A STUDY OF AXIAL AND RADIAL FLOWS FOR ANNULAR CHANNELS WITH ROUGHENED WALLS

KELLY M. BOONE

A Study of Axial and Radial Flows for Annular Channels with Roughened Walls

by

Kelly M. Boone

A thesis
submitted to the School of Graduate Studies
in fulfillment of the
thesis requirement for the degree of

Master of Engineering
in
Mechanical Engineering

Faculty of Engineering and Applied Science
Memorial University of Newfoundland
St. John's, Newfoundland, Canada, 2005

Abstract

The accurate prediction of pressure drop in production wells is very important to the petroleum industry. To decide if a reservoir is economically feasible, the underground reservoir's naturally occurring pressure should be properly determined.

In the initial stages of production, most oil is produced by natural lift production methods. In older reservoirs, unless injection methods are employed, the underground pressure eventually declines and oil will no longer naturally flow to the surface. Artificial lift techniques must then be used to extract the oil from the reservoir. Flow through an annulus, or casing flow, is used with artificial lift techniques. Due to the importance of casing flow, predicting pressure drop in these circumstances has become quite important.

Experiments were carried out using the multiphase flow loop at Memorial University of Newfoundland. Pressure differentials through varying sized annular channels with varying axial and radial flow rates were measured. For each of the three test sections incorporated into the design of the annulus, independent variables such as flow rate and pipe roughness were altered to study the effect each of these parameters would have on the pressure drop and hence the associated friction factors.

The data was collected and experimental friction factors were calculated. These values were plotted as a function of Reynolds numbers and compared to friction factors found theoretically.

Acknowledgements

There are many people to which I owe a thank you for helping me and supporting me during the completion of my masters degree. I would like to thank my supervisors Dr. Thormod Johansen and Dr. Yuri Muzychka. You have both helped me when I had questions and needed guidance. Thank you as well for the funding needed to support my research from CFI and NSERC. Thank you Dr. Johansen for giving me the opportunity to attend the short course in reservoir engineering at Leland Stanford University in 2003. It was an amazing learning experience that I will never forget.

I would also like to thank all the people that helped in getting the multiphase flow loop updated and ready to use. A great deal of work was required to prepare the flow loop for experimentation and I would not have been able to do it alone.

Finally, thank you to my friends, my family, and to Paul for your support and for being there for me through this time in my life. Thank you to my mother for helping me realize that continuing my education was exactly what I needed.

Contents

Abstract ii

Acknowledgements iii

List of Tables viii

List of Figures xi

Nomenclature xv

1 Why Study Flow in Annular Channels? 1

1.1 Introduction 1

1.2 Problem Discussion 8

2 Literature Review 12

2.1 Introduction 12

2.2 Pipe Flow 12

2.2.1 Single Phase Pipe Flow 13

2.2.2 Multiphase Pipe Flow 14

2.3 Horizontal and Inclined Flows 18

2.3.1 Horizontal Flow 18

2.3.2 Inclined Wells 20

2.4 Annular Flow Models 22
2.4.1 Single Phase Annular Flow 23
2.4.2 Multiphase Annular Flow 25
2.5 Radial Inflow 27
2.6 Smooth Wall and Rough Wall Piping 32

3 Pressure Gradient Comparison Methods **35**
3.1 Introduction 35
3.2 Simulation Theory 37
3.3 Simulation Results 39
3.3.1 When 'b' approaches Zero 39
3.3.2 When 'b' Approaches 'a' 42
3.4 Conclusion 45

4 Multiphase Flow Loop **46**
4.1 Introduction 46
4.1.1 Air Line Components 47
4.1.2 Pressure and Temperature Transducers 48
4.1.3 Flow Control System 49
4.1.4 Mixing Tanks and Separation Equipment 50
4.1.5 Main Pump 51
4.1.6 Data Acquisition System 52
4.1.7 MotionScope PCI High Speed Video System 52
4.2 Multiphase Flow Loop Upgrades 53
4.2.1 Main Pump and Inverter 53
4.2.2 Data Acquisition System 54
4.3 Addition of Annular Flow Capabilities 57

4.4 Addition of Radial Inflow Capabilities 60

5 Benchmarking Experiments 64

5.1 Benchmarking of Circular Pipe Flow 64

5.1.1 Experimental Procedures 65

5.1.2 Experimental Analysis 66

5.1.3 Theoretical Analysis 71

5.1.4 Results 73

5.2 Benchmarking of Annular Pipe Flow 78

5.2.1 Experimental Procedures 78

5.2.2 Results 79

6 Radial Inflow Through an Annular Channel 82

6.1 Experimental Set-up 82

6.2 Investigating Pressures and Flow Rates as a Function of Position . . . 85

6.2.1 Experiments with a 2" ID Annular Channel 85

6.2.2 Experiments with a 3" ID Annular Channel 88

6.2.3 Experiments with a 4" ID Annular Channel 92

6.3 Investigating Friction Factors for Radial Inflow into an Annular Channel 96

6.3.1 Theoretical Evaluation Considering Section P_3 to P_4: 96

6.3.2 Results for Section P_3 to P_4: 101

7 Axial Flow Through an Annular Channel 106

7.1 Experimental Setup 106

7.1.1 Smooth Axial Flow Through an Annular Channel 106

7.1.2 Rough Wall Annular Flow 108

7.2 Theoretical Evaluation 111

7.2.1 Smooth Axial Flow Through an Annular Channel 111

7.2.2 Axial Flow Through an Annular Channel with Rough Pipe Walls 113

7.3 Results 117

7.3.1 Smooth Axial Flow Through an Annular Channel 117

7.3.2 Axial Flow Through an Annular Channel with Rough Pipe Walls 124

8 Conclusions and Recommendations 135

8.1 Benchmark Experiments 135

8.2 Radial Inflow Experiments 137

8.3 Axial Flow Experiments 139

8.3.1 Experiments with Smooth Pipe Walls 139

8.3.2 Experiments with Roughened Pipe Walls 140

8.4 Recommendations 141

8.4.1 Radial Inflow Experiments 141

8.4.2 Axial Flow Experiments with Roughened Pipe Walls 142

8.4.3 General Recommendations 143

References 145

Appendicies 150

A Simulator Code for Pressure Gradient Comparison 150

B Operating and Maintaining the Multiphase Flow Loop 155

B.1 Turning on the Flow Loop 155

B.2 Shutting Down the Flow Loop 156

C Benchmarking Calculations 157

D Radial Inflow Experimental Results **160**

E Smooth Axial Flow Calculations **185**

F Rough Axial Flow Calculations **195**

List of Tables

5.1 Circular Pipe Flow - Trial 1 65

5.2 Circular Pipe Flow - Trial 2 66

5.3 Circular Pipe Flow - Trial 3 66

5.4 Radial Flow Benchmarking Tests 79

5.5 Annular Flow Benchmarking Results 79

5.6 Error Results 80

6.1 Radial Inflow Test Matrix 84

7.1 Test Matrix for the Annular Channel with 3" Diameter Inner Walls . 107

7.2 Test Matrix for the Annular Channel with 4" Diameter Inner Walls . 107

7.3 Test Matrix for the Annular Channel with 5" Diameter Inner Walls . 108

7.4 Test Matrix with Roughened Outer Walls and Smooth Inner Walls . . 109

7.5 Test Matrix with Roughened Outer and Inner Walls 109

A.1 Benchmark Data Analysis: Trial 1 157

A.2 Benchmark Data Analysis: Trial 2 158

A.3 Benchmark Data Analysis: Trial 3 159

B.1 Data Summary for Radial Inflow with a 2" ID Annular Channel 167

B.2 Data Summary for Radial Inflow with a 3" ID Annular Channel 175

B.3 Data Summary for Radial Inflow with a 4" ID Annular Channel 183

B.4 Friction Factors Evaluated at P_3 to P_4 for Varying Annular Channels . 184

C.1 Part 1: Smooth Axial Flow Through a 3" ID Annular Channel - Horizontal Analysis 185

C.2 Part 2: Smooth Axial Flow Through a 3" ID Annular Channel - Horizontal Analysis 186

C.3 Part 3: Smooth Axial Flow Through a 3" ID Annular Channel - Horizontal AnalysiS 187

C.4 Part 1: Smooth Axial Flow Through a 3" ID Annular Channel - Annular Flow Analysis 187

C.5 Part 2: Smooth Axial Flow Through a 3" ID Annular Channel - Annular Flow Analysis 188

C.6 Part 1: Smooth Axial Flow Through a 4" ID Annular Channel - Horizontal Analysis 189

C.7 Part 2: Smooth Axial Flow Through a 4" ID Annular Channel - Horizontal Analysis 190

C.8 Part 1: Smooth Axial Flow Through a 4" ID Annular Channel - Annular Flow Analysis 191

C.9 Part 2: Smooth Axial Flow Through a 4" ID Annular Channel - Annular Flow Analysis 192

C.10 Part 1: Smooth Axial Flow Through a 5" ID Annular Channel - Horizontal Analysis 193

C.11 Part 2: Smooth Axial Flow Through a 5" ID Annular Channel - Annular Flow Analysis 194

D.1 Part 1: Horizontal Pipe Flow with 1 Roughened Surface in the Annular Channel 195

D.2 Part 2: Horizontal Pipe Flow with 1 Roughened Surface in the Annular Channel 196

D.3 Part 3: Horizontal Pipe Flow with 1 Roughened Surface in the Annular Channel 197

D.4 Part 1: Annular Flow with 1 Roughened Surface in the Annular Channel 197

D.5 Part 2: Annular Flow with 1 Roughened Surface in the Annular Channel 198

D.6 Part 3: Annular Flow with 1 Roughened Surface in the Annular Channel 199

D.7 Part 1: Horizontal Pipe Flow with Two Roughened Surface in the Annular Channel 200

D.8 Part 2: Horizontal Pipe Flow with Two Roughened Surface in the Annular Channel 201

D.10 Part 1: Annular Flow with Two Roughened Surface in the Annular Channel 202

D.11 Part 2: Annular Flow with Two Roughened Surface in the Annular Channel 203

D.12 Part 3: Annular Flow with Two Roughened Surface in the Annular Channel 204

List of Figures

1.1 Oil and Gas Production System (Brill & Mukherjee, 1999) 4

1.2 Cross Section of A Typical Wellbore (Brill & Mukherjee, 1999) 5

1.3 Options for Well Completions (Economides et al., 1994) 6

1.4 Schematic of a Petroleum Trap (EIA Supply, 2004) 7

1.5 Schemiatic Description of a Pumping Well (Papadimitriou & Shoham, 1991) 9

2.1 Horizontal Flow Patterns (Beggs & Brill, 1973) 16

2.2 Eccentricity Degrees in Annuli (Caetano, 1985) 22

2.3 Schematic of Pipe with Radial Inflow (Schulkes & Utvik, 1998) 30

3.1 Visual Representation of Extreme Simulation Cases 36

3.2 As 'b' approaches Zero 40

3.3 As 'b' approaches Zero - A Closer Look 41

3.4 As 'b' Approaches 'a' 43

3.5 As 'b' approaches 'a' - A Closer Look 44

4.1 Original Multiphase Flow Loop 47

4.2 Pressure and Temperature Transducers from Omega 48

4.3 Pressure and Temperature Sensors with Clamp-on Saddles 49

4.4 Flow Meters from Omega 50

4.5 Original Flow Loop Pump 51

4.6 New Flow Loop Pump 53

4.7 Lab View 7.0 Data Acquisition Screen 54

4.8 New Wiring Set-up for Data Acquisition 55

4.9 Holding Ring Design and Assembly 58

4.10 Flow Spacings in Holding Rings 58

4.11 Radial Flow Setup 61

4.12 New Pressure Sensor Configuration 63

5.1 Location of Pressure Transducers for Circular Pipe Flow 70

5.2 Benchmarking Results for Circular Pipe Flow 75

5.3 Benchmarking Results for Circular Pipe Flow 77

5.4 Location of Valves on Radial Inflow Section 78

6.1 Radial Inflow Setup 83

6.2 Pressure and Flow Rate as a Function of Position in a 2" ID Annular Channel 86

6.3 Pressure and Flow Rate as a Function of Position in a 2" ID Annular Channel 87

6.4 Pressure and Flow Rate as a Function of Position in a 3" ID Annular Channel 90

6.5 Pressure and Flow Rate as a Function of Position in a 3" ID Annular Channel 91

6.6 Pressure and Flow Rate as a Function of Position in a 4" ID Annular Channel 93

6.7 Pressure and Flow Rate as a Function of Position in a 4" ID Annular Channel 94

6.8 Radial Inflow Setup 97

6.9 Radial Inflow Represented by Nozzle Flow 101

6.10 Friction Factors Evaluated at P_3 to P_4 Using a Discharge Coefficient . 103

6.11 Viscous Flow Patterns (White, 1991) 104

7.1 Friction Factors vs Reynolds number for Horizontal Flow Through an 3" ID Annular Channel 118

7.2 Friction Factors vs Reynolds number for Annular Flow Through a 3" ID Annular Channel 120

7.3 Friction Factors vs Reynolds number for Horizontal Flow Through a 4" ID Annular Channel 122

7.4 Friction Factors vs Reynolds number for Annular Flow Through a 4" ID Annular Channel 123

7.5 Friction Factors vs Reynolds number for Horizontal Flow Through a 5" ID Annular Channel 125

7.6 A Comparison of the Effect of Roughness Coefficients on Friction Factors 126

7.7 Friction Factor verses Reynolds Number for Horizontal Flow with 1 Roughened Surface in the Annulus 127

7.8 Friction Factor verses Reynolds Number for Annular Flow with 1 Roughened Surface in the Annulus 129

7.9 Friction Factor verses Reynolds Number for Horizontal Flow with 2 Roughened Surfaces in the Annulus 132

7.10 Friction Factor verses Reynolds Number for Annular Flow with 2 Roughened Surfaces in the Annulus 133

B.1 Fluid Flow Behaviour with a 2" ID Annular Channel with Radial Inflow Through Q_3 160

B.2 Fluid Flow Behaviour with a 2" ID Annular Channel with Radial Inflow Through Q_4 161

B.3 Fluid Flow Behaviour with a 2" ID Annular Channel with Radial Inflow Through Q_5 162

B.4 Fluid Flow Behaviour with a 2" ID Annular Channel with Radial Inflow Through Q_3 and Q_5 163

B.5 Fluid Flow Behaviour with a 2" ID Annular Channel with Radial Inflow Through Q_3 and Q_4 164

B.6 Fluid Flow Behaviour with a 2" ID Annular Channel with Radial Inflow Through Q_4 and Q_5 165

B.7 Fluid Flow Behaviour with a 2" ID Annular Channel with Radial Inflow Through Q_3, Q_4 and Q_5 166

B.8 Fluid Flow Behaviour with a 3" ID Annular Channel with Radial Inflow Through Q_3 168

B.9 Fluid Flow Behaviour with a 3" ID Annular Channel with Radial Inflow Through Q_4 169

B.10 Fluid Flow Behaviour with a 3" ID Annular Channel with Radial Inflow Through Q_5 170

B.11 Fluid Flow Behaviour with a 3" ID Annular Channel with Radial Inflow Through Q_3 and Q_5 171

B.12 Fluid Flow Behaviour with a 3" ID Annular Channel with Radial Inflow Through Q_3 and Q_4 172

B.13 Fluid Flow Behaviour with a 3" ID Annular Channel with Radial Inflow Through Q_4 and Q_5 173

B.14 Fluid Flow Behaviour with a 3" ID Annular Channel with Radial Inflow Through Q_3, Q_4 and Q_5 174

B.15 Fluid Flow Behaviour with a 4" ID Annular Channel with Radial Inflow Through Q_3 176

B.16 Fluid Flow Behaviour with a 4" ID Annular Channel with Radial Inflow Through Q_4 177

B.17 Fluid Flow Behaviour with a 4" ID Annular Channel with Radial Inflow Through Q_5 178

B.18 Fluid Flow Behaviour with a 4" ID Annular Channel with Radial Inflow Through Q_3 and Q_5 179

B.19 Fluid Flow Behaviour with a 4" ID Annular Channel with Radial Inflow Through Q_3 and Q_4 180

B.20 Fluid Flow Behaviour with a 4" ID Annular Channel with Radial Inflow Through Q_4 and Q_5 181

B.21 Fluid Flow Behaviour with a 4" ID Annular Channel with Radial Inflow Through Q_3, Q_4 and Q_5 182

Nomenclature

A	=	Cross sectional area
A_{ann}	=	Area of the annular channel
ACFM	=	actual cubic feet per minute
a	=	outer radius of an annular channel
b	=	inner radius of an annular channel
C_d	=	discharge coefficient
C_t	=	turbulent geometry factor for the annulus
C_{to}	=	turbulent geometry factor for a circular pipe
C_l	=	laminar geometry factor for the annulus
C_{lo}	=	laminar geometry factor for circular pipe
DBC	=	the distance between pipe centers in an annulus
D	=	pipe diameter
D_h	=	hydraulic diameter
D_{eff}	=	effective diameter
-dp/dx	=	rate of pressure drop in the overall flow direction
e	=	eccentricity of an annulus
f	=	friction factor
f_{lam}	=	friction factor for laminar flow
g	=	acceleration of gravity ($9.81 m/s^2$)
GOR	=	gas to oil ratio
GPM	=	gallons per minute
HP	=	horse power
K	=	permeability
K_{exp}	=	expansion loss coefficient for minor losses in pressure
K_{red}	=	reduction loss coefficient for minor losses in pressure
L	=	pipe length
LPM	=	liters per minute
$\dot{m}$	=	mass flow rate
md	=	millidarcy
MPFM	=	Mutiphase Flow Meter
P_3	=	Pressure in bottom radial inflow section

P_4	=	Pressure in middle radial inflow section
P_5	=	Pressure in top radial inflow section
psi	=	pressure per square inch
psia	=	atmospheric pressure per square inch
Q	=	Constant flow rate
Q_3	=	Flow rate in bottom radial inflow section
Q_4	=	Flow rate in middle radial inflow section
Q_5	=	Flow rate in top radial inflow section
Re	=	Reynolds Number
rpm	=	rotations per minute
UBD	=	Underbalanced Drilling
u	=	Darcy velocity or volumetric flux
v	=	fluid velocity
v_{ann}	=	fluid velocity in the annulus

ΔP_{acc}	=	Pressure due to acceleration of the fluid
ΔP_c	=	correction term for total pressure loss
ΔP_f	=	Pressure due to friction
Δz	=	vertical distance between pressure readings
ϵ	=	wall roughness
ϵ/D	=	relative roughness of a pipe
μ	=	fluid viscosity
ϕ	=	volume flux ratio
ρ	=	fluid density
σ	=	area ratio
θ	=	angle between the positive x-axis and the positive flow direction

Chapter 1

Why Study Flow in Annular Channels?

1.1 Introduction

To understand the need to investigate aspects of reservoir and completions engineering such as wellbore pressures, one must first begin to understand the reservoirs themselves and how oil is formed. Formed millions of years ago, oil is made up of compressed hydrocarbons having undergone extreme pressures and temperatures. Aquatic plant and animal remains were covered by layers of sediment and over time they endured varying pressures and heat. Different mixes of plant and animal remains, as well as pressure, temperature, and time have caused hydrocarbons to turn up today in an assortment of forms such as crude oil, natural gas, or even coal (EIA Supply, 2004).

The porosity of a reservoir is a very important characteristic. Porosity is the ratio of pore volume (V_p) to bulk volume (V_b) and has values varying from over 0.3 to less than 0.1. If the reservoir does not have the desired porosity, it will not be explored. The height of the reservoir is also an important characteristic. It describes the thickness of the porous medium contained between two impermeable layers. An attractive hydrocarbon saturation is another critical variable that must be determined before a well can be tested or completed. If a large fraction of the pore volume is occupied by hydrocarbons in a reservoir of substantial height, it may be a desirable well to develop (Economides, Hill, & Ehlig-Economides, 1994).

Probably the most important characteristic is the permeability of the reservoir. Permeability is a measure of the ease with which fluids flow through a porous rock. Many rocks, such as clays, shales, and chalk are impervious to the movement of fluids, even though they are porous (Allen & Roberts, 1993).

Permeability relates the amount of interconnectivity between the pores (Nind, 1981) and can be defined using Darcy's Law (Johansen, 2004) where:

$$u = \frac{Q}{A} = -\frac{K}{\mu}\left[\frac{dp}{dx} + \rho g sin\theta\right] \quad (1.1)$$

where:	u	=	Darcy velocity or volumetric flux
	Q	=	Volumetric flow rate (m^3/s)
	A	=	Cross sectional area (m^2)
	-dp/dx	=	rate of pressure drop in the overall flow direction
	μ	=	fluid viscosity (Pa s)
	K	=	permeability (m^2)
	θ	=	angle between the positive x-axis and the positive flow direction
	g	=	acceleration of gravity $(9.81m/s^2)$

The same reservoir rock can have different permeabilities at different locations. Generally, reservoirs with permeabilities greater than 250 millidarcies (md) will have wells that are good producers. It should be noted, however, that this generalization does not account for problems that may exist in an individual well such as high water cut, high gas-oil ratios (GOR), or sand. Not only can permeability vary from place to place but it can also vary directionally. The vertical permeability can be quite different from the horizontal permeability and in most cases it will not be the same (Nind, 1981).

Finding oil occurs in a series of steps. The first step is to test the rock at the location of interest to identify whether the site has the potential to be a reservoir. When it has been deemed a prospect for oil, an exploration well is then drilled. From data taken from these exploration wells, reservoir dimensions are determined and it is decided whether or not the reservoir is commercially viable. Production wells are than installed and pipelines are assembled to transport the oil for further shipment and processing (EIA Supply, 2004).

During oil production, fluids will flow from the drainage areas in the reservoir to the separator at the surface, as shown in Figure 1.1. The reservoir pressure is the average pressure in the drainage area and it controls the flow through the system. The reservoir pressure is assumed to remain constant for a fixed time during the depletion of the reservoir. When this pressure changes, the performance of the well changes and hence the well may then need to be re-evaluated. At the surface, the separator pressure is designed to optimize production and to keep the lighter hydrocarbon components in the liquid phase. Pressure regulators are used to maintain this pressure (Brill & Mukherjee, 1999).

A typical production well can be composed of many layers, from the flowing fluids down to the formation as shown in Figure 1.2.

As fluids enter the wellbore they will flow through a well completion region that can be quite complicated (Brill & Mukherjee, 1999). As part of the well completion, many wells are cemented and cased which helps to support the casing and provide zonal isolation at formation depths. A cemented and cased well must be perforated to obtain connection with the reservoir so oil can flow into the well to eventually be extracted. A well is usually cemented and cased when stability problems are anticipated. To combat the problems of sands, slotted liners can be placed between

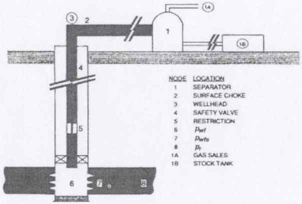

Figure 1.1: Oil and Gas Production System (Brill & Mukherjee, 1999)

the well and the formation. Gravel packing can also be used as another method to keep permeability-reducing fine grains away from the well (see Figure 1.3)(Economides et al., 1994).

Fluid flow in a pipe with mass transfer did not interest petroleum engineers until horizontal well technology was introduced and widely applied in the petroleum industry in the 1980s (Ouyang & Aziz, 1996). Although perforated pipe sections may be up to a few kilometers long, the pressure drop in the pipe can severely limit its actual production length. It is often assumed that the inflow rate per unit wellbore length is the same everywhere along the whole wellbore, but this is not necessarily true. Due to wellbore pressure drop, the wellbore pressure near the well toe is higher than the pressure at the well heel, therefore the pressure drawdown near the well toe is less than the pressure drawdown near the well heel. This makes the specific inflow rate near the well toe smaller than near the well heel (Ouyang, Arbabi & Aziz, 1997). Frictional effects are the most significant contribution in the drop in pressure between the heel and the toe of the well. Due to the acceleration of the fluids, an accelerational pressure component will exist over the area. This is given by $\Delta P_{acc} = \rho(v_2^2 - v_1^2)$.

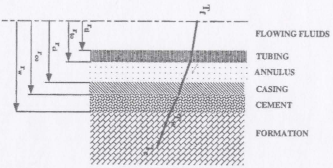

Figure 1.2: Cross Section of A Typical Wellbore (Brill & Mukherjee, 1999)

Usually ΔP_{acc} only contributes to less than 10% of the total pressure loss, though values as high as 40% have been found (Johansen, 2004). These pressure effects have a great influence on the production of the well and must be carefully considered to ensure optimal well production.

The accurate prediction of pressure drop in production wells is very important to the oil and gas industry. To decide if a reservoir is economically feasible, the underground reservoir's naturally occurring pressure should be properly determined. This pressure fluctuates depending on the characteristics of the trap, the reservoir rock and the production history (see Figure 1.4).

In the initial stages of production, most oil is produced by natural lift production methods, occurring because the reservoir pressure is large enough to push the oil to the surface. In older reservoirs, unless injection is carried out, the underground pressure eventually declines and oil will no longer naturally flow to the surface. Using artificial lift techniques, the oil must then be pumped out by gas or mechanical or electrical pumps (EIA Supply, 2004).

The primary production methods will become ineffective over time and in order to

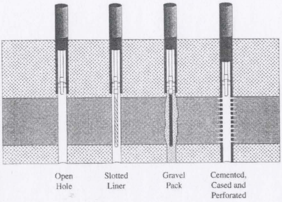

Figure 1.3: Options for Well Completions (Economides et al., 1994)

continue producing from the well, secondary production methods need to be implemented. Waterflooding is a common method that uses water to displace oil and force it into the wellbore. When the secondary production methods have been exhausted, tertiary or enhanced oil recovery methods may be required. These techniques focus on increasing the oil's flow characteristics by using steam, carbon dioxide, and other gases or chemicals (EIA Supply, 2004).

If the pressure drop through a vertical, horizontal, or inclined well is accurately conveyed, production from these wells can be optimized for economical advantages. It is important to understand pressures in reservoirs and wellbores and to understand what happens if the pressure drop along the length of the well is of the same magnitude as the pressure required to extract the oil from the reservoir. Also, if the permeability of the formation is large, pressure drop between the well and the reservoir will increase significantly as the toe of the well is approached. If the production profile is skewed in such a way, with one end of the well producing more than the other, early breakthrough of water or gas may occur. This would have an associated drop in revenues which is not desired by any company (Schulkes, Rinde & Utvik, 1999). This occurrence should be preventable and with more knowledge on pressure

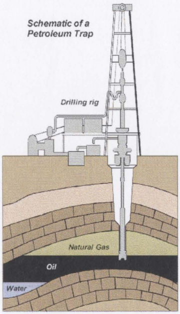

Figure 1.4: Schematic of a Petroleum Trap (EIA Supply, 2004)

drop through production wells, oil companies can produce in wells that may have not been feasible to produce from in the past.

1.2 Problem Discussion

In the petroleum industry, production systems encounter a broad range of pressures and temperatures. Wells can vary in length from a few hundred feet to over 20,000 feet while pipelines can run from a few feet to several hundred miles long. Pipe roughness, diameter, inclination, and shape all vary significantly. For all of these situations engineers are required to predict the relationships between flow rates, pressure drop, and piping geometry for the fluids produced from a reservoir over the entire life of a field (Brill, 1987).

Oftentimes when oil is produced, gas and even water can also be produced simultaneously. For these processes the flow column is ordinarily a jointed pipe of uniform diameter commonly called the production tubing. Occasionally flow through the annulus between the casing and the production tubing is also found (Govier & Aziz, 1972). This can occur for high production rates in the well and is usually dictated by economics, multiple completions, and regulated production rates. Wells that produce oil through the annulus make up a significant part of the world's oil production, even though only a small number of them exist in comparison to the total number of producing wells (Brill & Mukherjee, 1999).

Other applications involving flow through an annulus, or casing flow, can be found in wells using artificial lift techniques. A rod string is installed inside the tube string and fluids are pumped upward through the tubing-rod string annulus. Casing flow can also occur in gas production wells. A siphon tube is installed inside the tubing string and to prevent unwanted liquids from accumulating at the bottom of the wells, they will flow up through the tubing-string/siphon-tube annulus and be removed (Brill & Mukherjee, 1999).

More than eighty percent of North American oil wells require some type of artificial lift system to operate. The sucker-rod pump is the most widely used lift system in the petroleum industry and can be seen in Figure 1.5. Included in the wellbore is a tubing string and a casing. A liquid column can be found in the casing-tubing annulus due to the open completion of the well. Two separate regions will result after gas is vented through the annulus. Only single phase gas exists in the upper region, z_G, while the lower section, z_L, will consist of two-phase flow. This can complicate determining the pressure gradients in the annulus of the pumping wells (Papadimitriou & Shoham, 1991).

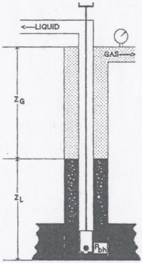

Figure 1.5: Schemiatic Description of a Pumping Well (Papadimitriou & Shoham, 1991)

Due to the importance of casing flow, predicting pressure drop in these circumstances has become quite important. Normally in the earlier attempts, the general application of systems with different fluid properties, pipe sizes, and flow rates were not certain. Most of the research in the past focused on partial or total flow pattern identification (Caetano, 1985).

Investigating flow through an annulus has also become important in the field of underbalanced drilling (UBD). An operation is classified as UBD when the hydrostatic head of a drilling fluid is intentionally designed to be lower than the pressure of the formation being drilled. In horizontal UBD, a gas-liquid mixture is injected through the drill string, where it passes through the bottom-hole assembly and provides energy to drive the downhole motor that drives the drill bit. The injected fluids flow from the bit into the rough-walled annulus, which is formed from the drill string and the open hole. The resulting multiphase fluids then flow from the well heel, up the casing-drill string annulus and to the surface (Smith, Gergory, Murno & Muqeen, 1998).

Annular flow is also of interest because it is a flow case which may provide some insight into the general problem of fully developed turbulent shear flows. It combines two boundary layers that may be very different from each other in distributions of velocity, shear stress, and turbulence quantities. Studying this flow type is also relevant since its limiting cases are flow in circular pipe and flow between parallel plates, which have been extensively studied (Brighton & Jones, 1964).

In 1997 a multiphase flow loop was designed and constructed in the Engineering Building's Fluid's Laboratory at Memorial University of Newfoundland. This project was a joint venture between Instrumar Ltd. and C-CORE/Memorial University of Newfoundland (MUN). At that time, the flow loop's main use was to aide in developing a Multiphase Flow Meter which would be used to measure real time flow rates of each component of the gas-oil-water flows of the unprocessed well streams (Multiphase Flow Loop, 1997).

The flow loop was also used to test the effectiveness of velocity inversion algorithms. These tests were essential for validating the fluid modeling and to meet the specification requirements of the meter (MPFL, 1997). Since then, the multiphase flow loop was dormant but had much potential for many other projects. In particular, it can have many applications in the oil and gas industry.

Experiments I designed to measure the pressure differentials through varying sized annular channels with varying axial and radial flow rates were carried out using the multiphase flow loop. For each of the three test sections incorporated into the design, independent variables such as pipe roughness and flow rates were altered to study the effect each of these parameters would have on the pressure drop and hence the associated friction factors.

Chapter 2

Literature Review

2.1 Introduction

Studies on pressure drop in piping has been carried out in the past with the main focus on many different aspects. Some of these studies include vertical flow, horizontal flow, inclined flow, radial flow, axial flow or a combination of these. As well as the direction of the flow, the type of flow, such as single phase or multiphase, has also been studied. There has also been research carried out on the shape of the piping, whether it be circular pipes, square ducts, or annular sections to name a few. Research with circular and annular piping is of great importance to the oil and gas industry. In combination with the above there have been investigations carried out to determine the effect of the pipe walls and to what effect rough pipe walls have on the flow and flow characteristics. All of these areas have great importance in investigating pressure gradients and friction factors in oil wellbores and are looked at in further detail.

2.2 Pipe Flow

A general wellbore flow model should be comprised of frictional, acceleration, gravitational, and inflow pressure drops (Ouyang & Aziz, 1996). The flow in a wellbore can be either single phase or multiphase. In most production wells, the flow is multiphase although most wells do experience single phase flow initially. Single phase flow exists mostly in injection wells. The flow geometry in wellbores is generally through a circular pipe, although flow though an annular spacing does occur between the tubing and the casing (Economides et al., 1994).

For fluids in a production well there are three different flow regions along the wellbore, including the laminar flow region, the partially developed turbulent flow region, and the fully developed turbulent flow region (Ouyang & Aziz, 1996). In laminar flow through piping with a constant cross section there are no components of velocity normal to the flow direction. Turbulent flow is characterized by fluctuating components of velocity in all directions. Between laminar flow and turbulent flow, the transitional flow stage occurs. This type of flow is most easily characterized by the Reynolds number obtained from the flow parameters. For Reynolds numbers less than 2000 the flow is considered laminar, for Reynolds numbers greater than 4000 the flow can be characterized as turbulent, and for Reynolds numbers between 2000 and 4000, the flow is in the transitional stage (Govier & Aziz, 1972).

How well one can predict flow behaviour for turbulent flow conditions depends on extensive experimental studies of velocity profiles and pressure gradients, which are very sensitive to pipe wall characteristics. A practical approach to defining friction factors for this type of flow would be to start with smooth wall pipe, which would be the simplest case. From there, one would proceed to partially roughened walls and then fully roughened walls (Brill & Mukherjee, 1999).

2.2.1 Single Phase Pipe Flow

It is important to understand single phase pipe flow before one can go further in this area. The single phase flow problem has significant practical value since during the initial stages of production, mainly oil will enter the well. It is only later that the flow becomes multiphase. It is important to understand single phase flow, since the early stages of oil production are are normally the most economical (Schulkes & Utvik, 1998).

The basis for all calculations involving fluid flow in pipes is conservation of mass, momentum, and energy. By applying these principles, changes in pressure and temperature with distance can be established (Brill & Mukherjee, 1999).

The flow behavior of single phase fluids is largely dependent on the density and viscosity of the fluid. The flow behavior of multiphase fluids is not only dependent on these parameters but it also depends on the consistency of the individual phases, the interfacial tension, the state of their dispersion, and their relative quantities. From this it is clear that multiphase flows are more complex and are therefore more complex to study. In any flow calculation we should seek to use accurately measured values of the parameters such as pressures and temperatures from single phase flows (Govier & Aziz, 1972).

2.2.2 Multiphase Pipe Flow

Multiphase flows occur throughout the entire production system and can be a mixture of natural gas phase, a hydrocarbon liquid, and a water phase. In an oil well whenever the pressure drops below the bubble point gas will evolve and from that point to the surface, gas-liquid two phase flow occurs. In a well producing from an underbalanced reservoir, two-phase flow will occur in the wellbore, in the tubing, or both unless the surface pressure remains above the bubble point. Many oil wells also produce substantial amounts of water, which can result in two or even three phase flow in the wellbore (Economides et al., 1994).

Multiphase flows in the oil and gas industry are unique from other industries and can behave very differently than single phase flows (Brill, 1987). Two-phase flow occurs in pipelines and in oil and gas wells. Often, some liquid is produced with most gas-producing wells and some gas is usually produced by most oil wells. As the reservoir becomes depleted, artificial lift systems such as a gas lift are used to aid in the production. Knowledge of two-phase flow pressure gradients is required to design these lift systems, making multiphase flows very important (Beggs & Brill, 1973).

The contact between two immiscible liquids such as oil and water is found in liquid-liquid extraction equipment and in pipelines for liquid transportation to name a few. Knowledge of the flow characteristics for such a fluid combination is required for the design of these systems (Charles, Govier & Hodgson, 1961). When two or more phases flow simultaneously in pipes, the phases tend to separate because of differences in density which cause differences in shear stresses at the pipe wall for each phase. As a result of the expansion of the gas phase, the gas and liquid phases do not normally travel at the same rate inside the pipe (Brill & Mukherjee, 1999).

Multiphase flows have been extensively researched over the past five decades (Beggs & Brill, 1973). In modeling multiphase flows, one must consider the differences in two-phase flows and three-phase flows. These multiphase flows can be best modeled by drift flux modeling techniques (Shi, Holmes, Diaz & Aziz, 2004). Since they are simple, continuous, and differentiable, drift flux models can be used for two and three phase pipe flows in reservoir models. Data from experiments of five centimeter diameters or less have been used in the past, but there is a need for data from larger diameter experiments for more accurate input parameters for modeling. Shi et al. (2004) evaluated the optimization of two-phase drift flux parameters and found that two-phase water-gas drift flux parameters can be used to estimate three-phase gas hold-up. However, two-phase oil-water drift flux parameters cannot be used due to large errors incurred (Shi et al., 2004).

In 1961 Charles, Govier, and Hodgson investigated what effect equal density oil-water mixtures had on pressure gradients. The major interest was if there were any beneficial effects from adding water in controlled amounts into pipelines with heavy crude. They found that when initially in laminar flow, increasing the amount of water to oil lowers the pressure gradient to a minimum. If more water is continually added, the pressure gradient will increase and will eventually exceed the pressure gradient for the case with only oil flowing (Charles et al., 1961).

The distribution of the phases inside the piping are quite distinguishable in multiphase flow. Existing flow patterns depend on relative magnitudes of the forces acting on the fluids. Several different flow patterns can exist in a well as a result of the large changes in pressure and temperature that the fluids are subject to. As the flow patterns change, the pressure gradients associated with the flows also change. It is therefore important to be able to predict flow patterns in multiphase flow (Brill & Mukherjee, 1999). For horizontal flow, Beggs and Brill (1973) investigated segregated flow, intermittent flow, and disturbed flow which are shown in Figure 2.1 obtained from this study.

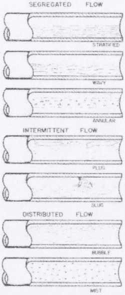

Figure 2.1: Horizontal Flow Patterns (Beggs & Brill, 1973)

Various flow patterns have been studied in the past by many different people. Govier, Sullivan, and Wood (1961) published the first comprehensive analysis on two phase oil/water vertical flows. Flow regimes studied here included oil bubbles, oil froth/water droplets, and water droplets. This research also found that oil behaved similar to high density gas. Curves showing the effect of oil-water ratios on pressure drop and the flow patterns were similar to those observed in the vertical flow of gas-liquid mixtures.

Hasson, Orell and Finik (1971) studied pressure drop, hold up, and flow regimes for water-kerosene mixtures. Flow regimes found in these experiments included annular, disturbed annular, and other flows. Shean (1976) carried out experiments investigating the upward flow of oil/water mixtures and oil/water/air mixtures obtaining flow patterns, holdup and pressure loss. From these experiments, he was able to identify the oil slugs, water froth, oil froth and water drop flow regimes. Woods, Spedding, Wattenson and Raghunathan (1998) studied three phase oil/water/air vertical flow in vertical pipes and reported data for the slug to annular flow regimes.

2.3 Horizontal and Inclined Flows

2.3.1 Horizontal Flow

Flow in oil wellbores can exist in horizontal piping, inclined piping, or vertical piping. From a reservoir engineering point of view, horizontal wellbores are important to investigate since a large amount of the presently known oil reserves are contained within layered reservoirs. In these situations, production through vertical wells is unattractive because of the limited contact area with the reservoir. The best way to extract oil between these layers is to use horizontal producers since they would provide a larger contact area with the reservoir (Dikken, 1989).

From a reservoir perspective, a horizontal well is typically inclined approximately 80^o from a vertical position and it's productivity is dependent on the well length. They can be completed as an open hole, with slotted liners, pre-packed liners, liners with external casing packers, or with cemented and perforated liners. Open hole or slotted liners are the most common completion methods used in such wells (Lacy, Ding & Joshi, 1992).

Horizontal wells have been employed for many situations including thin reservoirs, naturally fractured reservoirs, formations with gas and water coning problems, heavy oil reservoirs, gas reservoirs, enhanced oil recovery, and more recently secondary recovery applications (Lacy et al., 1992). One important factor that may limit the useful length of a horizontal producer is the frictional losses in the wellbore. For high flow rates or for long wells, the pressure drop in the wellbore may be of the same magnitude as the drawdown pressure at the producing side, defined as the difference in pressure between the reservoir and the wellbore. If this were the case, a section of the well downhole would not produce. The time and expense in drilling that portion of the well would be lost (Novy, 1992).

In a perforated horizontal well, depending on the completion type, fluid can enter the wellbore at different locations along the well. One must be sure the distance between the perforations is adequate enough to achieve a stabilized velocity profile. If not, this can lead to a different pressure behavior than that for fully developed flow (Yuan, Sarica & Brill, 1996).

It is difficult to find fully developed turbulent flows in perforated horizontal wells. Fluids enter the wellbore through the perforations so that the volume flux inside the perforated pipe increases toward the heel. The distortion of the pipe flow due to the numerous radial inflow points is quite complex and the pressure drop for these pipes is not readily determined (Schulkes & Utvik, 1998).

Beginning in the late 1980s, the petroleum industry started conducting analytical and experimental studies to investigate many aspects of horizontal well flow behavior. Horizontal wells can be very long and therefore the drawdown pressure can be strongly affected by the frictional pressure drop (Landman, 1994). The first analytic model which could predict the turbulent flow frictional pressure drop in horizontal wells was presented by Dikken (1989). Brice (1992) carried out a study which confirmed the high frictional pressure drop in the production section of a horizontal well as was proposed by Dikken (1989). Landman (1994) extended Dikken's model making it able to describe selectively perforated completions.

Since this time, horizontal well technology has become well established. Substantial analytical and experimental work has been published for an assortment of horizontal well production aspects. In 1992, Novy investigated pressure drops in horizontal wells. He discovered that the ratio of wellbore pressure drop to drawdown at the producing end was an important criterion. If this ratio goes above 10% to 15%, the wellbore friction will have a significant effect on productivity and may reduce it by more than 10%. Any oil well that produces more than 1500 STB/D and any gas wells that produce more than 2 MMscf/D are at risk (Novy, 1992).

In 1997, Ouyang, Arbabi, and Aziz investigated pressure drops along a horizontal wellbore. They showed that because of inflow through perforations, the accelerational pressure drop can be important and can considerably influence the well flow rates for certain flow conditions (Ouyang et al., 1997).

Due to inclinations and trajectories that vary along the length of the wellbore, a horizontal well is not truly horizontal. To accurately study horizontal wells, one must consider flow through inclined perforated pipes (Schulkes & Utvik, 1998).

2.3.2 Inclined Wells

As the search for petroleum moves into unexplored areas, the number of inclined wells is increasing. Several inclined or directional wells are usually drilled in offshore drilling for economical reasons. In Canada and Alaska, where permafrost exists, several directional wells are usually drilled from one location. In these areas, the cost of drilling is very high and it is more difficult to transfer the petroleum after production. Gathering lines from offshore wells are usually laid along the seabed and slope upward to the shore. The pressure gradient due to height changes for these pipelines can be much greater than the pressure gradient due to friction and must therefore be accurately predicted. Pressure gradients in an inclined well with inclination angles of 15^o to 20^o from the vertical can be greater than pressure gradients in a vertical well (Beggs & Brill, 1973).

Studies have been performed in the past on two-phase flow in inclined small diameter pipes. Beggs & Brill (1973) studied inclined liquid-gas flow in small diameter pipes and their work has been widely used in the petroleum industry. They were able to provide empirical relationships to predict holdup and pressure drop.

In 1988 Hasan and Kabir carried out experiments in a 12.5 cm pipe and an annular channel with varying sized inner diameters. They inclined the piping up to a maximum of 32^o from a vertical position. These experiments were all carried out at very low flow rates and it was found that this model performed as well as the Beggs & Brill (1973) model.

More recently, Tshuva, Barnea & Taitel (1999) also carried out a study on two-phase flow in small diameter inclined pipes. Upward water-air flows a different inclinations were studied and it was found that the flow distribution could be either symmetric or asymmetric. This would depend on the inclination of the pipe as well as the conditions of the flow. The authors proposed a model to explain their findings.

In 2003, Oddie et al., studied multiphase flows in large diameter inclined pipes. They used a large scale apparatus to carry out the experiments and were able to obtain unique holdup data for steady-state and transient flows. They evaluated the effects of flow rates on the different phases and pipe deviations studied. Detailed flow pattern maps were produced for the complete range of flow rates and pipe inclinations and it was found that the maps for the water-gas and oil-water-gas systems were quite similar. A mechanistic model developed by Petalas and Aziz (2000) predicted with great accuracy the experimentally observed flow patterns and it was able to predict holdup reasonably accurate as well.

2.4 Annular Flow Models

Annuli are characterized by the existence of two circular pipes, where the flow area is bounded by the inner wall of the outer pipe and the outer wall of the inner pipe. Annuli can be either eccentric, partially eccentric, or concentric, as shown in Figure 2.2. A concentric annulus occurs when the pipe centers are coincident and the eccentricity value is zero. When an annulus is fully eccentric, the eccentricity value is equal to one and both pipe walls have a point of contact .

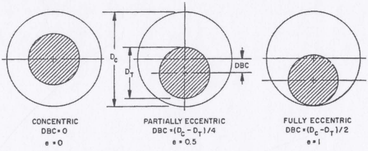

Figure 2.2: Eccentricity Degrees in Annuli (Caetano, 1985)

Flow through an annulus is encountered in various industrial applications, including the oil and gas industry. Although it is often encountered in practical applications, little literature has been published on the subject. The oil and gas industry's past interest in this subject was limited to investigating high productivity wells flowing through the casing-tubing annulus (Caetano, 1985), but more recently people are becoming interested in this topic for other reasons such as looking into underbalanced drilling technology. Since the accurate prediction of downhole pressure is very important for this technology, annular flow is becoming more relevant (Lage & Time, 2002).

In the past annuli have been evaluated on the basis of hydraulic diameter, but this may not always be the best way to represent the dimension for flow in an annulus. To more appropriately determine this parameter, a better understanding of flow through an annulus is required (Caetano, 1985).

2.4.1 Single Phase Annular Flow

For annular conduits with single phase flow, the friction factors are often determined using the hydraulic diameter characteristic. This concept is most suited for high turbulent flows (Caetano, 1985).

Experiments were carried out by Sadamomi, Sato and Saruwatari (1982) for vertical flow in non-circular channels. One of the shapes studied here was the concentric annulus with an annular channel space of approximately one inch. The inner core rod was held in place by three pins two millimeters in diameter inside the annular spacing located every half meter. The friction factor for fully developed turbulent single phase flow was correlated with Reynolds number. This correlation used a turbulent geometry factor, C_t, that is a function of the laminar geometry factor, C_l.

$$\frac{C_t}{C_{to}} = \sqrt[3]{(0.0154\frac{C_l}{C_{lo}} - 0.012)} + 0.85 \tag{2.1}$$

where: C_t = turbulent geometry factor for the annulus

C_{to} = turbulent geometry factor for a circular pipe

C_l = laminar geometry factor for the annulus

C_{lo} = laminar geometry factor for circular pipe

Sadamomi et al. (1982) were able to determine the friction factor for the channel considered according to $f = C_t Re^{-0.25}$, using the turbulent geometry factor for the annulus.

This equation is comparable to that developed by Paul H. R. Blasius (1873-1970). For turbulent flow and considering the Fanning friction factor, the Blasius equation can be represented by $f = 0.0791Re^{-0.25}$. The Blasius equations fits that which was discovered by Sadamomi et al. (1982) for the case where $C_t = 0.0791$.

In 1964 Brighton and Jones studied fully developed turbulent flow in annuli with a range of Reynolds numbers from 46,000 to 327,000. The test section included two concentric aluminum pipes. The outer pipe had a eight inch nominal inside diameter and four different inner pipe sizes were used. Friction factors were determined with a water flow apparatus for Reynolds numbers between 4000 and 17,000 and were found to be six to eight percent higher than what was generally accepted for flow through an annulus with smooth walls in this range. Brighton and Jones found that friction factors for air flows through an annulus with smooth walls were one to ten percent higher than the pipe flow values for those with same Reynolds numbers. They found that these results depended very little on the ratio of the inner pipe radius to the outer pipe radius.

Velocity profiles were studied by Brighton and Jones (1964) and were found to deviate from the normal correlations when the radial distribution of Reynolds stress is non-linear. They also found that in turbulent flow, the point of maximum mean velocity will occur at a smaller radius than in laminar flow. They were also able to determine mixing lengths from accurate measurement of the velocity gradients. Physically, the mixing length is the distance a particle travels before exchanging momentum with fluid particles of different layers. Brighton and Jones found that the mixing length goes to infinity as the maximum velocity is approached. Mixing lengths of this magnitude would be physically impossible and hence their findings supports the findings of the physical incorrectness of the mixing length theory.

In 1985 Caetano calculated friction factors for annular single phase flow. He found that using the hydraulic diameter characteristic was inaccurate for low turbulent

Reynolds numbers. He deduced that for flow through an annular spacing, the friction factor depended on Reynolds number, pipe diameter ratio, and degree of eccentricity. For a given set of flow conditions, he discovered that friction factor decreased with increasing degree of eccentricity and was less pronounced as the Reynolds number increased.

Caetano (1985) also discovered that the error involved in predicting friction factor values in an annulus when using the hydraulic diameter characteristic can be as high as 40% to 50%. This depended on the degree of eccentricity:

$$e = \frac{2DBC}{D_C - D_T} \tag{2.2}$$

and the annulus pipe diameter ratio:

$$K = \frac{D_T}{D_C} \tag{2.3}$$

where: D_T = outer diameter of the inner pipe
D_C = is the inner diameter of the outer pipe
DBC = the distance between pipe centers

By investigating the frictional pressure loss, he was able to conclude that the friction pressure gradient for an annulus is a function of pipe diameter and the degree of eccentricity.

2.4.2 Multiphase Annular Flow

Two-phase flow in an annular channel is important to study since it occurs in a variety of practical applications. For instance, two-phase flow exists in an annulus when an influx of gas enters an oil wellbore (Kelessidis & Dukler, 1989).

Kelessidis and Dukler (1989) studied upward annular two-phase flow as well with experiments carried out in a 2 x 3in annulus. This study focused on developing a flow pattern identification method and did not investigate frictional effects.

Papadimitriou and Shoham (1991) slightly improved this model, but only for bubble and slug flow patters. They also carried out a sensitivity analysis for pumping wells. The effects of the system and flow characteristics such as casing pressure, gas flow rate, and degree of eccentricity of the annulus were demonstrated.

Nakoriakov, Kuzentsov and Vitovsky (1992) studied upward flow in vertical narrow channels. The friction factor for two-phase flow was obtained for the experimental data collected and a mathematical model that can predict the friction factor in a narrow annular channel was developed. A calculation method for finding friction factors based on the empirical relationship of the mean gas to liquid velocity ratio was suggested and these calculations agree with the data obtained experimentally (Nakoriakov et al. 1992).

It is noted that the oil and gas industry use annular configurations which are much bigger than the ones investigated by Nakoriakov et al. (1992) so further study into this area is still desired.

Hasan and Kabir (1992) studied annular flow, but did not investigate pressure gradients or frictional effects. Their focus was on flow pattern prediction through an experimental investigation using vertical and inclined piping. They developed void fraction expressions for each flow regime studied.

Lage and Time (2000) studied upward flow in annuli for the purpose of developing a steady state mechanistic model. They focused on developing a procedure for flow pattern prediction for two-phase flow regimes and did not investigate friction factors associated with the flow.

2.5 Radial Inflow

The inflow through the perforations along a completed wellbore contributes to the pressure loss through unconventional friction factor correlations. This inflow effect is significant in most wells, and will affect both the pressure loss along the wellbore and the inflow performance of the well (Asheim, Kolnes & Oudeman, 1992).

There are many studies that have been carried out for single phase flow without radial inflow. The classic Moody Chart allows the pressure drop to be predicted with an accuracy of 10% to 15%. When radial inflow is added, the pressure variation in the piping is significantly altered and existing correlations without radial inflow can no longer be used. Radial inflow causes axial pipe flow to never reach fully developed flow in the areas where the inflow occurs (Schulkes, Rinde & Utvik, 1999). As well, for laminar flow the local friction factor increases with an increase in the injection Reynolds number, while it decreases for turbulent flow (Ouyang et al., 1997). It is important to understand radial flow in pipes because it relates to how oil enters the production wells and is extracted from the reservoir.

Ouyang et al. (1997) found that the influence of inflow to a wellbore and outflow from it depends on the flow regime present. Inflow, in production wells, increases the wall friction for laminar flow while decreases for turbulent flow. Outflow, in injection wells, has the opposite reaction. The wall friction is decreased for laminar flow and increased for turbulent flows. Calculation results show that the acceleration pressure drop may or may not be important compared to the frictional component depending on the specific pipe geometry, fluid properties, and flow conditions. Due to the existence of perforation inflow, the accelerational pressure drop can be important relative to the frictional part and can significantly influence the well flow rates under some flow conditions (Ouyang, 1996).

Yuan and Finkelstein (1956) were the first to study the effects of uniform injection and suction through a porous pipe wall on the two-dimensional steady state laminar fluid flow. They solved the Navier-Stokes equations in cylindrical co-ordinates for both very large and very small wall Reynolds numbers. They found that wall friction is increased with injection at the pipe wall and that suction will decrease the wall friction.

Dikken (1989) suggested a theoretical basis for understanding and predicting how the wellbore flow resistance affects the inflow performance. According to the theory, flow resistance may have a critical impact on the inflow rate distribution along the wellbore which is very important for horizontal wells in permeable reservoirs. In these areas, the pressure drop over the wellbore can become comparable to the drawdown pressure.

Asheim et al. (1992) studied pressure loss with only one or two radial inlets. Their experimental data was compared with a simple model taking into account both friction and acceleration pressure losses. They stated that the total pressure drop along a perforated pipe is made up of wall friction and inflow acceleration. The wall friction was computed in the same way as for regular unperforated pipe. They found that the model compared well with experimental data when the radial inflow was less than three times the axial velocity, but for larger velocities the model underpredicted the measured pressure loss.

Su and Gudmundsson (1995) investigated single phase pipe flow with radial inflow attempting to account for the effects of radial inflow. They assumed that the pressure drop for a perforated pipe had three contributions; frictional pressure drop, accelerational pressure drop, and a 'mixing' term. They show that most of the pressure drop is due to the first two components, but a significant contribution does come from the mixing term. For small flux ratios, the mixing term gives a negative contribution to the pressure drop in the pipe. This implies that the flow in the pipe is lubricated by the radial inflow. For large flux ratios, when the radial velocity is of the same order of magnitude of the axial velocity, the correction term gives a positive contribution which indicates the radial flow obstructs the pipe flow, thus increasing the pressure drop. The experiments show that the correction term in the pressure loss (Δp_c) is also highly dependent on the geometry of the perforated pipe.

A study by Schulkes, Utvik and Rinde (1997) was carried out and the effects of radial inflow on single phase and multiphase flows were investigated. With small perforations along a certain length of piping, it was discovered that a pressure correction factor for the radial inflow was required to determine the overall pressure drop. This correction term considers that the flow is not a fully developed turbulent flow near the radial inflow area. Frictional pressure loss can only be accurately calculated for fully developed turbulent flow and when radial inflow is introduced, the flow field is under continuous development. It is not yet clear how this effects the frictional pressure losses.

Experiments similar to Su and Gudmundsson (1995) were performed by Schulkes and Utvik (1998) with the main difference being the size of the experimental set-up. These experiments were carried out to near actual production pipeline dimensions.

In 1998 Schulkes and Utvik studied pressure drop in a perforated pipe with radial inflow for single phase flows. They wanted to find out the effect radial flow had on the evolution of the pressure flow field inside the pipe. They decided that the total pressure loss could be broken down into components of friction and acceleration effects according to:

$$\left.\begin{aligned} \Delta Ptotal &= \Delta P_f + \Delta P_{acc} \\ \Delta Ptotal &= f\tfrac{L}{D}\tfrac{1}{2}\rho v^2 + \rho(v_1^2 - v_o^2) \end{aligned}\right\} \tag{2.4}$$

and that it would be affected by an correction factor which would come from the radial flow. The total pressure drop would be represented as:

$$\Delta P_{total} = \Delta P_f + \Delta P_{acc} + \Delta P_c \tag{2.5}$$

The experiments were setup according to Figure 2.3 and were carried out in a 15m long pipe with a diameter of 0.15m. The pipe contained 56 perforations 9 mm in diameter. Using experimentation, they discovered that depending on the volume flux ratio $\phi = (q/Q)$ of radial to axial flow, the outcomes were quite different.

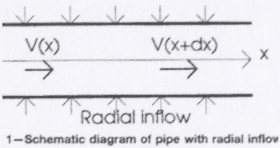

Figure 2.3: Schematic of Pipe with Radial Inflow (Schulkes & Utvik, 1998)

In this study Schulkes & Utvik (1998) were able to show that the correction term needed in the total pressure equation can be ±10% of the frictional pressure drop term and that it is highly dependant on the gemoetry in the system. They showed that for small flux ratios, the correction gives a negative contribution. In other words, the flow is lubricated by the radial flow. For large flux ratios, the correction term gives a negative contribution because it obstructs the pipe flow and therefore increases the pressure drop.

In 1999, Schulkes, Utvik, Rinde carried out experiments to determine the pressure loss for single phase pipe flow with radial inflow. Their aim was to establish a model to predict the pressure loss in such a system. The experiments were carried out with commercially available pipes used in oil production; the first was a perforated steel pipe and the second was a wire wrapped screen.

Schulkes et al. (1999) first conducted experiments without radial inflow to establish the friction factor for pipe flow. For these experiments a given axial flow volume, Q, was set and the radial volume, q, was increased in a stepwise manner. The main focus of these experiments was to modify the friction factor to include radial inflow effects. They found that radial inflow leads to a lower frictional pressure loss when compared to those computed for fully developed turbulent flow. This lead to including a correction term in the friction pressure loss in their model which accounted for the changes due to the radial inflow.

2.6 Smooth Wall and Rough Wall Piping

It is very important to investigate the effects of the wall roughness on pressure gradients in piping. Pressure gradient determination with smooth piping is important since it is less complex than if a roughness were introduced. Various correlations for hydraulically smooth pipe have been developed in the past by such people as Dodge and Metzner (1959), Bogue and Metzner (1963), Hall (1969), and Desouky and El-Emam (1990).

In most practical applications, the inside wall of a pipe is not hydraulically smooth. Under turbulent flow conditions, the wall roughness may have a noticeable effect on the pressure gradient due to friction. A pipe may be rough because of the nature of the material the pipe is constructed from or it may become rough over time due to erosion or corrosion of the material. Roughness can also be created artificially by attaching sand grains or small channels to the surface of the pipe walls (Govier & Aziz, 1972).

To fully describe roughness, one would need information about the geometry, including height, length, width, and shape of any protrusions as well as how they are dispersed. Since this is not often possible, roughness is usually measured in terms of the mean height of the protrusion. A relative roughness is defined as ϵ/D where ϵ is the mean height of the protrusion and D is the pipe diameter. This shows that the effect of roughness is due to dimensions relative to those of the pipe (Govier & Aziz, 1972).

Colebrook and White (1937) reported that a pipe may be viewed as perfectly smooth when $\frac{\rho V_\star k}{\mu}$ is less than 4 where ρ = fluid density (kg/m^3), $V_\star = \sqrt{\tau_o/\rho}$ and τ_o = shear stress at the wall, μ = fluid viscosity, and k = diameter of the roughness grains. They also reported that a pipe can be looked upon as completely rough when $\frac{\rho V_\star k}{\mu}$ exceeds 60. Between these two values, flow can be viewed as in the transitional state where both viscosity and grain size influence the flow.

For turbulent flow, wall roughness also depends on the Reynolds number as well as the effective roughness. A laminar sublayer exists and is in contact with the pipe wall. For high Reynolds numbers, this laminar sublayer is thin compared to the roughness of the wall, and therefore the roughness will be significant (Govier & Aziz, 1972).

In 1996, a series of experiments were carried out by Jayanti and Hewitt (1996) to investigate the response of flow to a step change in surface roughness in a cylindrical pipe. The change in roughness was introduced by joining a smooth pipe and a sand-roughened pipe having a roughness ratio of 55. Measurements were made in one and a half diameter increment lengths. The results of this experiment show that an abrupt change of wall roughness does affect the whole velocity field immediately. The flow becomes fully developed only after ten to fifteen diameters.

Other types of experiments were carried out in the past to investigate roughness. Instead of using rough pipes, roughness elements were added to the inside of the piping and the protrusion caused a disturbance in the flow. In 1997, a study was done by Siuru and Logan (1997) where the region of change between fully developed smooth and rough wall flows of air in circular tubes were investigated. In these experiments, the tubes were artificially roughened by equally spaced rectangular rings. Static pressure probes were used to measure the axial pressure drop and thus the friction factor for the section of pipe. One of the main findings from this experiment was that the longitudinal pressure gradient responded very quickly to a change in roughness and that it was not necessary to have a length of tube long enough to attain fully developed flow to determine the friction factors for a given roughness configuration (Siuru & Logan, 1977).

Work was also done by Su and Gudmundsson (1993) where perforations in a pipe acted as roughness elements. They investigated how perforation roughness affects the pressure drop in normal pipe flow. With no flow through the perforations, the roughness function was found to increase linearly with the perforation/casing diameter ratio. The authors were also able to obtain an empirical relationship for the friction factor in pipes with perforation roughness. They demonstrated that the roughness function depended only on the geometrical characteristics of the pipe and perforations.

Experiments were carried out to investigate the flow in a pipe following an abrupt increase in surface roughness by Logan and Jones (1963). They selected an eight inch diameter pipe because velocity profiles were known for smooth and rough pipes and the turbulence structure for smooth pipe had been determined. The rough portion of pipe was sand roughened and had a roughness ratio of radius to average grain size of 55. Air was used as the working fluid and the Reynolds number in the smooth pipe at the exit was 400,000 for all the data. It was found that for this Reynolds number, fully developed flow for the rough pipe was not attained for a length of 15 diameters. In the transition region of the rough pipe, velocity gradients and Reynolds stresses were higher than that for fully developed rough pipe flow.

Two-phase flow in rough pipes was studied by Chisholm and Laird (1958). They investigated pressure drop and saturation for air-water mixtures in smooth and rough tubes. Improvements in several two-phase flow correlations were presented. Approximate formulas were developed using these improvements correlated most of the data agreeing within $\pm$ 15% with a maximum of $\pm$ 25% of experimetal values were developed by the authors (Chisholm & Laird, 1958).

Chapter 3

Pressure Gradient Comparison Methods

3.1 Introduction

Flow through an annular channel can be modeled by computer simulation techniques. Many complex commercial software programs exist that can model the fluid interactions and complex mathematical equations behind the flows. Work has been carried out in the past involving single phase frictional pressure drops in a smooth concentric annulus. A paper by Jones and Leung (1981) entitled *An Improvement in the Calculation of Turbulent Friction in Concentric Annuli* discusses how to solve for pressure gradients using the effective diameter of piping instead of the hydraulic diameter, which is more commonly used. Only more recently has it been realized that the hydraulic diameter may not be sufficient to accurately describe the observed behavior.

Using the Java programming language, a short simulation program based on the equations presented in this paper was written (see APPENDIX A). The simulation program compares calculated pressure gradients using two different methods to express diameter. One method calculates the pressure gradient in an annular flow system using the hydraulic diameter, while the other uses the effective diameter in the calculations. The results were plotted to compare and contrast both methods.

Before the simulation program performs any calculations, the user must input the values for the outer radius (m), the inner radius (m), the fluid density (kg/m^3), the wall roughness, the fluid viscosity ($Pa{\cdot}s$), and start and end flow rates. The simulations were carried out for two extreme conditions, represented in Figure 3.1. In the first situation, the inner diameter is approaching the outer diameter ($b \rightarrow a$), while in the second situation, the inner diameter is approaching zero ($b \rightarrow 0$).

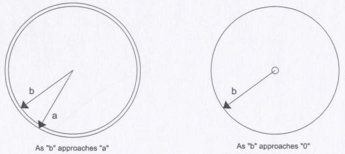

Figure 3.1: Visual Representation of Extreme Simulation Cases

3.2 Simulation Theory

Assume the following input parameters are known:

- outer radius, a
- inner radius, b
- fluid density, ρ
- fluid viscosity, μ
- wall roughness, ϵ
- flow rate, Q

The area of the annulus is:

$$A = \pi(a^2 - b^2) \tag{3.1}$$

and the perimeter of the annulus is:

$$P = 2\pi(a + b) \tag{3.2}$$

The hydraulic diameter is therefore:

$$\begin{aligned} D_h &= \frac{4A}{P} \\ &= \frac{4\pi(a+b)(a-b)}{2\pi(a+b)} \\ &= 2(a-b) \end{aligned} \tag{3.3}$$

For laminar flow, it has been proven (White, 1991) that the flow in a concentric annulus can be found from:

$$Q = \frac{\pi}{8\mu}\frac{dp}{dx}\left[a^4 - b^4 - \frac{(a^2 - b^2)^2}{ln(a/b)}\right] \tag{3.4}$$

The frictional pressure loss defined by Equation 3.5 can be substituted into Equation 3.4 to produce Equation 3.6:

$$\frac{dp}{dx} = \frac{f_{lam}\rho v^2}{2D_{eff}} \tag{3.5}$$

$$Q = \frac{\pi}{8\mu}\frac{f_{lam}\rho v^2}{2D_h}\left[a^4 - b^4 - \frac{(a^2-b^2)^2}{ln(a/b)}\right] \tag{3.6}$$

Solving Equation 3.6 for f_{lam} and substituting in the definition of flow rate, $Q = vA$, gives:

$$f_{lam} = \frac{16\mu D_h(a^2-b^2)}{\rho v\left[a^4 - b^4 - \frac{(a^2-b^2)^2}{ln(a/b)}\right]} \tag{3.7}$$

An equation has not yet been established to express the laminar friction factor required to determine the effective diameter. To find the pressure gradient for a concentric annulus, the frictional pressure gradient similar to Equation 3.5, given by Equation 3.8 is used.

$$\frac{dp}{dx} = \frac{f_2\rho v^2}{2D_{eff}} \tag{3.8}$$

From White (1991), the effective diameter is given by:

$$D_{eff} = \frac{64D_h}{f_{lam}Re_{lam}} \tag{3.9}$$

Equation 3.7 is solved for f_{lam} and from White (1991), Reynolds number is defined as:

$$Re_{lam} = \frac{\rho v D_{eff}}{\mu} \tag{3.10}$$

Using the Haaland friction factor defined by:

$$f_2 = 4\left[1.8\log\left(\frac{6.9}{Re_{D_{eff}}} + \left(\frac{\epsilon}{3.7D_{eff}}\right)\right)^{10/9}\right]^{-2} \tag{3.11}$$

for turbulent flow, the pressure gradient can now be obtained.

3.3 Simulation Results

3.3.1 When 'b' approaches Zero

Simulations were carried out as the inner diameter (b) of the annular channel approaches zero. In this case, the inner diameter becomes smaller and smaller and the flow approaches circular pipe flow. In examining the first scenario, it is observed that the size of the annular channel is essentially increasing.

By examining Figure 3.2 which shows the plots obtained from the simulations, it is observed that there is a significant difference in the two methods. The method of solving for the pressure gradient, which uses the effective diameter, gives a higher result than the method using the hydraulic diameter. We can also see that as the inner diameter gets closer and closer to zero, the difference in the two methods becomes smaller and smaller, as is expected.

Figure 3.3 shows a closer look at how both methods used to find the pressure gradient vary. The solid lines represent the simulations performed with a very small inner diameter when b=0.0005m. The dashed lines represent simulations carried out at a larger inner diameter when b=0.0127m. From this figure it is clearly seen that at b=0.0005m, the difference between both methods is much smaller than for the other case with b=0.0127m. From this it is inferred that if the simulations could be carried out with b=0, both methods would produce the same results for pressure gradient.

Another observation made from Figure 3.3 is that as the inner diameter becomes smaller and smaller, the pressure drop for both cases decreases but for the method using the effective diameter, it decreases at a faster rate than using the hydraulic diameter.

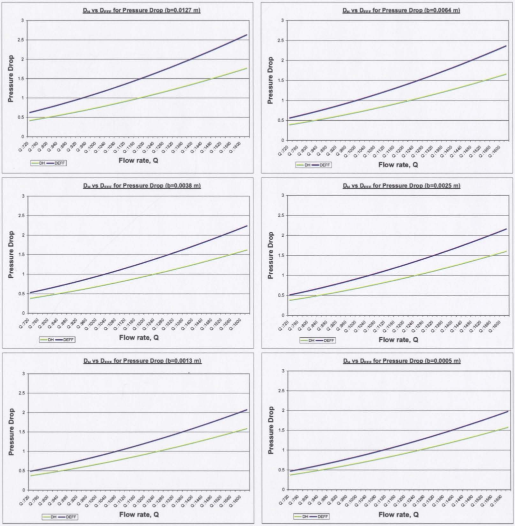

Figure 3.2: As 'b' approaches Zero

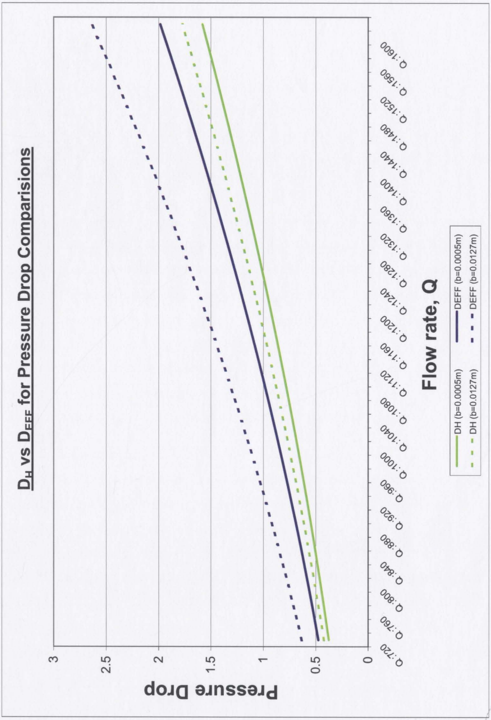

Figure 3.3: As 'b' approaches Zero - A Closer Look

3.3.2 When 'b' Approaches 'a'

In examining the second case where the inner diameter of the annular channel approaches the outer diameter, another very distinct result is observed. By carrying out experiments where the inner diameter of the annular channel becomes very close in value to the outer diameter, the annulus is becoming very small and approaching a solid circular pipe.

From Figure 3.4, it is evident that there is a significant difference in both methods. The method of solving for the pressure gradient which uses the effective diameter once again gives a higher result than the method using the hydraulic diameter. We can also see from Figure 3.4 that as the inner diameter gets closer to the outer diameter, the difference in the two methods becomes larger and larger. The fourth plot displayed in Figure 3.4 has a different scale on the y-axis than the other three. If this scale from the final plot was employed on the first three plots in this figure, the differences would not be clearly presented. It is evident that there is a much greater difference in the two methods in the fourth plot than there is in the third plot.

Figure 3.5 shows a closer look at how both methods used to find the pressure gradient vary as the inner diameter approached the outer. The solid lines represent the simulations performed with an inner diameter close to the size of the outer diameter when b=0.1460m. The dashed lines represent simulations carried out at a smaller inner diameter and a larger annular channel size when b=0.1270m. From this figure it is apparent that at b=0.1270m, the difference between both methods is much smaller than for the other case with b=0.1460m. From this it can be inferred that if the simulations could be carried out with b=a, the difference in both methods would continue to grow.

From Figure 3.5 it is observed that as the inner diameter becomes larger and larger for both cases, the pressure drop increases but for the method using the effective

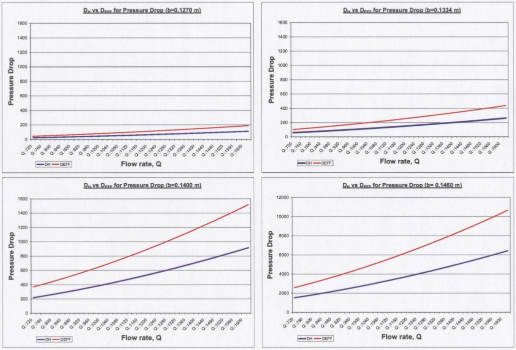

Figure 3.4: As 'b' Approaches 'a'

diameter, it increases at a faster rate than with the hydraulic diameter.

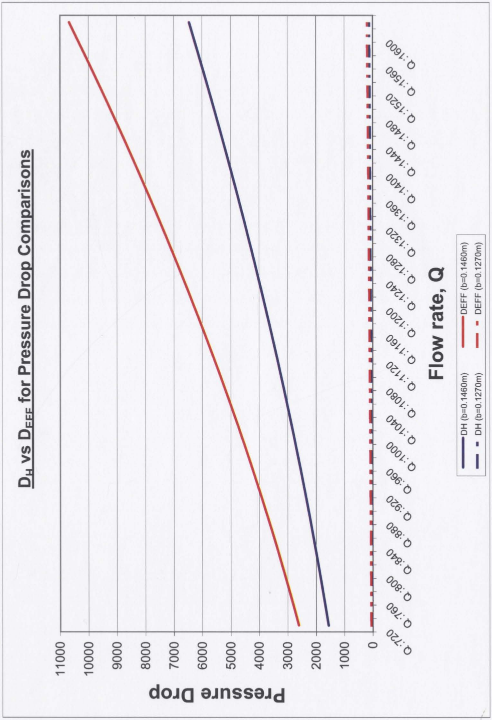

Figure 3.5: As 'b' approaches 'a' - A Closer Look

3.4 Conclusion

When the annular channel is very large and approaches circular open pipe flow, some general conclusions can be made. With small inner diameters, both methods produce similar results for pressure gradients. The outcome of the experiments may not be largely influenced if one were to use one method of describing the diameter over the other in such an instance.

If the annular channel is very small the diameter must be carefully defined. If the diameter is described using an effective diameter, much larger pressure drops will be obtained. Both methods are a legitimate way to define a diameter, but from these experiments it is concluded that if one is studying small annular channels the outcome of the experiment will be affected by the way in which the diameter is defined.

Chapter 4

Multiphase Flow Loop

4.1 Introduction

In 1997 a new multiphase flow loop was fabricated at Memorial University of Newfoundland in the Fluids Lab of the Engineering Building. Designed as an open loop re-circulating system (see Figure 4.1), it was initially used for hot film anemometry experiments with two-phase flow. The facility was designed to support the development of an electroquasistatic multiphase flow meter (MPFM) to measure the individual oil-water-gas flow rates of unprocessed oil well streams (MPFL, 1997).

To ensure proper phase mixing and allow the flow patterns to properly develop, the flow loop was built 65 meters long. It was constructed of three inch diameter schedule 40 PVC pipe. Clear horizontal and vertical test sections were incorporated throughout the system for flow visualization and long radius elbows were used to minimize flow disturbances. The pipe supports were carefully designed to minimize the influence of system vibrations. Instrumentation on the flow loop included several pressure and temperature transducers as well as flow meters located on each of the liquid and air lines. Electro-pneumatic control valves were installed on these lines to facilitate control of the flow conditions. Operational control of the loop was implemented through a fully integrated computer system, which also handled the data acquisition (MPFL, 1997).

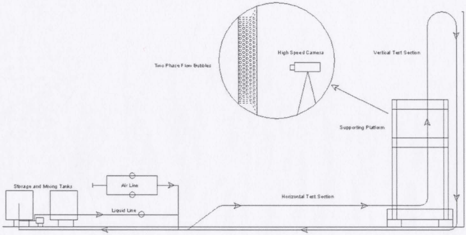

Figure 4.1: Original Multiphase Flow Loop

4.1.1 Air Line Components

The air lines, which are made from mild steel, branch into two components; a one inch line and a one-half inch line. Steel pipe was chosen as the preferred material to easily connect the air lines to the flow meters and other components. A one inch ball check valve is located on this line before the air and liquid lines meet and is used to prevent any liquid from entering the air line and its components.

The air used with the flow loop is supplied by the Fluids Laboratory. A one inch union and ball valve acts as a connection point allowing for a quick disconnection if necessary. A high pressure rubber hose is used to transfer the air from the main supply to the steel piping assembly.

4.1.2 Pressure and Temperature Transducers

All the pressure and temperature transducers in the multiphase flow loop were purchased from *Omega*. The pressure gradients were evaluated by measuring two pressures along a test sections with the PX603 series cable style transducers. Shown in Figure 4.2, these thin film transducers are compatible with both liquid and gas and are fitted with a one quarter inch male NPT fitting used for installation. For the liquid line the PX603-100G5V was used which is rated from 0 to 100 psi. Installed on the air line was the PX603-200G5V, which was rated for 0 to 200 psi. Both transducers produced a one to five volt signal read into the data acquisition system (Omega PX603, 2002).

Also shown in Figure 4.2 are the Pipe Plug Probe T-style thermocouples. They have a rugged 304 stainless steel design with a strain relief spring with a 1/4 NPT fitting. They produce a millivolt signal which must be gained before it can be read into the data acquisition system (Omega TC-NPT, 2002).

Figure 4.2: Pressure and Temperature Transducers from Omega

Fittings for both the steel air lines and the PVC liquid lines were needed to install the transducers. Tees with one quarter inch bushings were used to mount the transducers onto the steel air lines. To mount the transducers onto the PVC piping, single socket outlet *Clamp-it* saddles with an o-ring seal were purchased from *JJ Downs Industrial Plastics Inc.*, shown in Figure 4.3 (JJ Downs, 2004). The o-ring seal, located between the pipe and the clamp, prevented leaks from occurring at the point of contact.

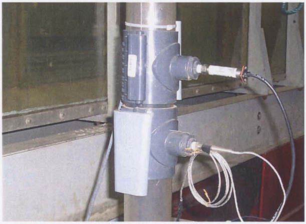

Figure 4.3: Pressure and Temperature Sensors with Clamp-on Saddles

4.1.3 Flow Control System

To properly manage the flow rates of each working fluid, electro-pneumatic control valves were installed on the liquid and air lines. A three inch valve controlled the liquid line flow rates and a one inch valve operated those of the air lines. A second three inch control valve was installed on the return line to allow control of the back pressure for the flow loop. Using this valve, the flow loop could be pressurized to 60 psia (MPFL, 1997)].

Separate flow meters were used to measure the rates of each of the fluids in the multiphase flow loop with each meter positioned on its respective line before the location where the fluids unite. An *Omega* FTB-730 turbine flow meter was installed to measure flow rates on the liquid line with a k-factor (pulses per gallon) of 10.14, as shown in Figure 4.4. This three inch flow meter measures between 3 and 400 gallons per minute (GPM). A PVC body was selected with 150 Class ANSI flanged ends that can be directly attached to the liquid line piping (Omega, FTB-730, 2002).

The air is separated from the liquid on the return line as it enters the mixing tank. Two separate flow meters are used on the air lines, an Omega FTB-931 on the one-half inch line and an Omega FTB-936 on the one inch line, shown in Figure 4.4. The FTB-931 and FTB-936 are economical ball bearing turbine flow meters with male NPT fittings suitable for use with gases with a minimum density of 0.025 lb/ft. They operate between 0.35 to 3.5 actual cubic feet per minute (ACFM) and 4.0 to 60.0 ACFM respectively. Valves were installed to direct the air through the desired meter based on the required flow. In addition, each flow meter has a signal conditioner attached to it which allows the signal to be properly read into the DAQ system (Omega FTB-930, 2002).

Figure 4.4: Flow Meters from Omega

4.1.4 Mixing Tanks and Separation Equipment

Included in the equipment for the flow loop are two large tanks. If two-phase liquid-liquid flow is required, oil and water can be premixed in a 750 liter mixing tank that will also hold them for recirculating the fluids through the flow loop. The second tank is a 630 liter transfer/settling tank used for separating fluids after they have been mixed. The two tanks are connected by piping with a 1.5 HP centrifugal pump that can transfer the fluids from one tank to the other if needed (MPFL, 1997).

4.1.5 Main Pump

The main pump used to pump the fluids from the mixing tank through the flow loop was a five horsepower, three inch centrifugal pump (see Figure 4.5) (MPFL, 1997). The pump's motor required three phase 230/460 VAC which was taken from one of the electrical panels in the fluids lab (Card, 2004).

This pump was salvaged from another project and originally incorporated into the flow loop to minimize cost. This pump could only be set in either the ON or OFF position and was therefore difficult to locate a desired speed. The only means for controlling flow was by opening and closing the pneumatic actuators manually.

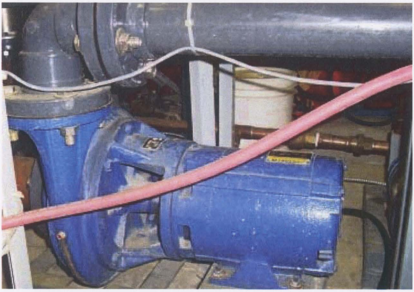

Figure 4.5: Original Flow Loop Pump

To ensure the pump's output does not exceed the pressure rating of the PVC piping, a 1.5 inch Jaybell pressure relief valve was added. If the pressure were to surpass the 100 psi rating, which is slightly lower than the 130 psi working pressure of the PVC piping, the valve would discharge the excess pressure and direct the fluid back to the mixing tank (Card, 2004).

4.1.6 Data Acquisition System

A fully integrated computer system was used to operate the multiphase flow loop. A data acquisition system was needed to accept input signals from the equipment in the flow loop such as the flow meters and pressure and temperature transducers. Signal conditioning, analog to digital conversion, and digital to analog conversions abilities were all necessary. Labtech Notebook Pro software was used to operate the data acquisition and control systems (MPFL, 1997).

4.1.7 MotionScope PCI High Speed Video System

The MotionScope PCI system included a camera head, a camera cable, and a full length PCI Controller board with appropriate software. The MotionScope High Speed Digital Imaging System can record a sequence of digital images of an event. A frame rate of 60 to 8000 frames per second can be used to record the data.

The system stores these images in an Image Memory on the Controller Unit. These images can be viewed forward or reverse at selected frame rates from 1 to 8000 frames per second. The motion can be analyzed frame-by-frame and by freeze framing. These AVI files can be saved as a complete sequence of events or if desired only the relevant part of the sequence can be saved.

4.2 Multiphase Flow Loop Upgrades

For the multiphase flow loop to return to operational status, many upgrades to the system were necessary. Until now, there had been limited upkeep on this facility and hence many pieces of equipment were either becoming obsolete, or were not functioning properly.

4.2.1 Main Pump and Inverter

With limited use, stagnant water in the system had caused rust to form and deposit on the flow loop's components and cloud the piping. The major contributor to the rust formation was the main pump, since it was not stainless steel. To correct this problem a 316 stainless steel pump, size 4 x 3 x 8, 5HP 460V 3 phase 1750rpm Goulds pump was purchased from *Electric Motor and Pump* to replace the original (see Figure 4.6) (Card, 2004).

Figure 4.6: New Flow Loop Pump

To compliment the new pump, a *TB Wood's* inverter was purchased and installed. The fluid flow through the system could now be controlled by this inverter instead of having to manually control the pump speed. This conserves energy, puts less strain on the pump, and provides more options for flow regimes, if desired.

4.2.2 Data Acquisition System

A new data acquisition system (DAQ) was designed and created using LabView 7.0. It has a friendly graphical user interface and allows the user to create input/output programs quickly without having to use many lines of programming code. The LabView program can interpret the input signals from all equipment. Included in the DAQ front screen are waveform plots for pressure, temperature, and flow, as can be seen in Figure 4.7. Numeric values are displayed in the top left hand corner of the screen for any active sensor inputs.

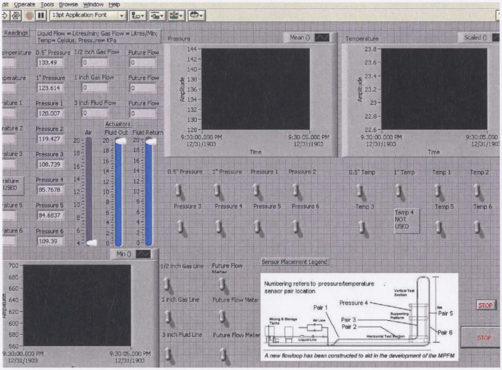

Figure 4.7: Lab View 7.0 Data Acquisition Screen

The new design of the DAQ system allows the user to control the amount of fluid entering and circulating through the system. Using sliders, the flow rates of both air and water can be controlled. To view the exact quantity of fluids passing through the flow loop, a display box for each of the gas flow and fluid flow was incorporated into the screen. Pressure and temperature measurements are also displayed for every sensor on the multiphase flow loop. The final component needed to carry out axial and radial inflow experiments was the control and display of the three radial inflow sections. On Figure 4.7, these components are labeled as FUTURE FLOW but were later renamed appropriately.

The updated DAQ program accepts input signals from the transducers and meters and outputs the signals to the control valves. The system was designed with a maximum of 30 inputs and 3-4 analog outputs. It also requires signal conditioning, analog to digital conversion, and digital to analog conversion. New equipment purchased to upgrade the DAQ system included two PCI cards and a 32 channel multiplexing card with built in Cold Junction Compensation and gain control for thermocouple inputs, all from *CyberResearch Inc.* (see Figure 4.8).

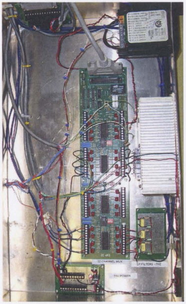

Figure 4.8: New Wiring Set-up for Data Acquisition

The analog signals from the pressure and temperature transducers and flow meters were multiplexed using two CYEXP 32 Mulitplexors. The multiplexor inputs the signals to the input card in the computer and performs signal conditioning functions that gains the input, which is needed to achieve a proper voltage input range.

The output from the flow meter also needed to be converted to a voltage signal. A rate meter, which takes the incoming pulse output from the flow meter and converts it to a current signal, was used to provide signal conditioning. At this point, the current now needs to be converted to a voltage. To accomplish this, a 250 ohm resistor was placed in parallel with the card resistor. The conditioned signals are then acquired by the computer using a CYDAS 8P PCI analog to digital conversion card. The analog output signals used to operate the control valves are provided by a PCICAD 08A output card (Card, 2004).

APPENDIX B describes the operation and maintenance procedures for the multiphase flow loop.

4.3 Addition of Annular Flow Capabilities

To incorporate annular flow into the multiphase flow loop, many changes were required. The vertical flow section was redesigned to replace a portion of the three inch diameter piping. The new design incorporated three test sections flanged together with the piping diameter increased to six inches to provide adequate space inside to create an annulus.

Two inch, three inch, four inch, and five inch diameter pipes were chosen to test in the experiments to give an array of annulus sizes. Clear acrylic piping was purchased from *G. E. Polymer Shades* to fabricate the new sections. To seal the inner pipes and make them watertight, each end was topped with a parabolic cap fabricated and installed by technical services in the engineering building. It was important to make sure everything was watertight since leaks could cause errors in the analysis due to inaccurate flow readings, or cause damage some of the equipment. To obtain the proper design length the inner piping required being joined together, which was also done by technical services. A sleeve was made to fit inside the piping and it was then sealed inside.

To hold the inner piping in place, holding rings were designed (see Figure 4.9). My design was given to technical services and the holding rings were fabricated from PVC on the CNC machine. Three rings were made for the two inch diameter piping as a prototype to determine their functionality.

With the testing of the holding ring prototype complete, it was decided that only two for each of the remaining inner piping sizes would be required. The main purpose of these holding rings is to hold the inner pipe in place and keep the annular spacing between the inner and outer pipes uniform without restricting the flow. Figure 4.10 shows that as the inner pipe diameter increases, the annular space decreases and the open annular spacing inside the holding rings correspondingly decreases. To limit the

Figure 4.9: Holding Ring Design and Assembly

total flow restrictions in the system, only two holding rings are used to hold the inner pipe in place.

Figure 4.10: Flow Spacings in Holding Rings

No holding rings were used for the five inch diameter piping because it was felt the flow would be too restricted. In place of these rings, on each end of the piping, four spacers made from acrylic were attached. These spacers held the piping in place without placing too much restriction on the flow.

The final consideration in designing and fabricating the annular section of the multiphase flow loop was to make sure there was adequate space between the ends of the inner pipe and the flanged pieces so the fluid could easily flow up from the three inch diameter piping into the annulus and then out again on the top end. Each piece of inner piping was fabricated to a total length of 95 inches to give adequate space for the flow to enter and leave the annulus.

4.4 Addition of Radial Inflow Capabilities

To test radial inflow scenarios, many design changes to the multiphase flow loop were carried out. Three sections in series were designed to simulate rock layers in a reservoir with different permeabilities the layers may have. It was more feasible with less risk of damage to the materials to design for an average radial inflow value and only drill one hole in the pipe, rather than perforate the acrylic piping multiple times. A flow meter and ball valve to monitor and control the flow was installed on each of the inflow test sections.

To run experiments with radial inflow only, the original flow loop design was modified to no longer allow flow to enter from the bottom of the vertical test section. The lower end of this section was detached and the bottom was plugged so that fluid could only enter the annular channel through any of the three radial inflow sections.

The vertical, annular section now required additional support since it was disconnected from the flow loop and no longer being supported from below. A support made from three inch PVC piping with a flange on its end was fabricated and installed to allow the annular section to rest upon the flange and be supported by the floor of the Fluids Lab. A second method used to support the annular section was with a bracket made by the welding shop in the technical services department which was attached to the platform floor. This bracket is adjustable to accommodate the six inch piping and the three inch piping originally part of the multiphase flow loop.

In building the radial inflow section, flexible Tygon tubing was used since it was more feasible and allowed the radial inflow section to be assembled easier than if PVC piping were used. The size of the tubing was determined by the size of the end connection of the flow meters purchased for use on the radial inflow lines. I was able to determine that a $1\frac{1}{4}$ inch diameter tubing would fit the connections and would also be a common size to make finding fittings for the tubing easier.

From the horizontal section, a 3 inch to $1\frac{1}{4}$ inch reducer was purchased and installed to allow for flow into the tubing. The tubing was secured onto the reducing joint with a hose barb. From here, the flow split into three separate streams, each stream entering a different test section. The flow was split using two T-joints and a 90 degree elbow (see Figure 4.11).

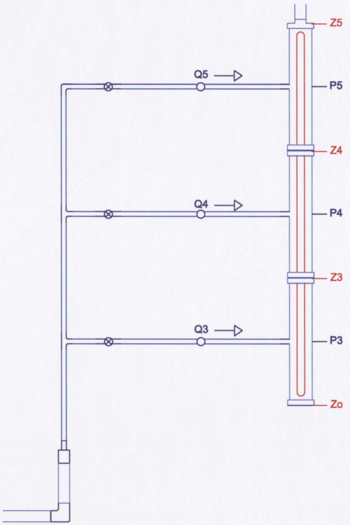

Figure 4.11: Radial Flow Setup

From these joints, the flow entered a short six inch length of tubing and then into a ball valve, which controlled the flow into each section. The tubing was secured onto the valves using hose clamps. Next, as the fluid leaves the valves it enters another length of tubing 20 inches long, which is an adequate length for flow development. It then enters a flow meter where the flow rate is monitored. The tubing is once again secured to each flow meter with hose barbs on both ends. The flow meters were incorporated into the data acquisition program so the user can determine the amount of fluid entering each of the test sections.

When the flow leaves each flow meter, it enters another section of tubing 20 inches long again. Holes were drilled and tapped in the outside of the annular piping and the tubing was connected to hose barbs screwed into these holes. Technical Services drilled and tapped these holes into the outer six inch section and through the clamp on saddles for added security.

On the side of the outer pipe opposite from the point where the flow enters the piping, a pressure transducer purchased from *Omega* is located which will measure the pressure at that point in each section. Each transducer is attached to the flow loop clamp-on saddles purchased from *JJ Downs Limited* in the same manner as the others.

With all of the equipment installed, it then had to be wired and programmed into LabView 7.0 for data acquisition. The pressure sensors were reconfigured and calibrated. The two pressure sensors previously located on the downward vertical section were disconnected from Labview since these pressure readings were not needed for these experiments. In their places on the DAQ board were two new sensors located on the middle and top sections of the annular test section. The pressure sensors were then re-configured in Labview and listed in sequential order (see Figure 4.12). A voltage signal was read from the pressure sensors and through Labview, this voltage was converted into a kilopascal output and displayed onto the Labview screen.

The three newly added flow meters were programmed into Labview. A voltage signal

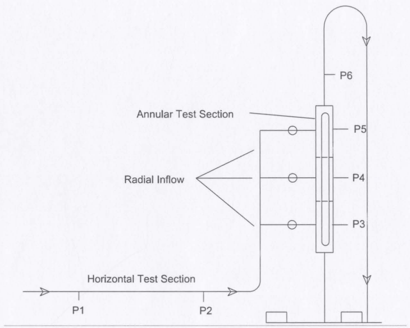

Figure 4.12: New Pressure Sensor Configuration

was read from each meter which was converted into a flow reading. The calibration equations obtained from the flow meters were entered into Labview and from there the flow rate was displayed in gallons/second. A conversion was then performed to display the flow rate in liters per minute for each of the new flow meters.

Chapter 5

Benchmarking Experiments

5.1 Benchmarking of Circular Pipe Flow

The precision of a piece of equipment denotes how well it can reproduce a certain reading with a given accuracy (Holdman, 2001). To ensure the multiphase flow loop would produce precise and reliable data, benchmarking experiments were carried out with axial flow through a circular pipe. This type of experiment has been done in the past with well documented results. The data collected during experimentation was analyzed to determine the friction factors for the circular pipe flow. These experiments are necessary to establish if reliable results could be obtained from the flow loop. By carrying out well documented experiments, it can be shown whether or not the data collected from the multiphase flow loop compared well with published theoretical data.

For all benchmarking tests, single phase experiments were carried out with water used as the working fluid. Three sets of data were collected in three inch diameter schedule 40 PVC piping at different times to show repeatability of the results. For each set of experiments the flow rates varied from a minimum of approximately 10 liters per minute to a maximum of approximately 1000 liters per minute. When exact flow rates could not be duplicated, values were chosen as close to the previous flow rate as possible and recorded as such.

The pump speed was modified for some experiments to obtain flow rates outside the normal bounds of the pump operating at 60 Hz. I chose to alter the pump speed by $\pm$ 15 Hz because the pump could still be operated safely at the highest speed. It is not recommended to run the pump any higher than 75 Hz for fear of causing any damage to it. At the lower pump speed of 45 Hz, the maximum flow rate that could be reached was approximately 750 liters per minute. At the highest pump speed of 75 Hz, a top flow rate of approximately 1200 liters per minute was obtained and at this speed focus was placed on recording data for flow rates that could not be obtained at 60 Hz, therefore a full test matrix of experiments was not carried out.

5.1.1 Experimental Procedures

For each set of experiments carried out in the laboratory, I created a test matrix to be followed. Each text matrix detailed various pump operation speeds for which a series of flow rates were tested. The test matrix for the first set of benchmarking experiments is displayed in Table 5.1. For all experiments carried out, more than one trail of data was collected to ensure repeatability.

Table 5.1: Circular Pipe Flow - Trial 1

Pump Speed	*Flow Rate (LPM)*					
60 HZ	1020	850	550	350	130	20
45 HZ	770	690	500	240	110	12

The first test matrix was followed as closely as possible for the second set of benchmarking experiments with some minor alterations. For each pump speed tested, additional flow rates were added to obtain more data points on the friction factor verses Reynolds number plots that would later be generated. The addition of the extra data points would help to show the data trends more clearly. The second test matrix used is displayed in Table 5.2.

Table 5.2: Circular Pipe Flow - Trial 2

Pump Speed	*Flow Rate (LPM)*							
60 HZ	1000	950	850	550	350	230	115	45	7
45 HZ	750	690	530	250	125	43	10		

The text matrix followed for the third set of benchmarking experiments is slightly different in make up than the previous two shown in Table 5.1 and Table 5.2. Instead of running the experiments at the pump speed of 45 Hz, a higher speed of 75 Hz was now tested. Preliminary analysis and plotting did show that an adequate amount of data at 45 Hz had been obtained. For the third trial of benchmarking experiments, the pump was set to 75 Hz to obtain flow rates beyond 1000 liters per minute which would produce points on the friction factor verses Reynolds number plot beyond the range of data previously collected. For the 60 Hz tests, flow rates were not chosen to correspond with the previous experiments, but instead values were selected between those already chosen to collect new data points to fall on different places on the plot. The third test matrix displayed in Table 5.3:

Table 5.3: Circular Pipe Flow - Trial 3

Pump Speed	*Flow Rate (LPM)*						
75 HZ	1200	1125	1030	875			
60 HZ	950	870	780	630	410	290	120

5.1.2 Experimental Analysis

Calculations were performed on the data collected to determine their associated friction factors. In these calculations, the Fanning friction factor was found instead of the Darcy friction factor where $f_{Darcy} = 4f_{Fanning}$ (Hodge & Taylor, 1999).

The Bernoulli equation is very widely used and is probably used more often in fluid flow applications than any other equation. This equation assumes inviscid flow, steady flow, flow along a streamline, constant density, and an inertial reference frame. The Bernoulli equation can be used with external flows around objects submerged in fluids, with internal flows over relatively short distances, and with flow from a plenum (Potter & Wiggert, 1997).

The Bernoulli equation expresses the conservation of the sum of pressure, kinetic, and potential energy according to Equation 5.1.

$$\frac{1}{\rho}\int_1^2 dP + \frac{1}{g}\int_1^2 v dv + \int_1^2 dz = 0 \tag{5.1}$$

Integrating Equation 5.1 knowing that the flow is incompressible gives Equation 5.2, known as the Bernoulli equation.

$$P + \frac{1}{2}\rho v^2 + \rho g z = Const \tag{5.2}$$

The first term in Equation 5.2 represents the pressure head, the second term represents the velocity head, and the final term represents the static head differences. The constant of integration is called the Bernoulli constant and relies heavily on steady, frictionless, incompressible flow (Hodge & Taylor, 1999).

The Bernoulli equation cannot be used when general losses in the system are to be accounted for. An equation derived from the conservation of energy formula can be used for such situations. The conservation of energy equation used is shown in Equation 5.3 (Hodge & Taylor, 1999).

$$\frac{\delta q}{\delta t} - \frac{\delta W_s}{\delta t} = \frac{\delta}{\delta t}\int_{CV} \rho e d\mathcal{V} + \int_{CS}\left(e + \frac{P}{\rho}\right)\rho\overline{V}\cdot d\overline{A} \tag{5.3}$$

Considering the specific total energy, e, to be made up of the specific internal energy, the potential energy, and the kinetic energy, in the absence of heat transfer the energy equation becomes Equation 5.4 (Hodge & Taylor, 1999).

$$dW_s + \frac{dP}{\rho} + VdV + gdz = d(losses) = 0 \tag{5.4}$$

Integrating Equation 5.4, gives Equation 5.5 (Hodge & Taylor, 1999).

$$\frac{P_1}{\gamma} + \frac{{V_1}^2}{2g} + z_1 = \frac{P_2}{\gamma} + \frac{{V_2}^2}{2g} + z_2 + \frac{W_s}{g} + losses \tag{5.5}$$

The total pressure losses in a system are comprised of both major and minor losses. Major losses are associated with pipe wall friction over the entire length of a pipe (Hodge & Taylor, 1999). Pressure losses due to friction is a major contributor that effects flow. Frictional pressure loss can be calculated according to the Darcy-Weisbach equation for the frictional pressure drop in pipes (shown in Equation 5.6).

$$\frac{dP}{dx} = \frac{f\rho v^2}{2D} \tag{5.6}$$

Incorporating the Fanning friction factor into Equation 5.6 gives:

$$\frac{dP}{dx} = \frac{4f_f\rho v^2}{2D} \tag{5.7}$$

For laminar flow the friction factor is only a function of the Reynolds number, shown in Equation 5.8, but for turbulent flow it may depend on both the Reynolds number and the relative roughness of the pipe ([Economides et al., 1994).

$$f_f = \frac{16}{Re_D} \tag{5.8}$$

Rearranging and integrating Equation 5.7 gives:

$$\Delta P_f = f_f \frac{2L}{D} \rho v^2 \tag{5.9}$$

where: ΔP_f = frictional pressure gradient (Pa)

f_f = Fanning friction factor

L = pipe length (m)

D = pipe diameter (m)

ρ = fluid density (kg/m^3)

v = fluid velocity (m/s)

To determine the friction factor in the test section under consideration, calculations were carried out between the second pressure transducer P_2 and last pressure transducer P_6, as shown in Figure 5.1.

P_2 is located on the horizontal test section just before a 90^o long radius bend which turns the piping vertically upward. There are two more bends located inside the test section as can be seen in Figure 5.1. The second 90^o bend turns the piping horizontal at the highest point in the system and the third such bend turns the piping vertically downward. P_6 is the last pressure transducer the fluid must pass through before being re-circulated back through the system. It is located approximately 1.07 meters above the horizontal test section.

Applying Equation 5.5 directly to this test section, the equation becomes:

$$\left.\begin{aligned} \frac{P_2}{\gamma} + \frac{V_2{}^2}{2g} + z_2 &= \frac{P_6}{\gamma} + \frac{V_6{}^2}{2g} + z_6 + \Delta P_{loss} \\ P_2 + \frac{V_2{}^2\rho}{2} + (\rho g z_2) &= P_6 + \frac{V_6{}^2\rho}{2} + (\rho g z_6) + \Delta P_{loss} \end{aligned}\right\} \tag{5.10}$$

Equation 5.10 can be simplified since the datum is located at z_2 and is therefore

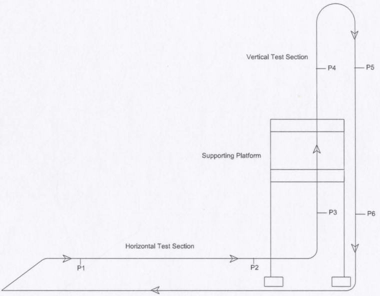

Figure 5.1: Location of Pressure Transducers for Circular Pipe Flow

zero. Hence, the value of z_6 is the vertical distance above z_2 from zero. Since the entire multiphase flow loop was comprised of only three inch nominal diameter piping and there is no other source of inflow besides the main mixing tank, the flow rate and hence the flow speed remains constant throughout the entire flow loop. For this reason, $v_2 = v_6 = Q/A$ or $v_2 - v_6 = 0$. Equation 5.10 becomes:

$$\Delta P_{26} + (\rho g \Delta z_{26}) = \Delta P_{loss} \tag{5.11}$$

In calculating the friction factor for the section of piping specified, minor losses need to be considered. Minor losses exist when fluid flows through fittings, valves, and process equipment and are not necessarily smaller than major losses (Hodge & Taylor, 1999). Each of the three 90^o bends has an associated pressure loss with a corresponding k-value. A value of 0.22 can be used as the k-value for a long radius 90^o bend (Western

Dynamics, 2004) where :

$$\Delta P_{loss} = \frac{1}{2} K_E \rho v^2 \tag{5.12}$$

The system also experiences major losses in the form of frictional pressure in the piping. This frictional pressure loss can be calculated according to Equation 5.9. Considering both the minor losses and major losses in the piping and using Equation 5.10, the experimental friction factor can be calculated according to Equation 5.13:

$$f_{exp} = \frac{(\Delta P_{16} + \rho g \Delta z_{16} - (\frac{3K_E \rho v^2}{2}))D_h}{2L_T \rho v^2} \tag{5.13}$$

where: D_h = hydraulic diameter of annulus (m)

ΔP_{16}= pressure difference from P_1 to P_6 (Pa)

g = gravitational constant (9.81 m/s^2)

Δz_{16} = vertical distance from z_1 to z_6 (m)

L_T = total length of section (m)

ρ = fluid density (kg/m^3)

v = fluid velocity (m/s)

This is the equation used to analyze the data collected during experimentation and to determine the friction factors for the various flow rates in these benchmarking experiments.

5.1.3 Theoretical Analysis

To determine the theoretical friction factor values, an equation which describes the same conditions is used. For turbulent flow and considering the Fanning friction factor, the following formula developed by Paul H. R. Blasius (1873-1970) was used (Equation 5.14):

$$f_{theory} = \frac{0.0791}{\sqrt[4]{Re}} \tag{5.14}$$

If one were use the Darcy friction factor the above equation would become $f_{theory} = \frac{0.3164}{\sqrt[4]{Re}}$, since the friction factor would be multiplied by a factor of four. The Blasius equation which was founded in 1913, is entirely empirical and fits reliable data acquired in the past to a good degree of accuracy. It can be used for steady state, turbulent flows in pipes of varying shapes (Govier & Aziz, 1972).

The Reynolds number must be determined before the friction factors can be calculated. Reynolds number is based on the flow rate (which was set in each of the experiments), the diameter of the pipe, and the viscosity of the working fluid. The fluid speed was determined from the flow rate and used in calculating the Reynolds number according to Equation 5.15:

$$Re = \frac{\rho v D}{\mu} \tag{5.15}$$

Knowing that water was used as the working fluid in these experiments, the density and viscosity are therefore known values. The dimensions of the piping in the flow loop are also known and hence the Reynolds number can be calculated. With the Reynolds numbers found, the theoretical friction factors are then be calculated according to Equation 5.14. With both an experimental and a theoretical friction factor obtained for the same set of parameters, both could be compared. If they were to agree within an acceptable percentage of error, it can be concluded that the multiphase flow loop can be used for determining pressure differentials for fluid flows.

5.1.4 Results

The friction factors were determined for each experiment set forth in the test matrices depicted in Section 5.1.1. These friction factors were plotted against Reynolds number as shown in Figure 5.2. For calculation details of the analysis, see Appendix C.

In addition using the Blasius equation, the Swamee and Jain and Churchill equations were also used to determine theoretical friction factors. The Swamee and Jain equation provides an explicit method to calculate friction factors for turbulent flow as shown in Equation 5.16 (Hodge & Taylor, 1999).

$$f = \frac{0.0625}{\left[log\left(\frac{\epsilon}{3.7D} + \frac{5.74}{Re^{0.9}}\right)\right]^2} \tag{5.16}$$

A single expression that represents the friction factor for laminar, turbulent, and transitional flows was devised by Churchill. This explicit expression can be solved if Reynolds number and relative roughness are known and is advantageous since the friction factor in the transition region is a continuous function which smoothly links the laminar and turbulent flow regions. The Churchill equation used is shown in Equation 5.17 (Hodge & Taylor, 1999).

$$\left.\begin{aligned} f &= 2[(\frac{8}{Re_{Dh}})^{12} + (\frac{1}{(A+B)^{(3/2)}})]^{(1/12)} \\ A &= (2.457\ln[\frac{1}{(\frac{7}{Re_{Dh}})^{0.9}}]^{16} \\ B &= (\frac{37530}{Re_{Dh}})^{16} \end{aligned}\right\} \tag{5.17}$$

The Haaland equation shown in Equation 5.18 is valid for $\epsilon/D > 10^{-4}$ for turbulent flow, considering the Darcy friction factor (Hodge & Taylor, 1999).

$$f = \frac{0.3086}{\left\{\log\left[\frac{6.9}{Re} + \left(\frac{\epsilon}{3.7D}\right)^{1.11}\right]\right\}^2} \tag{5.18}$$

Incorporating the Fanning friction factor into Equation 5.18 gives:

$$f = \frac{0.07715}{\left\{\log\left[\frac{6.9}{Re} + \left(\frac{\epsilon}{3.7D}\right)^{1.11}\right]\right\}^2} \tag{5.19}$$

For other turbulent flow situations where ϵ/D is very small, as in the case for smooth pipe flow, Equation 5.20 can be used (Hodge & Taylor, 1999).

$$f = \frac{0.07715n^2}{\left\{log\left[\frac{7.7}{Re} + \left(\frac{\epsilon}{3.7D}\right)^{1.11n}\right]\right\}^2} \tag{5.20}$$

Equation 5.20 was used to plot the friction factor verses Reynolds number curves as described by Haaland on Figure 5.2.

All three equations were plotted together on Figure 5.2 and error bars with a range of $\pm 15\%$ were depicted for the Blasuis and Haaland equations. The Blasuis equation gives the lowest values of friction factors while the Haaland equation gives the highest. Any data point that falls within either the range from the Blasius equation, the range from the Haaland equation, or anywhere in between is said to have good agreement with proven theory.

By examining Figure 5.3 it was observed that overall the experimental solutions compared quite well with theoretical results. Trendlines for each of the data sets were plotted against the Blasuis equation in Figure 5.3. The trendline for trial 1 data, depicted in blue, closely follows the curve set forth by the Blasius equation within approximately $\pm$ 5% to $\pm$ 7%. The trendline for trial 2 data, shown in red, agrees within approximately $\pm$ 9% to $\pm$ 16%. This curve does not follow the Blasuis

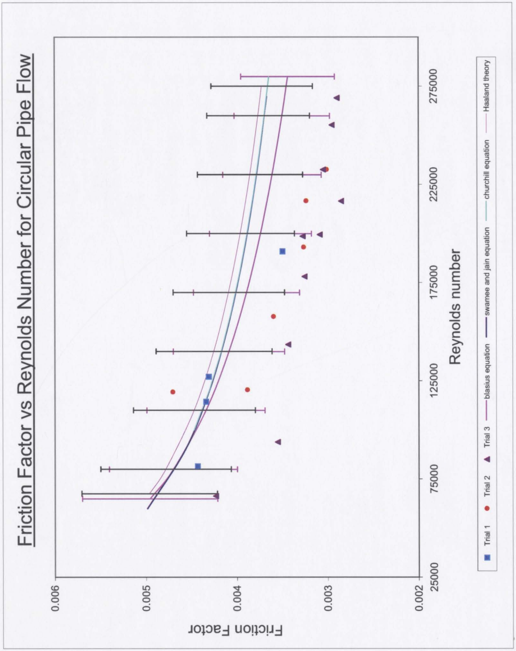

Figure 5.2: Benchmarking Results for Circular Pipe Flow

findings as closely as those from trial 1, but does follow the data trend within a reasonable range. The trendline for trial 3 results, shown in purple, lies just outside the $\pm$ 15% range but still follows the curve set forth by Blasius in a steady manner. These experimental results show the multiphase flow loop to be a system that can provide reliable results for fluid flow investigations.

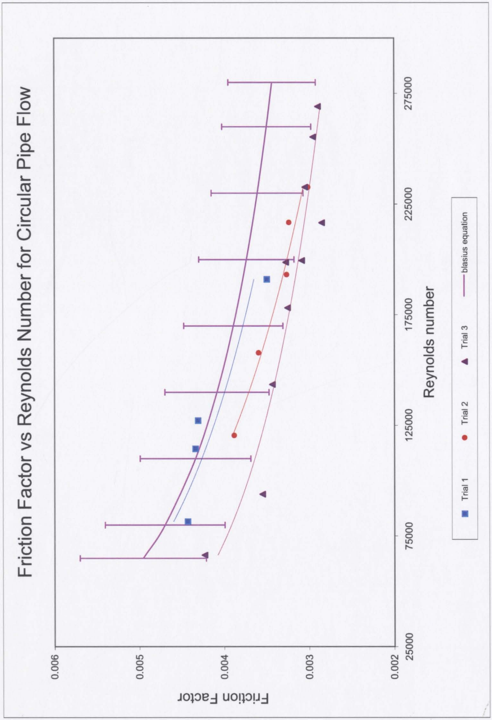

Figure 5.3: Benchmarking Results for Circular Pipe Flow

5.2 Benchmarking of Annular Pipe Flow

In addition to the circular pipe flow benchmarking experiments, some simple annular flow experiments were carried out to ensure the new flow meters purchased and installed on the radial sections of the annulus were in working order. This testing was necessary to be sure these flow meters would give reliable measurements.

5.2.1 Experimental Procedures

A series of experiments with varying flow rates were carried out to determine if the multiphase flow loop would produce predictable results which would follow expected trends. Three pump speeds were used and for each speed a different sequence of valves on the radial inflow lines were open, as shown in Table 5.4, with the X's representing the open valve during each experiment. The location of the valves on the test section is shown in Figure 5.4. By varying the pump speed, it was investigated whether the results were as accurate for the higher flow rates as they were for the lower rates.

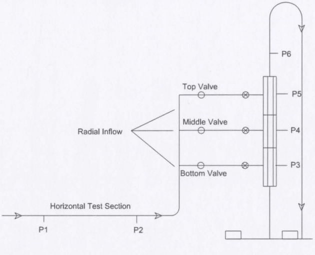

Figure 5.4: Location of Valves on Radial Inflow Section

Table 5.4: Radial Flow Benchmarking Tests

	30 Hz				*45 Hz*				*60 Hz*			
Top Valve	X			X	X			X	X			X
Middle Valve		X		X		X		X		X		X
Bottom Valve			X	X			X	X			X	X

5.2.2 Results

The data collected from the experiments conducted according to the test matrix in the above section can be seen in Table 5.5.

Table 5.5: Annular Flow Benchmarking Results

	Radial Flow Rates			**Bulk Flow Rate**
Pump Speed	*Bottom Inflow*	*Middle Inflow*	*Top Inflow*	
30 Hz			71.27 LPM	73.32 LPM
30 Hz		108.26 LPM		115.10 LPM
30 Hz	112.09 LPM			117.86 LPM
30 Hz	58.79 LPM	78.14 LPM	53.03 LPM	189.96 LPM
60 Hz			153.37 LPM	149.80 LPM
60 Hz		222.25 LPM		234.05 LPM
60 Hz	208.74 LPM			219.48 LPM
60 Hz	140.86 LPM	159.94 LPM	102.85 LPM	396.71 LPM
75 Hz			190.54 LPM	184.19 LPM
75 Hz		222.25 LPM		264.84 LPM
75 Hz	maxed out			289.74 LPM
75 Hz	150.98 LPM	204.28 LPM	136.22 LPM	498.44 LPM

The total radial inflow for each experiment was calculated and compared with the bulk total flow rate measured in a different section of the flow loop. The error percentage between the radial inflow meters and the bulk flow meter was calculated with results shown in Table 5.6.

From Table 5.6 it is clear that as each valve is opened individually, the flow rates measured by the bulk flow meter agree quite well with the ball bearing liquid turbine flow

Table 5.6: Error Results

Valve Opened	*Pump Speed*	*Radial Inflow Total*	*Bulk Flow Total*	*Percent Error*
Top Valve	30 Hz	71.27 LPM	73.32 LPM	2.79%
Middle Valve	30 Hz	108.26 LPM	115.10 LPM	5.94%
Bottom Valve	30 Hz	112.09 LPM	117.86 LPM	4.89%
All Valves	30 Hz	189.96 LPM	199.62 LPM	4.84%
Top Valve	60 Hz	153.37 LPM	149.80 LPM	2.38%
Middle Valve	60 Hz	222.25 LPM	234.05 LPM	5.04%
Bottom Valve	60 Hz	208.74 LPM	219.48 LPM	4.89%
All Valves	60 Hz	403.66 LPM	396.71 LPM	1.75%
Top Valve	75 Hz	190.54 LPM	184.19 LPM	3.45%
Middle Valve	75 Hz	222.25 LPM	264.84 LPM	16.08%
Bottom Valve	75 Hz	208.74 LPM	289.74 LPM	27.96%
All Valves	75 Hz	491.48 LPM	498.44 LPM	1.40%

meters on the radial inflow sections. Generally, all measured values are in agreement within plus or minus six percent, except for two instances with the pump operating at 75 Hz. In both cases, the flow meter in question had reached its maximum flow rate. The main bulk turbine flow meter is rated for 3-400 gallons per minute (GPM) while the three ball bearing liquid turbine flow meters located on the radial inflow section are only rated for 4-60 GPM (Omega FTB-930, 2002). If the flow were to exceed 60 GPM, the ball bearing liquid turbine flow meters would not accurately convey the proper flow rates.

It was also observed that the bottom inflow section incurs a higher flow through it than the middle and top sections. As the height increases on the vertical test section, the flow measured at each inflow section is decreasing. This is quite logical because as the height increases, there is more resistance acting on the flow and this resistance leads to a lower measured flow rate. For this reason, the flow rates observed follow expected trends.

It has been shown that the new ball bearing liquid turbine flow meters do compare quite well with the main bulk meter which has also been shown to produce reliable results. It can therefore be concluded that the new flow meters will give reliable results and can therefore be used in experiments using the multiphase flow loop.

Chapter 6

Radial Inflow Through an Annular Channel

6.1 Experimental Set-up

The radial inflow section of the multiphase flow loop was fabricated and assembled as described in Chapter 4. Figure 6.1 shows the actual equipment as it was assembled in the laboratory. The bottom and middle inflow section are easily depicted, with the top section hidden slightly behind the floor of the platform. In this photograph, the two inch diameter inner pipe is installed with water flowing through the multiphase flow loop. The water flows up into the tubing from the PVC piping where it then splits into the sections of tubing with a ball valve in the open position. In this picture, the ball valves are slightly visible from their location just right of the platform leg.

The hydraulic diameter of the annulus and radial fluid inflow rate through the system are the main variables investigated during these experiments. The hydraulic diameter can be best defined as the cross sectional area divided by the whetted perimeter of the pipe multiplied by four, or $D_h = 4A/P$. The hydraulic diameter is an approximation that is more accurate for turbulent flows than for laminar. The hydraulic diameter theory for eccentric annuli often fails because the eccentricity affects the losses in the piping and the hydraulic diameter does not vary with respect to eccentricity [Hodge and Taylor (1999)].

Figure 6.1: Radial Inflow Setup

For the radial inflow experiments, two pump speeds were used during data collection with various flow rates set at each pump speed. To obtain different sizes for the hydraulic diameter of the annulus the inner piping was changed while the outer pipe remained constant. For every pump speed each of the top, middle, and bottom valves were opened and closed in various sequences and combinations as shown in Table 6.1, with each column representing a new experiment.

The experiments in the test matrix presented in Table 6.1 were carried out for three

Table 6.1: Radial Inflow Test Matrix

	Valve Opened						
Top Valve	X			X		X	X
Middle Valve		X		X	X		X
Bottom Valve			X		X	X	X

sizes of clear acrylic inner piping which was purchased from *GE Polymer Shades.* The piping was fabricated to incorporate parabolic end caps required to prevent fluid from entering inside the inner pipe. To obtain the desired total length of 2.42 meters, two sections of pipe were joined using a sleeve seated inside the piping. This work was performed by the Technical Services Group located in Memorial University of Newfoundland's Engineering building.

The first inner piping size tested with radial flow was the nominal two inch diameter piping which produced the largest flow area in the annulus. The next size was a nominal three inch diameter piping, which gave an intermediate sized flow area. The last size inner to be tested with radial flow was a nominal four inch diameter piping. This gave the smallest flow area in the annulus and therefore the highest pressure readings.

6.2 Investigating Pressures and Flow Rates as a Function of Position

6.2.1 Experiments with a 2" ID Annular Channel

To demonstrate the behaviour of the fluid, the pressures in the annulus and their corresponding flow rates were plotted against position for each of the annular channel sizes. The flow rates were measured at each of the radial inflow meters and the total flows through the system were summed accordingly. For the case with the nominal two inch inner diameter pipe, the results are shown in Figure 6.2.

Although the data trends can be seen, Figure 6.2 may be unclear and somewhat confusing. To more clearly show the behaviour of the fluid, Figure 6.3 includes only the results where all three ball valves on the radial inflow sections were open.

For all other experimental plots and analysis, see Appendix D.

The pink lines in Figure 6.3 represent experiments when the pump was set to 40 Hz and the blue lines represent those with the pump set at 75 Hz. The two lines increasing from left to right denote flow rate as a function of position, or the height at which the data point was collected.

The first point on these lines is located at a position of 0.43 meters above the base of the test section. At this position, the bottom radial inflow section is positioned and the fluid flowing through here will enter the annulus. The second data point is located 1.29 meters above the base of the test section and 0.86 meters above the first point. This point denotes the middle radial inflow section and any fluid in this section will enter the annulus at this location. The third data point on these lines is found at 2.15 meters above the base of the test section. Each radial inflow section was designed to be symmetric, therefore the distance between each inflow section is 0.86 meters. The third point on Figure 6.3 is 0.86 meters above the second point.

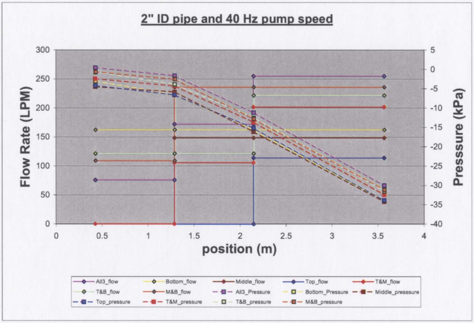

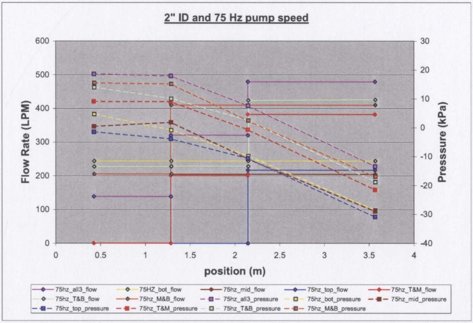

Figure 6.2: Pressure and Flow Rate as a Function of Position in a 2" ID Annular Channel

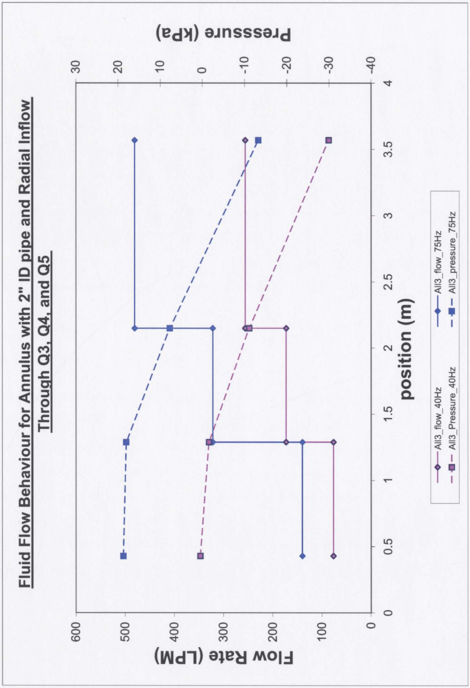

Figure 6.3: Pressure and Flow Rate as a Function of Position in a 2" ID Annular Channel

This is the last data point inside the annulus.

The final point on the curves in Figure 6.3 is located 3.57 meters above the last point in the test section. This point represents the location of the sixth pressure transducer, P_6, located above the annulus on the original three inch diameter piping. It was included in the plot to show the flow behaviour after the fluid leaves the annulus.

These lines show that at each consecutive point, the flow rate is increasing in a stepwise manner. Figure 6.3 depicts the experiments where all three valves in the radial inflow lines are open with fluid is flowing through them all. The flow rate should therefore increase at each point inside the annular channel. As stated, the final point is located outside the annular test section and at this location there is no fluid inflow. Beyond the third point, the flow rate should become constant as shown in Figure 6.3.

The two dashed lines decreasing from left to right represent pressure verses position. The first two points on these lines show a slight decrease in pressure as the fluid travels from the bottom section up into the middle section inside the annulus. The second and third points show that from the middle section to the top section, an even larger decrease in pressure is observed. The third and fourth points show a further decrease in pressure as the fluid leaves the annular spacing and enters the three inch PVC pipe. This should be expected because the fluid is leaving a larger volume entering a smaller one. The pressure needs to increase to allow the fluid to pass through the smaller space.

6.2.2 Experiments with a 3" ID Annular Channel

The second annular channel size studied with radial inflow was with a nominal three inch diameter inner pipe in the annulus. These experiments also followed the test matrix depicted in in Table 6.1. Again, pressures and their corresponding flow rates were plotted as a function of position for the data collected. The results are shown in Figure 6.4.

As with the results from the two inch inner diameter piping, Figure 6.4 may be unclear. Figure 6.5 shows only the results for the experiments where all three valves on the radial inflow sections were open and can be viewed to help clarify Figure 6.4.

As before, the pink lines in Figure 6.5 represent the experiments conducted at the lower pump speed while the blue lines signify experiments at the higher speed. In these experiments 60 Hz was used instead of 45 Hz as it was in the previous case. The two lines increasing from left to right in a stepwise manner represent flow rate verses position and the two dashed lines decreasing from left to right represent pressure verses position.

Figure 6.5 shows that the flow rate increases as the distance from the base of the annulus increases. Since this plot depicts the experiments where all three ball vales in the radial inflow lines are open and fluid is flowing through them, the flow rate should increase at each point located inside the annular channel. After the third point on the line, no more fluid can enter the system so the line on the plot levels off and becomes constant, as it should.

It can also be noted that the line segment between points one and two has a steeper slope than the segment between points two and three. As the distance from the base of the annulus increases, more resistance is acting on the flow causing less fluid to travel through the upper inflow sections. This can be supported by using data collected during experimentation, as provided in APPENDIX D. For the experiments carried out at 75Hz, the summation of the flow rates through the bottom and middle sections was 355.25 LPM while the top and middle sections experienced a flow total flow rate of 340.50 LPM.

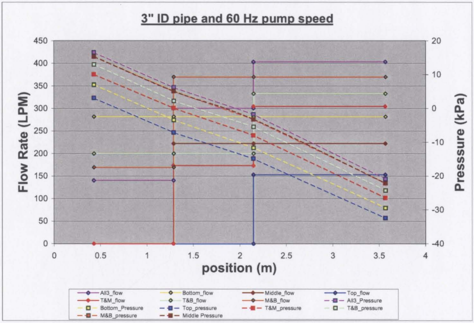

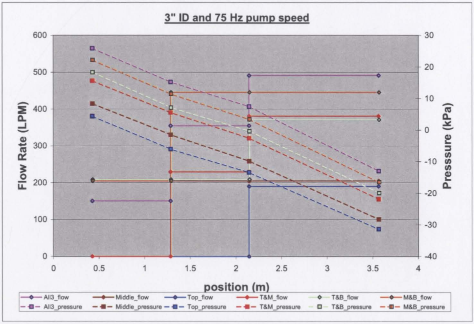

Figure 6.4: Pressure and Flow Rate as a Function of Position in a 3" ID Annular Channel

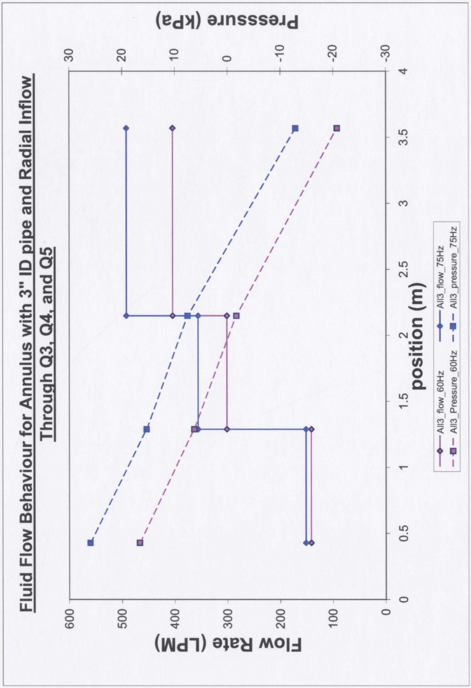

Figure 6.5: Pressure and Flow Rate as a Function of Position in a 3" ID Annular Channel

By looking at Figure 6.5 it is shown that the pressure verses position curves do follow expected trends. The line segment between point one and point two is sloping downwards which shows a decrease in pressure as the fluid travels from the bottom section up into the middle section inside the annulus. The segment between second and third points show that in the next section the pressure continues to decrease at approximately the same rate as in the first section. The third and fourth points show a further decrease in pressure as the fluid leaves the annular spacing and enters the three inch PVC pipe, which was expected to occur.

6.2.3 Experiments with a 4" ID Annular Channel

The final annular channel size studied with radial inflow was with a nominal four inch diameter inner pipe inside the annulus. These experiments also followed the test matrix depicted in in Table 6.1. Again, pressures and their corresponding flow rates were plotted as a function of position for the data with the results shown in Figure 6.6.

Figure 6.7 can be studied to help clarify Figure 6.6. Figure 6.7 shows only the results for the experiments where all the valves on the radial inflow sections were open.

The pink lines in Figure 6.7 represent the experiments conducted at 60 Hz while the blue lines denotes experiments at 75 Hz. The two lines increasing from left to right in a stepwise manner represent flow rate as a function of position and the two dashed lines decreasing from left to right characterize pressure as a function position.

The line segment between points one and two has a steeper slope than the segment between points two and three. Data provided in APPENDIX D proves that more resistance is acting on the flow as the distance from the base of the test section increases. For the experiments carried out at 75Hz, the summation of the flow rates through the bottom and middle sections was 369.18 LPM while the top and middle

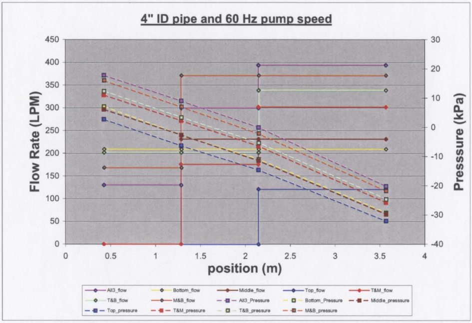

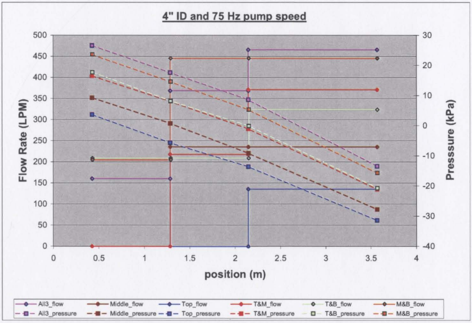

Figure 6.6: Pressure and Flow Rate as a Function of Position in a 4" ID Annular Channel

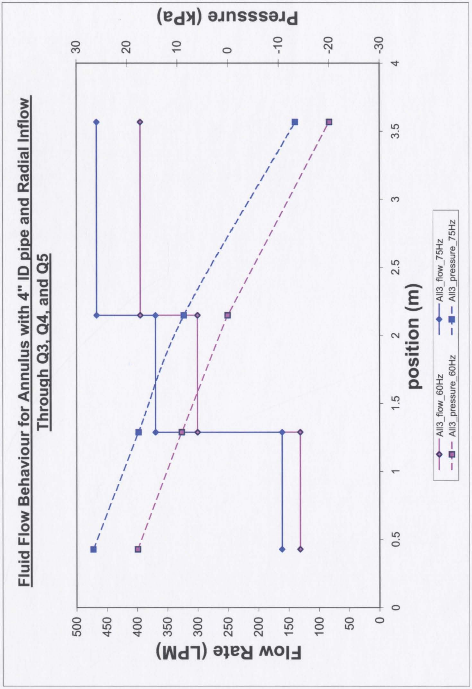

Figure 6.7: Pressure and Flow Rate as a Function of Position in a 4" ID Annular Channel

sections experienced a flow total flow rate of 305.62 LPM.

Like the other annular channel sizes, Figure 6.7 illustrates that the curves plotted show trends that were expected. A decrease in pressure as the fluid travels from the bottom section and up through the annular channel is shown. A further decrease in pressure is depicted as the fluid leaves the annular spacing and enters the three inch diameter PVC pipe. This was also expected since the fluid is leaving a larger volume entering a smaller one.

By studying the same experiments with different annular channel sizes, one can see that the same trends are found in each of the experimental results. It is important to show the plots for each experiment to properly portray that with all annular channels studied, the same fluid trends were displayed each time.

6.3 Investigating Friction Factors for Radial Inflow into an Annular Channel

6.3.1 Theoretical Evaluation Considering Section P_3 to P_4:

To calculate the friction factors in an annular channel with radial inflow using simplified equations where one does not need to integrate, the flow between any two pressure transducers in the annulus at any time must be constant. For example, the friction factor could not be calculated between P_3 and P_5 if there was inflow through the middle section, Q_4. Due to this constraint, there were a limited number of situations where the friction factors were determined.

A section of piping between the bottom pressure sensor, P_3, and the middle pressure sensor, P_4, was first considered. For these calculations, the case with where fluid is entering the annular channel through the bottom inflow section only was first studied (see Figure 6.8 for locations).

From Figure 6.8, it is shown that the flow rates are recorded at the flow meters on the radial inflow section located on the 1 $\frac{1}{4}$ inch diameter braided Tygon tubing. To determine the fluid speed in the annulus, the mass flow of the fluid is obtained. Since water is the working fluid for all the experiments carried out with a known density of 1000 kg/m^3, the mass flow is obtained from Equation 6.1.

$$\dot{m} = \frac{Q}{time} = \frac{[L][min]}{60[min][s]} = \frac{Q}{60}\frac{[kg]}{[s]} \tag{6.1}$$

The velocity of the fluid in the annulus can then be calculated according to:

$$v = \frac{\dot{m}}{\rho A_{ann}} \tag{6.2}$$

The hydraulic diameter is represented by the equation $D_h = \dfrac{4A}{P}$ where A is the area and P represents the perimeter. Since the perimeter of an annulus is $P = \pi(D_o + D_i)$,

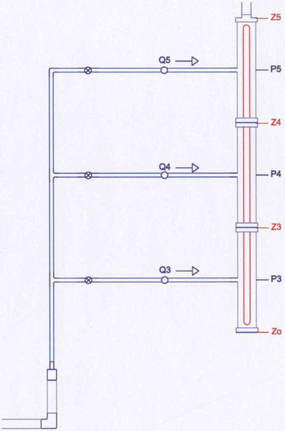

Figure 6.8: Radial Inflow Setup

the hydraulic diameter equation can be solved for the area and the equation becomes:

$$A = \frac{D_h \pi (D_o + D_i)}{4} \tag{6.3}$$

By substituting the area into Equation 6.2, the velocity in the annulus can be calculated using Equation 6.4.

$$v_{ann} = \frac{4\dot{m}}{\pi \rho D_h (D_o + D_i)} \tag{6.4}$$

To determine the friction factor between pressure transducers P_3 and P_4, the equations presented in Chapter 5 are used. Assuming the fluid speed is constant, $v_3 = v_4 =$

v_{ann}. Using the Fanning friction factor, the frictional pressure drop,ΔP_{fric}, can be represented by Equation 6.5 (Hodge & Taylor, 1999):

$$\Delta P_{fric} = \frac{4 f_{fanning} L_T}{D_h} \frac{\rho v_{ann}^2}{2} \tag{6.5}$$

From Equation 5.13 in Chapter 5, the experimental friction factor is calculated according to:

$$f_{exp} = \frac{(\Delta P_{35} + \rho g \Delta z_{35} - \Delta P_{acc}) D_h}{2 L_T \rho v_{ann}^2} \tag{6.6}$$

where: D_h = hydraulic diameter of annulus (m)

ΔP_{35} = pressure difference for the section (Pa)

g = gravitational constant (9.81 m/s^2)

Δz_{35} = vertical distance between pressure readings (m)

L_T = total length of section (m)

ρ = fluid density (kg/m^3)

v_{ann} = fluid velocity in the annulus (m/s)

Included in Equation 6.6 is the pressure drop due to the acceleration of the fluid in the channel ΔP_{acc}. This component is often not as large as the frictional component but should be calculated to determine its overall effect on the flow. For example, to determine the acceleration effects in the channel when there is only flow through the bottom flow meter, Q_3, Equation 6.7 can be used.

$$\Delta P_{acc} = \rho (v_3^2 - v_0^2) \tag{6.7}$$

In this particular case, there is no flow entering the section below the bottom flow meter, so v_o is zero. Hence, Equation 6.7reduces to:

$$\Delta P_{acc} = \rho {v_3}^2 \tag{6.8}$$

Equation 6.8 is then be substituted into Equation 6.6 and the experimental friction factors are calculated.

For annular flow with radial inflow a certain type of situation will arise where, in theory, the fluid exiting the tubing will have to change direction. It will have to stop traveling horizontally and will begin traveling vertically upward through the annular channel. Even though the pressure transducers are located on the opposite side of the piping from where the fluid enters, the readings will be somewhat affected. A stagnant pressure component is expected to exist in this area and should be accounted for. This stagnant pressure will only need to be accounted for on pressure readings that are taken when there is fluid entering the annular channel through the tubing directly across from them.

For example, if there is fluid flowing through Q_3 only, then the measured value at the corresponding pressure transducer will include a stagnant pressure component such that:

$$\left.\begin{aligned} P_{measured} &= P_3 + P_{stagnant} \\ &= P_3 + \frac{1}{2}\rho v_{tubing}^2 \end{aligned}\right\} \tag{6.9}$$

The velocity in the tubing will need to be determined in order to carry out this calculation. The inner diameter of the flexible tubing (D_{tubing}) was measured accurately to be $1\frac{1}{4}$ inches or 0.03175m. Using Equation 6.10, the tubing velocity was calculated.

$$\left.\begin{aligned} v_{tubing} &= \frac{Q}{A} \\ &= \frac{4Q}{\pi D_{tubing}^2} \end{aligned}\right\} \tag{6.10}$$

Using Equation 6.10 and Equation 6.9, the actual value of P_3 used to calculate the friction factors isl therefore:

$$P_3 = P_{measured} - \frac{1}{2}\rho v_{tubing}^2 \tag{6.11}$$

This value is one of the pressure measurements used to determine ΔP for the test section.

The experimental friction factors calculated according to Equation 6.6 were compared to theoretical values calculated according to the Blasius equation (see Equation 6.12).

$$f_{theory} = \frac{0.0791}{\sqrt[4]{Re}} \tag{6.12}$$

where: Re $=$ Reynolds number $= \dfrac{\rho v D_h}{\mu}$

6.3.2 Results for Section P_3 to P_4:

To study frictional effects in an annular channel with radial inflow, a section of piping between the bottom pressure sensor, P_3, and the middle pressure sensor, P_4, was first considered. The case with where fluid is entering the annular channel through the bottom inflow section only was first studied. Data was collected for three different annular channel sizes.

To help understand this type of flow, the radial inflow can be represented as nozzle flow with fluid traveling from a small area into a larger area (see Figure 6.9).

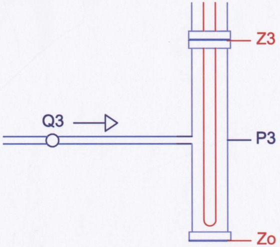

Figure 6.9: Radial Inflow Represented by Nozzle Flow

The actual flow rate through a nozzle rarely equals the theoretical flow rate. Blockage of the flow area by the boundary layer and dissipation due to viscous friction usually lowers the flow rate below what can be calculated theoretically.

A discharge coefficient, C_d, can be used to help correct the flow rate. The discharge coefficient is defined as the actual mass rate of flow divided by the theoretical mass rate of flow (Blevins, 1984). If C_d is equal to one, than the model should already agree with theory. The discharge coefficient is a function of the geometry of the nozzle, the Reynolds number, and Mach number if one is working with compressible flows such as gas where (Blevins, 1984):

$$C_d = F(geometry, UD/\nu, U/c) \tag{6.13}$$

where: U = inlet velocity

D = inlet diameter

c = speed of sound

Blevins (1984) lists various nozzle types and their associated discharge coefficients. The case which most resembles my setup would be the ring exit nozzle case he describes. The discharge coefficient can be found from the diameter ratio. From Blevins, the following discharge coefficients were obtained:

- For nominal two inch diameter piping: d/D = 0.33, $C_d = 0.61$
- For nominal three inch diameter piping: d/D = 0.45, $C_d = 0.61$
- For nominal four inch diameter piping: d/D = 0.71, $C_d = 0.68$

Incorporating these values into the friction factor equations, the results were plotted as shown in Figure 6.10. All calculation details are shown in Appendix D.

From this figure, it is evident that there exists a large amount of uncertainty in the results. We can see that the results obtained for the experimental friction factors have negative values which have no practical meaning. However, as the inner piping gets larger and the annular spacing becomes smaller, the data does begin to approach the theoretical results.

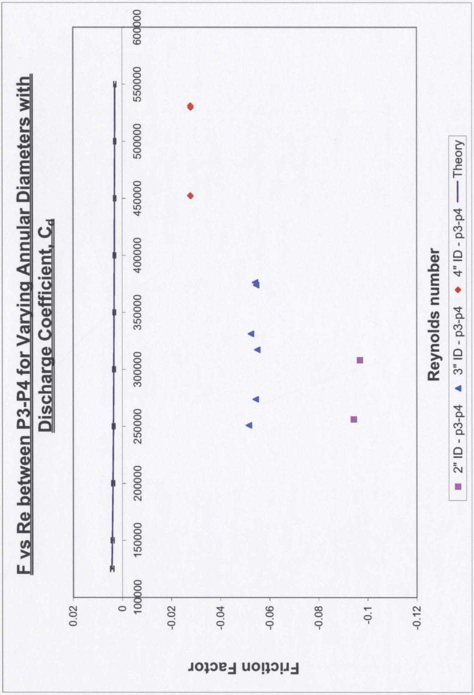

Figure 6.10: Friction Factors Evaluated at P_3 to P_4 Using a Discharge Coefficient

The negative values indicate that there are some errors in the measurements taken during testing. They indicate that for the small flow rates tested, the pressure gradients could not be accurately deduced. Although the pressure transducers were earlier said to be adequate for data measurements, it has been found that for measuring small pressure gradients these transducers cannot accurately portray the pressure differences within an acceptable level of certainty. The actual flow into the annular channel is quite complicated in nature and is not easily explained. White (1991) shows what a flow such as this would look like in Figure 6.11.

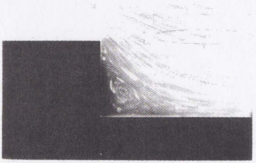

Figure 6.11: Viscous Flow Patterns (White, 1991)

The fluid is entering into a larger area from a smaller one and as the fluid pours into it, some very complicated interactions are taking place. The fluid sweeps in and tries to fill up the new volume. Eddies exist in the bottom corner of the space where the fluid is churned as it enters.

As the fluid enters the annular test section in the multiphase flow loop, one might expect to see a similar occurrence. Although no photographs were taken of this phenomenon during testing, it was witnessed that as the fluid entered the annulus from the radial inflow section, the fluid became very churned up. It was evident that some complex flow phenomenon was occurring.

As the fluid travels up through the test section it may begin to swirl. The average velocity used has been obtained from the flow meter readings located on the radial inflow sections outside the annular channel. If the fluid is swirling as it travels up through the vertical test section, the flow rates measured on the radial inflow section will no longer be accurate. This swirling would affect the local velocity and would have to be considered. If a local velocity value was obtainable, this value may improve upon the results that have been calculated for the friction factors in these experiments.

Chapter 7

Axial Flow Through an Annular Channel

7.1 Experimental Setup

7.1.1 Smooth Axial Flow Through an Annular Channel

In addition to investigating radial inflow in an annular channel, axial flow through the test section was also studied. Constant flow through the annulus at high flow rates could now be observed whereas with radial flow, at each inflow section more fluid was entering the annulus and the flow was not in steady state. For the radial experiments in which constant flow through the annular channel could be achieved, only low flow rates and hence low Reynolds were found. The annular channel was able to experience much higher flow rates with axial flow.

For the experiments where the fluid was driven axially through a smooth annular channel, a test matrix was constructed and followed (see Table 7.1). Three different pipe sizes were used for the inner piping to vary the size of the channel. After each test was complete for a particular inner pipe size, the entire test section would be disassembled and removed from the multiphase flow loop where the inner piping would then be removed and a new size installed. With the new inner piping in place, the test section was put back in position in the flow loop and reassembled.

Table 7.1: Test Matrix for the Annular Channel with 3" Diameter Inner Walls

Experiment	*Pump Speed (Hz)*											
Trial 1	73	67	60	52	45	37	30	22	15	12		
Trial 2	73	67	60	56	52	45	40	36	30	26	20	15
Trial 3	73	67	60	56	52	45	40	36	30	26	20	

The smallest sized inner piping used was a nominal three inch diameter acrylic pipe. For this setup, three trials were carried out during experimentation. After collecting the first trial of experiments and carrying out some preliminary calculations, it was evident that the results for the data collected at the lower flows were not as accurate as those from the higher flows. For this reason, some experiments with lower flow rates were removed from the text matrix and instead more experiments with higher flow rates were recoded. It was felt that the experiments held at the higher flow rates would produce more interesting results.

The second sized annular channel to be tested incorporated a nominal four inch diameter pipe inside the annulus. These experiments followed the text matrix depicted in Table 7.2. The text matrix was revisited once again and some additional experiments carried out at higher flow rates were added in the second and third trials of data collection.

Table 7.2: Test Matrix for the Annular Channel with 4" Diameter Inner Walls

Experiment	*Pump Speed (Hz)*													
Trial 1	73	67	60	56	52	45	40	36	30	26	20	15		
Trial 2	72	67	64	60	56	52	48	45	40	36	30	26	20	15
Trial 3	72	67	64	60	56	52	48	45	40	36	30	26	20	15

The third and final sized annular channel tested with smooth axial flow through an annulus incorporated a nominal five inch diameter piping. These experiments followed the text matrix depicted in Table 7.3. Only one trial of experiments was carried out for this setup due to damage incurred to the piping.

Table 7.3: Test Matrix for the Annular Channel with 5" Diameter Inner Walls

Experiment	*Pump Speed (Hz)*											
Trial 1	73	67	60	56	52	45	40	36	30	26	20	15

7.1.2 Rough Wall Annular Flow

Rarely in industry will one find perfectly smooth pipe flow. Wall roughness is therefore a very practical characteristic to investigate and may greatly effect the pressure gradients associated with the flows. For investigating the effect of wall roughness on the fluid flow through an annular channel, only the four inch diameter inner piping was chosen to show the roughness effects. It is speculated that the same trends would be evident for the other annular channels.

Rough - Smooth Wall Annular Flow

Two setups were considered to examine the effects of wall roughness on the flow through an annular channel. In the first setup, a smooth inner pipe and a rough outer pipe was studied. To roughen the walls of the clear acrylic piping, sandpaper of different grits was purchased and attached. Grit is a reference to the number of abrasive particles per inch of sandpaper. The lower the grit, the rougher the sandpaper (Metal Finishing Systems, 2005). A 20 grit sandpaper, which is classified as a course grit, was chosen and adhered to the inside of the six inch diameter pipe with the sand grains exposed to the the fluid. To attach the sandpaper, the multiphase flow loop had to be disassembled and the annular test section removed from it. Once this section was removed, each of the three sections it was comprised of were further disassembled to be able to attach the sandpaper to all areas of the piping. With the sandpaper in place, the test section was put back and reassembled.

These experiments were carried out in the same manner as in the smooth pipe flow experiments. A similar test matrix was created and followed as shown in Table 7.4.

Table 7.4: Test Matrix with Roughened Outer Walls and Smooth Inner Walls

Experiment	*Pump Speed (Hz)*													
Trial 1	72	67	64	60	56	52	48	45	40	36	30	26	20	15
Trial 2	72	67	64	60	56	52	48	45	40	36	30	26	20	15
Trial 3	72	67	64	60	56	52	48	45	40	36	30	26	20	15

Rough - Rough Wall Annular Flow

In the second setup considered, each of the pipe walls of the annulus were roughened. It was decided that both the inner wall of the outer piping and the outer wall of the inner piping would not have the same roughness value. In a practical situation, it is unlikely that both surfaces exposed to the fluid would be of the same roughness.

The outer piping of the annulus still has the 20 grit sandpaper attached but a grit less course than 20 was chosen for the inner piping. A 60 grit sandpaper was adhered to the outer walls of the inner piping. The flow differences should be evident by choosing a roughness value such as this when compared to experiments carried out with one smooth surface. The experiments were conducted as set out in the test matrix shown in Table 7.5.

Table 7.5: Test Matrix with Roughened Outer and Inner Walls

Experiment	*Pump Speed (Hz)*													
Trial 1	72	67	64	60	56	52	48	45	40	36	30	26	20	15
Trial 2	72	67	64	60	56	52	48	45	40	36	30	26	20	15
Trial 3	72	67	64	60	56	52	48	45	40	36	30	26	20	15

Care was shown in reassembling the annular test section with sandpaper attached to both surfaces. If the surfaces were bumped or scraped, sand grains would become detached from the backing and fall off. The holding rings were not secured in their usual position on the inner piping because with the sandpaper on the outer pipe they would not assemble properly. The lower holding ring was in its usual position near the bottom of the pipe just above the connection point between the pipe and the end cap. The upper holding ring was instead put on the pipe approximately one third of the way down from the top. At this position, it sits between the top and middle sections of the annular channel.

Once this holding ring was in position, the remaining sandpaper was installed and the test section reassembled. In all other experiments, the fluid would pass through the first holding ring before a pressure measurement was taken and would pass by the last holding ring after that pressure measurement was taken. As it is setup with sandpaper on both piping, the fluid passes through the upper holding ring before a pressure measurement is taken which will now contribute to the minor losses in the test section in the system.

7.2 Theoretical Evaluation

7.2.1 Smooth Axial Flow Through an Annular Channel

To accurately determine the friction factors for fully rough walls, it is logical to begin with the simplest case which would be where the pipe walls are smooth. From this point, the equations are expanded upon and a roughness coefficient is introduced.

Friction Factors for Horizontal Flow

Two separate sections of the multiphase flow loop were studied for the data analysis for the axial flow experiments. The first section considered was the horizontal test section which measures 4.68 meters in length. The friction factors were calculated between P_1 and P_2. P_1 is the first pressure transducer the fluid passes through located at the beginning of the horizontal test section. P_2 is the second pressure transducer the fluid will pass through in the flow loop and is located at the end of the horizontal section just before the fluid enters a 90^o long radius elbow. This section consists entirely of straight three inch diameter PVC pipe only; it is part of the original multiphase flow loop constructed in 1997.

For a circular pipe under turbulent flow, the friction factors are a function of Reynolds numbers only when the pipe is considered smooth (Caetano, 1985). For these calculations, a simplified version of the Bernoulli equation was used. The fluid speed in the section was constant, therefore Δv was zero and there was no change in height between the pressure sensors which makes Δz also zero. Equation 7.1 shows this simplified equation used to calculate the friction factors.

$$f_{exp} = \frac{D_h \Delta P}{2 L_T \rho v^2} \tag{7.1}$$

where: D_h = hydraulic pipe diameter (m)

ΔP = pressure difference for the section (Pa)

L_T = total length of test section (m)

ρ = fluid density (kg/m^3)

v = fluid velocity (m/s)

The theoretical friction factors for each experiment were calculated according to the Blasius equation (Equation 7.2) as they were in the previous chapters.

$$f_{theory} = \frac{0.0791}{\sqrt[4]{Re}} \tag{7.2}$$

These finding are compared to those obtained experimentally. It was important to carry out experiments in the horizontal test section as well as the annular test section since the data collected from the horizontal test section will give a measure of validity. If the results compare well with theory for this section, it can be concluded that the results from the annular test section should be reliable as well.

Friction Factors for Annular Flow

The other test section analyzed was the vertical, annular channel. When the piping becomes non-circular, the system becomes more complex. Although no single relationship exists between Reynolds number and friction factor for these configurations, the Blasius or Nikuradse equations are usually adequate (Caetano, 1985).

The friction factors were calculated for the test section between P_3 and P_5, with P_3 being the pressure sensor on the lower end of the annulus and P_5 being the pressure sensor located on the upper end. This section was 1.73 meters in length between the pressure transducers. In this section there were no bends, fittings or other such obstacles for which calculations for any minor losses would need to be considered.

In Chapter 5, equations were presented from the conservation of energy formula and were simplified for the case where the fluid speed is constant. These equations apply for axial fluid flow through an annular channel as well. The speed of the fluid through the annulus remained constant throughout each test carried out and therefore Δv is zero. For the annular test section, the height between the pressure transducers needed to be accounted for. This situation resembles the calculations depicted for radial inflow and therefore Equation 7.3, which was originally presented in Chapter 5 could be used to calculate the experimental friction factors here. It should be noted that the Δz is negative which makes the term $\rho g \Delta z$ negative.

$$f_{exp} = \frac{D_h(\Delta P + \rho g \Delta z)}{2 L_T \rho v^2} \tag{7.3}$$

For each experiment Equation 7.2 was used to calculate theoretical friction factors which are compared to those obtained experimentally.

7.2.2 Axial Flow Through an Annular Channel with Rough Pipe Walls

Whether one surface of the annular channel is rough or both surfaces are rough, the same equations are used for both situations. If both surfaces of the annular channel are roughened, they will not have the same roughness coefficients and an effective value would have to be determined. The first case studied here had an annular channel with one rough surface on the outer wall, with a smooth surface on the inner wall. The second scenario had the same roughness on the outer piping, but this time in inner pipe of the annulus was roughened as well.

There is some uncertainty in the actual size of the sand grains since every grain was not identical and it was not practical to measure each one individually. A maximum diameter was used as the size of the sand grains and this value was used to determine the roughness coefficient. If the diameter of the sand grains were varied, it would effect the roughness coefficient which in turn effects the theoretical friction factors that were determined for flow.

Friction Factors for Horizontal Flow

The friction factors were determined for the horizontal section of piping between P_1 and P_2. Although this section of pipe is smooth and does not show the roughness effects on any type of flow, it does show whether or not the data collected is reliable. If the calculations are carried out for smooth, horizontal pipe flow and the results are in good agreement with theory, it is a good assumption that the data collected is accurate and can be used to evaluate the friction factors in the annular channel. For this calculation as with the calculations for smooth pipe flow, Equation 7.1 was used to determine the friction factors. The experimental results could then be compared to Equation 7.2.

Friction Factors for Annular Flow

The next section studied was the vertical, annular section between P_3 and P_5. Between these two sensors there were no obstacles which would contribute to the minor losses in the system except for one holding ring to hold the inner piping in place. The upper holding ring is located approximately one third of the way down from the top of the piping and sits between the middle pressure sensor, P_4, and the top pressure sensor, P_5.

The same equation used in calculating the experimental friction factors for this section of piping for the case where the inner pipe walls were smooth was also used here. Δv is zero because the fluid speed through the test section is constant. The height difference between the pressure transducers needed to be accounted for as well as the pressure losses incurred due to the holding ring. Any minor losses between P_3 and P_5 needed to be included in the calculation to accurately model the flow. The fluid must pass through one holding ring in this section and this obstacle will contribute to the minor losses in the test section.

Minor losses are expressed in terms of a loss coefficient, K. To calculate the K factors for the fluid entering and exiting the holding ring Equation 7.4 could be used. These K factors are expressions of the areas before and after the joints that is contributing to the pressure loss.

$$\left.\begin{aligned} \sigma &= A_{holes}/A_{ann} \\ K_{exp} &= (1-\sigma)^2 \\ K_{red} &= 0.42(1-\sigma^2) \end{aligned}\right\} \tag{7.4}$$

The experimental friction factors for the vertical, annular section of piping with the outer pipe possessing a rough finish was found according to Equation 7.5.

$$f_{exp} = \frac{(\Delta P_{35} + \rho g \Delta z_{35} - (\frac{K_{total}\rho v^2}{2}))D_h}{2L_T \rho v^2} \tag{7.5}$$

where: D_h = hydraulic diameter of annulus (m)

ΔP_{35} = pressure difference from P_3 to P_5 (Pa)

g = gravitational constant (9.81 m/s^2)

Δz_{16} = vertical distance from z_3 to z_5 (m)

L_T = total length of test section (m)

ρ = fluid density (kg/m^3)

v = fluid velocity (m/s)

To calculate the theoretical friction factors when one must consider the roughness effects on the flow Blasius can no longer be used. Instead, an equation which expresses the friction factor as a function of Reynolds number and the relative roughness is needed. Shown in Equation 7.6, the Colebrook-White equation is an implicit equation that has been accepted as the most accurate representation of the Moody diagram for turbulence (Hodge & Taylor, 1999).

$$\frac{1}{\sqrt{f}} = log\left(\frac{\epsilon}{3.7D} + \frac{2.51}{Re_D\sqrt{f}}\right)^{-2} \tag{7.6}$$

It is widely used and several variations of it exist which are all implicit and must be solved iteratively. Though these equations can be solved numerically, explicit forms of theses equations are preferred in the industry. Some of these explicit equations have been proposed by Moody (1947), Wood (1966), Churchill (1977), Haaland (1981), and others. Most of these explicit equations have their own range of Reynolds numbers and roughness values for which they are valid (Ouyang & Aziz, 1996).

The Swamee and Jain equation (Hodge & Taylor, 1999) was used to calculate the theoretical friction factors for this data (see Equation 7.7). It was shown in the Benchmarking experiments that for smooth pipe flows, the Swamee and Jain equation compares quite well with Blasuis. It can therefore be deduced that it will provide trustworthy results for theoretical calculations with roughened surfaces.

$$f = \frac{0.0625}{\left[log\left(\frac{\epsilon}{3.7D} + \frac{5.74}{Re^{0.9}}\right)\right]^2} \tag{7.7}$$

The roughness factor was determined from the sandpaper grit. A 20 grit sandpaper has an equivalent minimum particle size of 0.026 inches and a maximum particle size of 0.063 inches (MFS, 2005) which is the roughness coefficient, ϵ. The roughness factor, ϵ/D is found by dividing ϵ by the diameter of the pipe and in this case it would be the hydraulic diameter of the annulus, D_h. By carrying out the calculations using both values, the effect of the actual value of the particle size on the roughness coefficient and hence on the friction factor as well is determined.

7.3 Results

7.3.1 Smooth Axial Flow Through an Annular Channel

Annular Channel with 3" Diameter Inner Piping

Using the equations presented, friction factors were plotted against Reynolds numbers for the data obtained for smooth axial flow in the annulus. For each of the annular channel sizes, two test sections were analyzed and friction factors were found for each of the test sections.

The first section studied was the horizontal test section. This section was comprised of three inch diameter PVC pipe and was an original part of the multiphase flow loop. Friction factors were calculated for the data collected during these experiments and were compared to the Blasius theory, as shown in Figure 7.1. This section of piping was not altered throughout the experimentation process so calculating friction factors here is a good show of whether or not the experimental data is reliable.

From examining the horizontal test section data included in APPENDIX E, there is good agreement between the theoretical calculations and the experimental data for Reynolds numbers greater than 100,000, which is evident from Figure 7.1. Run #1 and run #3 are both within an acceptable limit of $\pm 15\%$, shown by the dashed lines. Run #2 shows the same trends as the other data sets but is outside the acceptable limit and may be off due to flow sensor debris or other such bias errors that can be seen in experimental situations. By carrying out more than one data set, drift in results can be considered in the analysis. The maximum flow rate obtained for these experiments was approximately 1000 liters per minute or equivalently a maximum Reynolds number of approximately 230,000. This maximum was reached because of resistance in the piping and the maximum rating on the pump.

For Reynolds numbers lower than 100,000 there is substantial error between theory

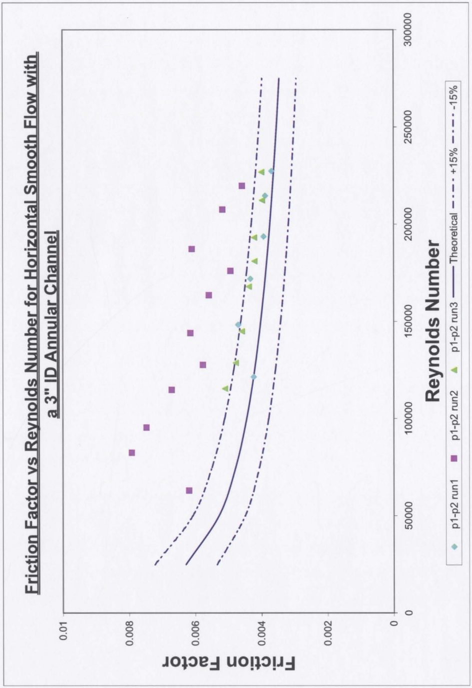

Figure 7.1: Friction Factors vs Reynolds number for Horizontal Flow Through an 3" ID Annular Channel

and experimental calculations. The pressures are read using pressure transducers suitable for reading gauge pressures. Although they can accurately read pressure at a certain location, it has been found through this study that they are not as accurate for determining pressure differences which are less than 1 kPa. In the horizontal section, the difference in pressure between the two transducers for low flow rates can be quite small, and to more accurately determine the pressure drop differential pressure transducers can be used. Differential pressure transducers are designed to measure differential pressures of liquids or gases and would have a smaller associated error reading (Omega DTP, 2002).

The second test section considered was the segment of piping between P_3 and P_5, located in the vertical, annular channel. From the plot shown in Figure 7.2, the friction factor results are somewhat scattered around the Blasius equation, and are all beyond the $\pm$ 15% error range.

The results from trial one were not included in Figure 7.2. Due to an equipment malfunction, no values were recorded from the bottom pressure transducer, P_3. Since this value is needed to calculate friction factors in the annular test section, no data could be plotted for trial one.

The results in the annular channel are somewhat scattered around the theoretical curve. If differential pressure transducers were used, it is anticipated that there would be a smaller error in the difference between the two readings. For smaller pressure drops, if one pressure transducer is reading low and the other one is reading high, or vice versa, the recorded pressure drops would be inaccurate which would affect the associated friction factors. For larger pressure drops, this error would not be as evident.

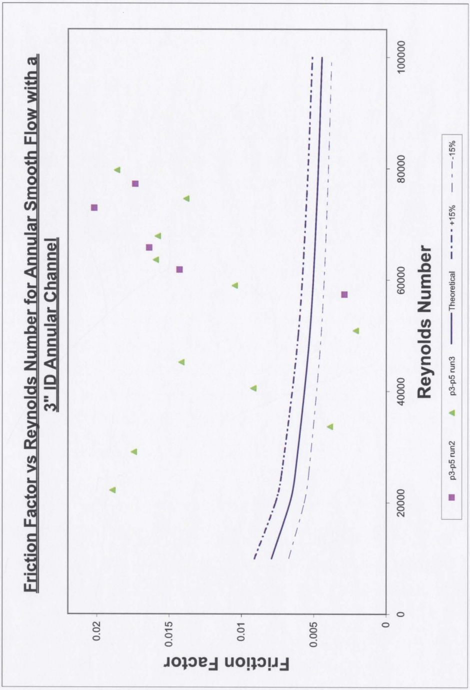

Figure 7.2: Friction Factors vs Reynolds number for Annular Flow Through a 3" ID Annular Channel

Annular Channel with a 4" Diameter Inner Piping

The next annular channel size incorporated a four inch diameter inner pipe inside the annulus. The data collected during these experiments was analyzed using the equations presented in the earlier sections. Using the data presented in APPENDIX E, the results for the horizontal test section are shown in Figure 7.3. The experimental friction factors were plotted against Reynolds number and these points were shown on the same plot as the Blasius theory curve. This curve is shown in dark blue with a $\pm$ 15% error margin, shown by the dashed lines.

From examining this section of piping, it is observed that there is good agreement between the theoretical calculations and the experimental data for Reynolds numbers greater than approximately 100,000. The maximum flow rate for these experiments was near 950 liters per minute which gives a maximum Reynolds number of approximately 215,000 that can be obtained. The maximum flow rate for this setup is slightly lower than that of the arrangement with the three inch diameter inner piping due to a smaller flow area in the annulus and hence an increased resistance in the line.

The second test section studied was the annular channel. The data that was collected in the laboratory was analyzed and experimental friction factors were again calculated. These results were compared to theoretical values calculated from Equation 7.2 and the results were plotted in Figure 7.4.

From this figure, it is observed that most of the data points reported fall within the specified error margin if $\pm$ 15%. Friction factors for other flow rates were calculated and these results can be seen in APPENDIX E, but it was observed from these computations that for Reynolds numbers below approximately 50,000, the data did not agree well with theory and were therefore not included in the plots.

A trend can be seen from the results of both the annular channels with a three inch diameter inner piping and the four inch diameter inner piping. Most of the data from

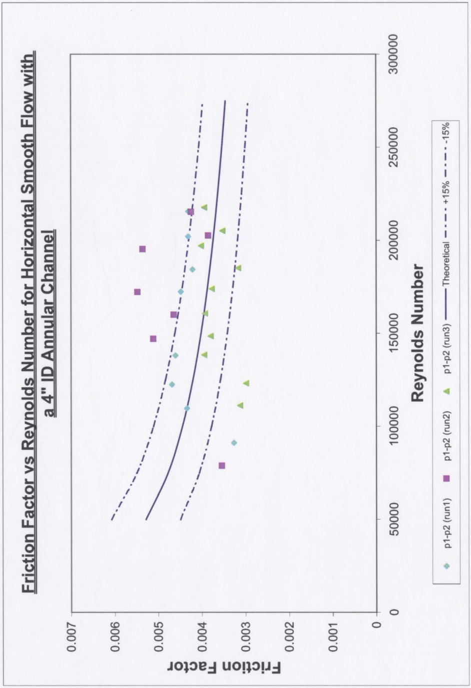

Figure 7.3: Friction Factors vs Reynolds number for Horizontal Flow Through a 4" ID Annular Channel

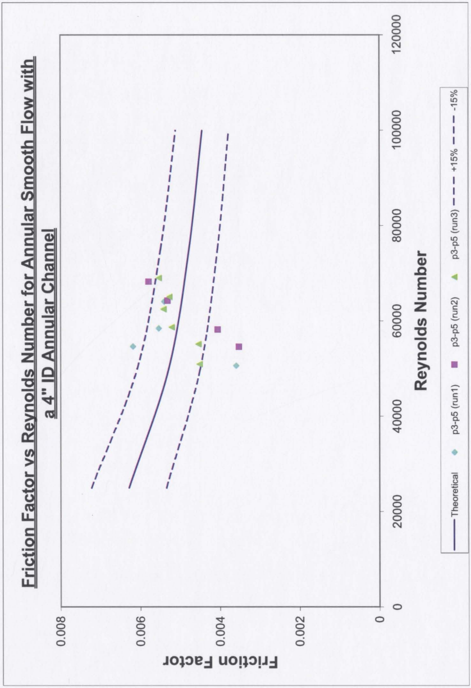

Figure 7.4: Friction Factors vs Reynolds number for Annular Flow Through a 4" ID Annular Channel

the three inch diameter inner piping did not agree with theory but as the size of the annular channel decreased, the results improved. It is believed that the smaller channel produces larger pressure gradients and these gradients would lead to more accurate results, since the pressure transducers in the flow loop are more accurate when measuring larger gradients.

Annular Channel with a 5" Diameter Inner Piping

The final annular channel studied with smooth flow was the nominal five inch diameter inner piping channel. Due to extensive damage incurred to the inner piping after the first trial was carried out, only one data set was collected. As with the other experiments, the first section studied was the horizontal test section. The friction factors were calculated in the same manner as previously described (see APPENDIX E) and the results were compared to theory and plotted on Figure 7.5.

Unlike the previous experiments studied, this figure shows all the data points collected outside the specified error range of $\pm 15\%$. With only one data set to study and showing results such as these, it was deduced that these results many not be reliable and should not considered.

7.3.2 Axial Flow Through an Annular Channel with Rough Pipe Walls

The Effect of Roughness Coefficients on Annular Flow

Calculations were carried out using equations previously presented to determine the friction factors for an annular channel with different surfaces. To demonstrate the effect the roughness coefficient has on flow and hence on friction factors, two sets of similar calculations were carried out with the difference being the particle size of the sand grains. Maximum and average values were used for particle diameter with the

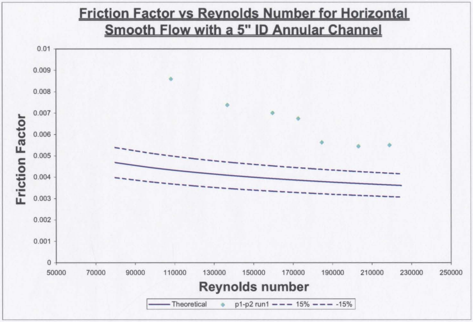

Figure 7.5: Friction Factors vs Reynolds number for Horizontal Flow Through a 5" ID Annular Channel

results for both plotted with the experimental friction factors as shown in Figure 7.6.

The size of the sand grain particles does have a relevant effect on the calculated results, as evident from Figure 7.6. This plot shows that the Swamee and Jain theoretical results with the maximum sand grain size is in closer agreement with the data obtained experimentally. It is evident that the outcome is largely influenced by altering this variable. Given these results, this issue should be further investigated.

Although the experimental results do not agree within a ± 15% error margin, shown in APPENDIX F, the data sets are consistent and they show the proper trends with Reynolds number decreasing with increasing friction factor. Uncertainty plays a factor in an experiment such as this and can come from places including accurate pressure differential measurements and the eccentricity of the annulus to name a few. To obtain results within this range indicates the flow through an annular channel

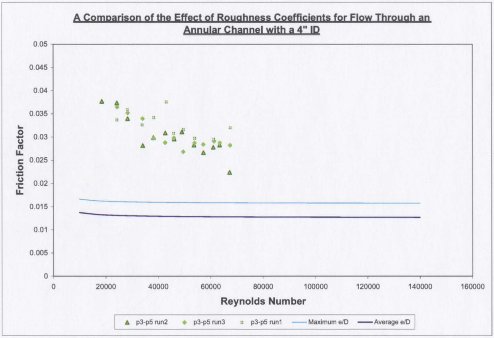

Figure 7.6: A Comparison of the Effect of Roughness Coefficients on Friction Factors

with roughened walls can be modeled to a certain degree.

Roughened Outer Pipe and Smooth Inner Pipe

Friction factor verses Reynolds number plots were generated for the data obtained for the case where the outer wall of the annulus was rough and the inner wall of the annulus was smooth. The first section of piping analyzed was the horizontal section. Here the fluids travels through a three inch diameter pipe which is considered smooth. This analysis was important to show the validity of the data obtained. The data was analyzed (see APPENDIX F), and the results of this analysis is shown in Figure 7.7.

This plot compares the experimental results to the Blasius theory. The piping in this section remains the same throughout the experiments and calculating the friction

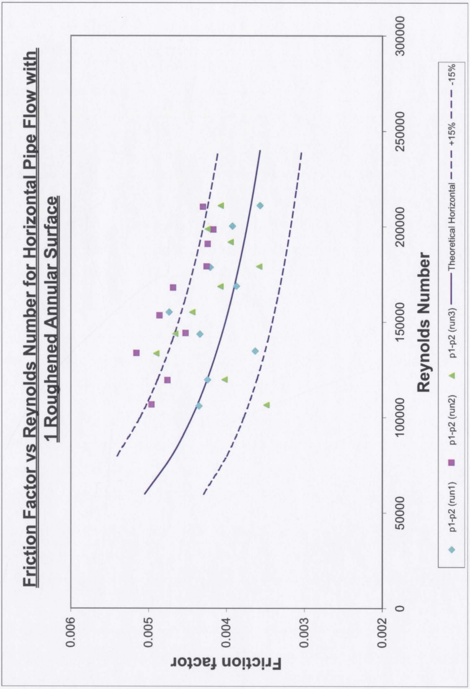

Figure 7.7: Friction Factor verses Reynolds Number for Horizontal Flow with 1 Roughened Surface in the Annulus

factors in this section is a good prediction of whether the experimental data is reliable. Each trial is depicted with a different symbol and colour and the Blasius theory line is shown as dark blue with a $\pm$ 15% error margin.

By examining Figure 7.7, it is observed that the experimental data is in good agreement with proven theory for most of the data obtained. The system cannot run flow rates higher than approximately 930 liters per minute with water as the working fluid due to the size of the pump, therefore the maximum Reynolds numbers to be plotted does not exceed approximately 215,000. From this plot, it is concluded that the results obtained are reliable and should produce dependable results for other test sections during these experiments.

The second test section studied was the vertical annular channel with one roughened wall. The friction factors calculated from these data points were all compared to the Swamee and Jain equation shown in Equation 7.7. The results from this analysis (see APPENDIX F for analysis) is shown in Figure 7.8.

As in the case with horizontal flow, each trial is depicted in a with a different symbol with a different colour. Trial one is shown in light blue, trial two in pink, and trial three in green. The theoretical line calculated from the Swamee and Jain equation is shown as dark blue with an error margin of $\pm$ 15%.

It is easily seen that these results do not fall withing the specified error margin. There are a number of factors which may influence the results. As mentioned in previous chapters, the instrumentation used to record the pressure readings has been found not to be the proper instrumentation for measuring small pressure differences. If each pressure measurement can fluctuate by a certain percentage than the possibility exists that one sensor may fluctuate above the correct reading while the other may fluctuate below the proper reading. The readings could also fluctuate in such a way that one deviates toward the correct reading, while the other deviates away. Such a situation as this would show a smaller pressure difference which would highly affect

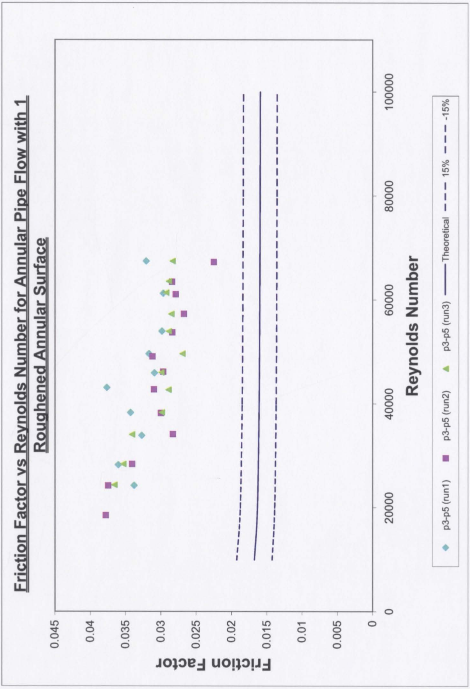

Figure 7.8: Friction Factor verses Reynolds Number for Annular Flow with 1 Roughened Surface in the Annulus

the outcome. All such scenarios would give an improper pressure drop across the test section and would cause the experimental friction factors to be out of the specified error range.

The degree of eccentricity of the annulus also can effect the experimental friction factors calculated. Studies by (Caetano, 1985) showed that friction factor decreased with increasing degree of eccentricity. If the inner pipe is able to move somewhat as the fluid passes by it, it may become more eccentric. As the eccentricity increases, the experimental friction factor would decrease according to Caetano (1985). With only two holding rings keeping it in place, there is a good possibility that this may be affecting the results obtained.

It is observed from Figure 7.8 that the value of the experimental friction factors are higher than the theoretical results. APPENDIX F shows the exact calculations carried out and compares both sets of data. The results do show the proper trends set out according to classic theory with friction factors decreasing with increasing Reynolds numbers. Overall the data does agree fairly well given the amount of uncertainty associated with the experiment.

Roughened Outer and Inner Pipe Walls

The last experiments carried out with axial flow through an annular channel was for the case with both the outer walls and the inner walls of the annular channel roughened. The outer wall was roughened to a higher degree than the inner wall and an effective roughness coefficient was determined.

The horizontal test section was evaluated to show the validity of the data collected, with all calculations found in APPENDIX F. Figure 7.9 shows most of the data point falling within the specified error margin of $\pm$ 15%. Four test trials were carried out due to equipment problems during the second trial. Only three data points were collected so this trial was carried out at a later time, but all resuts collected were recorded.

The experimental data agrees well with the theoretical results calculated for most all the data obtained. The sandpaper adds an increased resistance to the flow through the system. The maximum flow rate that could be obtained here was the lowest for all the axial flow experiments carried out. The maximum flow rate for these experiments was approximately 870 liters per minute and hence the maximum Reynolds numbers was approximately 63,000.

The second test section studied for the last set of experiments was with two roughened surfaces inside the annular channel, with each surface roughened to a different degree. Using the Swamee and Jain equation shown in Equation 7.7, the theoretical friction factors were calculated for which the experimental results were compared. The results from this analysis were plotted and are shown in Figure 7.10.

As in the other cases, each trial is depicted with a different symbol and colour. Trial one is in light blue, trial two in pink, trial three in green, and trial four in red. The line representing the theoretical results is shown as dark blue with a $\pm$ 15% error margin.

The experimental results for the case with two different roughened surfaces compared fairly well with theory with some of the data points falling within the specified margin of error, while the rest are slightly above. For Reynolds numbers above approximately 30,000 the data points are tending to drift further from theory. The higher the flow rate, and hence the higher the Reynolds number, the less accurate the experimental data was. This may be due to the increased flow rate inside the annulus causing the sandpaper to begin to come off the pipe walls. If the sandpaper moves inside the annulus, then the measures diameters are no longer accurate which would affect the calculations.

APPENDIX F shows the exact calculations carried out and compares both the data

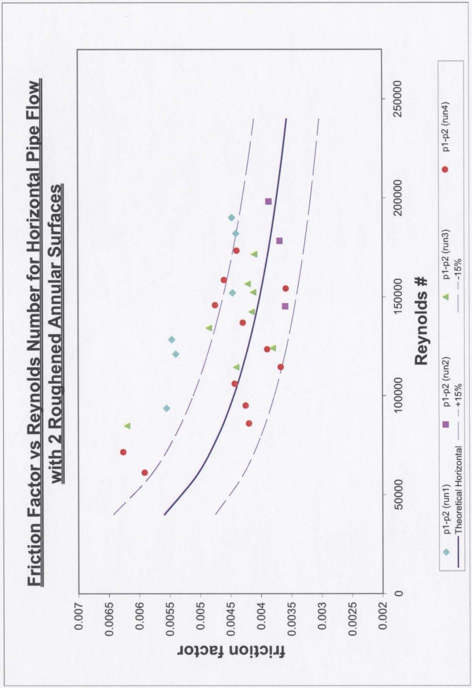

Figure 7.9: Friction Factor verses Reynolds Number for Horizontal Flow with 2 Roughened Surfaces in the Annulus

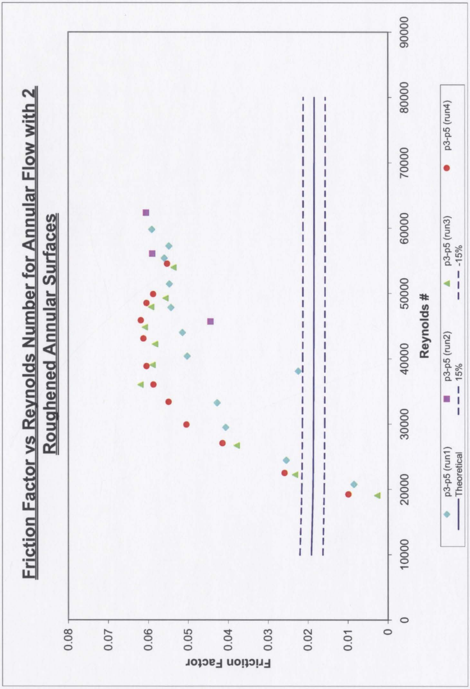

Figure 7.10: Friction Factor verses Reynolds Number for Annular Flow with 2 Roughened Surfaces in the Annulus

for the horizontal test section and the annular test section. The results do follow the trends set out according to theory and overall they do agree quite well.

Chapter 8

Conclusions and Recommendations

8.1 Benchmark Experiments

The benchmark experiments were required to determine whether or not the multiphase flow loop would provide reliable results. Experiments were carried out for circular pipe flow through a test section which incorporated both minor losses and major losses.

By plotting the experimental friction factors against Reynolds numbers along with calculated theory, I could determine that most of the experimental values were within plus or minus fifteen percent of the theoretical data plotted. Some data points on the plot were very close in proximity which shows the experiments are repeatable. From this graphical analysis I concluded that the flow loop produced reliable results.

Four different equations were used to plot the theoretical curves. The first theoretical method studied is one of the most widely used formulations and was developed by Blasius. It only considers friction factors for smooth pipe flow. Other equations by Swamee and Jain, Churchill, and Haaland were all studied and plotted on this benchmarking plot. All four equations produced very similar results with data from both Swamee and Jain and Churchill equations overlapping. From this information, I concluded that more than one theoretical method studied can be used to compare the experimental values. The Blasuis equation can be used for all cases with smooth pipe flow. When flow in roughened pipes is studied and the Blasius equation could no longer be used, one of the other equations which considered roughness effects can be used. The Swamee and Jain equation was chosen to evaluate these experiments theoretically.

8.2 Radial Inflow Experiments

Three annular channel sizes with radial inflow into an annular test section were investigated. For each experiment, a test matrix was created and followed. The valves on the inflow tubing were opened and closed in different sequences such that fluid could flow through one section, two sections, or all three sections.

Pressure and flow rates were plotted against position to determine the data trends. By examining any of the generated plots it is seen that as the height of the annular test section increases, the measured pressures decrease. The plots generated with all valves open and therefore inflow through all three radial sections showed that the pressures decreased and the flow rates increased as we get higher from the bottom of the test section. From this I concluded that the trends shown on these plots followed the trends expected for this type of flow.

Friction factor calculations were carried out with flow through the bottom radial inflow section only. In such a situation, complex fluid flow phenomena exists. As fluid enters the annular channel from the flexible tubing, it will tend to fill up the free space. As it does this, eddies will form in certain areas which will complicate the flow patterns. Entrance effects also play a significant role since the flow can become blocked at the entrance by boundary layer effects. As well, the actual flow rate can be lower than expected because of viscous friction effects. A discharge coefficient can be used in the calculations to help correct the flow rate.

After fluid enters the annular channel it will, in theory, have to stop flowing horizontally and then turn to flow vertically up through the annular test section and therefore a stagnant pressure component will have to be considered. As the fluid travels up through the test section it may begin to swirl. If this happens, the flow rates measured on the radial section will no longer be accurate. This swirling of the fluid would affect the local velocity and would have to be considered. One must also take into consideration accelerational effects inside the annular test section. Even though they may not be large, they may still have a substantial contribution to the overall pressures in the section under consideration.

The type of flow in this section is very complex and there are many factors that must be considered to accurately determine the friction factors. The method used to study radial inflow is a good approximation of what occurs when the reservoir fluid diffuses through the formation to the well in a parallel dual string or tubing-annulus completion, for example. It is concluded that simple analysis methods will not accurately model the radial inflow for this system. The experiments do not represent the actual inflow of reservoir fluid to the annulus, but are more of an approximation of the radial inflow.

8.3 Axial Flow Experiments

8.3.1 Experiments with Smooth Pipe Walls

Experiments were carried out for fluid flow through piping with smooth walls and varying sized annular channels. The first annular channel size studied was with a six inch diameter outer pipe and a three inch diameter inner pipe. The data was collected and friction factors were plotted against Reynolds numbers. When this data was compared to theory, scatter was observed in the data in the annular test section. It is believed that the low pressure drop in the measurements is contributing to this scatter.

The next annular channel size studied was with a six inch diameter outer pipe and a four inch diameter inner pipe. The results from these experiments produced data points within a plus or minus fifteen percentage range from theory and were not scattered as in the previous case. The pressure drops associated with these experiments were somewhat higher so this error was not as prominent.

The last annular channel size to be studied in these experiments was with a six inch diameter outer pipe and a five inch diameter inner pipe. Only one trial of experiments could be collected due to damage incurred to the inner piping. The results from only one trial could not be relied on so these experiments were not longer considered.

From the overall evaluation of axial flow through an annular channel, it can be concluded that flow with smooth walls can be modeled using the multiphase flow loop.

8.3.2 Experiments with Roughened Pipe Walls

Experiments were carried out to investigate frictional effects on flows through pipes with roughened walls. One annular channel size was studied with altering roughness values. The first experiments carried out were with a six inch diameter outer pipe with a roughened surface exposed to the fluid. The inner piping was four inch inner diameter with smooth walls. The second experiment carried out had the same roughness on the outer piping but with the inner surface roughened. Both surfaces did not have the same roughness value.

Friction factors were plotted against Reynolds numbers for the data collected and compared to Swamee and Jain theory. In both cases the experimental friction factors were higher and outside the fifteen percent error range than those determined experimentally. This type of flow, however, is more complex than smooth pipe flow with more uncertainty associated. To roughen the surfaces of the pipes, sandpaper was fastened to the walls and as the flow rates increased the sandpaper would become agitated and sometimes begin to move inside the test section. If this occurred during testing, the variable for hydraulic diameter used would not be accurate. If the fluid was traveling through a smaller diameter than was used in the calculations, the friction factors determined experimentally would be somewhat uncertain.

If a different method was used to roughen the walls of the piping, it is believe that better results would be found. Due to the methods used during these experiments, it is concluded that rough axial flow through an annular channel can be modeled decently well. With some adjustments to the test setup, it is speculated that this flow could be modeled better and would produce results that agreed a little closer with theory.

8.4 Recommendations

8.4.1 Radial Inflow Experiments

Some general recommendations can be made to improve the experiments carried out in this investigation. The radial inflow section can be redesigned to obtain better measurements. The measurements taken during during this study are affected by many factors since the flow measured is quite complex. The addition of more pressure sensors for the radial inflow experiments may help to explain what is happening to the complex flow system. In particular, a pressure measurement on the very bottom of the annular test section may be beneficial.

For some of the radial inflow analysis, pressure gradients could not be accurately deduced. Although the pressure transducers were earlier said to be adequate for data measurements, it has been found that for measuring small pressure gradients these transducers cannot accurately portray the pressure differences within an acceptable level of certainty. It is recommended to use differential pressure transducers when small pressure gradients are studied.

A large problem in particular for the radial inflow experiments is that the velocity in the annulus was not directly measured. The mean velocity is be calculated from the flow rate measured at the flow meters on the flexible tubing lines in the inflow sections. This velocity may not be the actual velocity traveling inside the annular test section. If the fluid is swirling as it rises up the section, the mean velocity calculated will not be the actual velocity in the annulus. This would cause the calculations carried out to be inaccurate.

To study annular friction losses with a permeable wall pipe, a wire or membrane filter wrapped perforated wall is suggested. To measure the turbulent velocity within the annuli, pitot tubes are recommended.

Consideration can also be given to visually recording the fluid at the point where it leaves the radial inflow section with the $1\frac{1}{4}$ inch diameter flexible tubing and enters the annular channel, which is a much larger volume. The fluid should fill the annular space in a cone-shaped manner and a visual recording of this may help to determine its size. More information on what is happening to the fluid will help explain why the measurements produce the values which were measured during experimentation.

8.4.2 Axial Flow Experiments with Roughened Pipe Walls

There is much uncertainty in the experiments with roughened pipes, partly caused by the method of choice used to roughen the piping in the test section. Attaching sandpaper was not the best method to use. As the flow rates increased, the fluid would agitate the sandpaper and eventually the sandpaper would start to dislodge. When this would happen, the multiphase flow loop would have to be drained and the test section would be removed where the test section would be taken apart so the sandpaper could be repositioned. With the sandpaper back in place, the test section was reassembled and returned to the multiphase flow loop which was then refilled with fluid and the testing could resume.

This was very time consuming and caused many delays during experimentation. In addition to this, the exact roughness coefficient also was uncertain because it was not practical to measure each particle on the sandpaper to determine its dimension. To remove some uncertainty involved in both of these issues, a different method to investigate roughness effects on flows could be used. Different materials have different known roughness coefficients associated with them, and it is recommended that instead of applying a type of roughness to a pipe, different materials can be purchased for the piping. This would eliminate the uncertainty in the roughness coefficients because they would be known. It would also eliminate some of the uncertainty in the measured values since there would be no sandpaper inside the test section to become dislodged from its position.

8.4.3 General Recommendations

A general recommendation which should improve the pressure measurements taken throughout the entire study is to choose a different type of pressure transducer to record the pressures in the test sections for when small gradients are measured. Differential pressure transducers are recommended instead of the gauge transducers that were used here.

A differential pressure transducer would record the difference in pressure and would have only one uncertainly value associated with it. By measuring pressures without using differential transducers, each pressure reading will have an associated uncertainty with it. One pressure could be reading too high and the other could be reading too low and this would cause the different in both readings to be too large. The opposite could also occur where one pressure could be reading too low and the second reading could be too high. This would cause the pressure difference to be too small. Either case would affect the values used and would cause any calculations carried out with these values to be incorrect.

In the experiments studied it seemed that as the pressure differentials became larger, the calculated friction factor values became closer to theoretical values. It was therefore concluded that an error in the values used in the calculations must be coming from the small pressure drops. If differential pressure transducers were used, the smaller pressure drops should be more accurate and the calculations carried out for these circumstances would better agree with theory formulated many years ago.

For further study of radial inflow and axial flow through an annular channel, one could consider two-phase flow. With two-phase flow, it is anticipated that the pressures recorded would be much higher and the issues of low pressure drops would not need to be addressed. A new range of Reynolds numbers could be studied which would give more information about flow inside an annular channel.

References

Allen, T.O., and Roberts, A.P. (1993). *Productions Operations, Well Completions, Workover, and Stimulation, Volume 1, fourth edition.* Tulsa, Oklahoma, Oil & Gas Consultants International Inc.

Asheim, H., Kolnes, J., and Oudeman, P.A. (1992). Flow Resistance Correlation for Completed Wellbore. *Journal of Petroleum Science and Engineering*, 8, 97-104.

Brighton, J.A., and Jones, J.B. (1964). Fully Developed Turbulent Flow in Annuli. *Journal of Basic Engineering*, 86, 835-844.

Beggs, H.D., and Brill, J.P. (1973). A Study of Two-Phase Flow in Inclined Pipes. *Journal of Petroleum Technology*, 25, 607-617.

Brice, B.W. (1992, 8-11 March). *Production Impacts on ΔP Friction in Horizontal Production Wells.* Presented at the SPE Second Latin American Petroleum Engineers Conference, Caracas, Venezuela.

Bogue, D.C and Metzner, A.B., (1963). Velocity profiles in turbulent pipe flow. *Industrial & Engineering Chemistry Fundamentals*, 2(2), 143-149.

Brill, J.P. (1987). Multiphase Flow in Wells. *Journal of Petroleum Technology*, 39(1), 15-21.

Brill, J. P., and Mukherjee, H. (1999). (1999) *Multiphase Flow in Wells, Volume 17.* Richardson, Texas, Society of Petroleum Engineers Inc.

Blevins, R.D. (1984). *Applied Fluid Dynamics Handbook.* Van Nostrand Reinhold Company Inc., New York.

Caetano, F.F. (1985). *Upward Two-Phase Flow Through an Annulus.* Ph.D. dissertation, University of Tulsa, Tulsa.

Card, J. (2004). *Design, Construction and Instrumentation of a Data Acquisition / Control System for the Multi-Phase Flow Loop at Memorial University of Newfoundland.* Unpublished Report, Memorial University of Newfoundland, Newfoundland.

Charles, M.E., Govier, G.W., and Hodgson, G.W. (1961). The Horizontal Pipeline Flow of Equal Density Oil-Water Mixtures. *The Canadian Journal of Chemical Engineering*, 39(1), 27-36.

Chisholm, D., and Laird, A.D.K. (1958). Two-Phase Flow in Rough Tubes. *Transactions of the American Society of Mechanical Engineers*, 80, 276-286.

Colebrook, C. F., and White, C. M. (1937, 3 August). Experiments with Fluid Flow in Roughened Pipes. *Proceedings of the Royal Society of London, Series A, Mathematical and Physical Sciences.* 161(906), 367-381.

Desouky, S.E.M., and El-Emam, N.A. (1990). A Generalized Pipeline Design Correlation for Pseudoplastic Fluids. *Journal of Canadian Petroleum Technology*, 29(5), 48-54.

Dikken, B. J. (1989, 8-11 October). *Pressure Drop in Horizontal Wells and its Effect on Their Production Performance.* Presented at the SPE 64^{th} Annual Technical Conference and Exhibition, San Antonio, Texas.

Dodge, D.W., and Metzner, A.B. (1959). Turbulent flow of a Non-Newtonian System. *American Institute of Chemical Engineering Journal*, 5(6), 189-204.

Economides, M. J., Hill, A. D., and Ehlig-Economides, C. (1994). *Petroleum Production Systems.* New Jersey: Prentice Hall PTR.

Govier, G.W., and Aziz, K. (1972). *The Flow of Complex Mixtures in Pipes.* New York: Van Nostrand Reinhold Ltd.

Govier, G.W., Sullivan, G.A., and Wood, R.K. (1961). The Upward Vertical Flow of Oil-Water Mixtures. *Canadian Journal of Chemical Engineering*, 39, 67-75.

Hall, C.D. (1969). General Turbulent Pipe Flow Scale-up Correlation for Rheological Complex Fluids. *Society of Petroleum Engineering Journal*, 9(3), 131-133.

Hasan, A.R., and Kabir, C.S. (1992). Two-Phase Flow in Vertical and Inclined Annuli. *International Journal of Multiphase Flow*, 18(2), 279-293.

Hasan, A.R., and Kabir, C.S. (1998) Predicting Multiphase Flow Behaviour In a Deviated Well. *Society of Petroleum Engineering Journal*, 3, 474-482.

Hasson, D., Orell, A., and Finik, M. (1971). A Study of Vertical Annular Liquid-Liquid Flow: Part I Laminar Conditions, Israel Institute of Technology, Haifa.

Hodge, B. K. and Taylor, R. P. (1999). *Analysis and Design of Energy Systems, third edition.* New Jersey, Prentice Hall.

Holdman, J.P. (2001). *Experimental Methods for Engineers, seventh edition.* New York, Mc-Graw Hill Companies Inc.

Jayanti, S., and Hewitt, G. F. (1996). Response of turbulent flow to abrupt changes in surface roughness and its relevance in horizontal annular flow. *Applied Mathematical Modeling*, 20, 244-251.

JJ Downs Industrial Plastics. *JJ Downs Industrial Plastics.*. Retrieved September 16, 2004 from http://www.jjdownsplastics.com/

Johansen, T.E. (2004). *Principles of Reservoir Engineering.* Unpublished, Memorial University of Newfoundland, St. John's, Canada.

Jones, O.C. Jr., and Leung, J.C.M. (1981). An Improvement in the Calculation of Turbulent friction in Smooth Concentric Annuli. *Journal of fluids Engineering*, 103, 615-623.

Kayode, C. (1991). Sizing Process Piping for Single Phase Fluids. *The Chemical Engineer*, 10, 19-25.

Kelessidis, V.C, and Dulker, A.E. (1989). Modeling Flow Pattern Transitions for Upwards Gas-Liquid Flow in Vertical Concentric and Eccentric Annuli. *International Journal of Multiphase Flow*, 15, 173-??.

Lacy, S., Ding, W., and Joshi, S.D. (1992, 8-11 March) *Horizontal Well Applications and Parameters for Economic Success.* Presented at the SPE 2^{nd} Latin American Petroleum Engineers Conference, Caracas, Venezuela.

Lage, A.C.V.M., and Time, R.W. (2000, 16-18 October) *An Experimental and Theoretical Investigation of Upward Two-Phase Flow in Annuli.* Presented at the SPE Asia Pacific Oil and Gas Conference and Exhibition, Brisbane, Australia.

Landman, M. J. (1994). Analytic Modeling of Selectively Perforated Horizontal Wells. *Journal of Petroleum Science and Engineering*, 10, 179-188.

Logan, E. JR., and Jones, J.B. (1963). Flow in a Pipe Following an Abrupt Increase in Surface Roughness. *Journal of Basic Engineering*, 35-39.

Memorial University of Newfoundland, Faculty of Engineering and Applied Sciences. (1997). *Multiphase Research Laboratory.* Retrieved September 5, 2004, from web site http://mpfl.engr.mun.ca/

Metal Finishing Systems. (2005). *Abrasive Grain Sizes - Grit Comparison.* Retrieved June 24, 2005, from web site: http://www.metalfinishingsystems.com/tt-abrasives.html

Nakoriakov, V.F., Kuznetsov, V.V., and Vitovsky, O.V. (1992). Experimental Investigation of Upward Gas-Liquid Flow in a Vertical Narrow Annulus. *International Journal of Multiphase Flow*, 3, 313-326.

Nind, T.E.W. (1981). *Principles of Oil Well Production, second edition.* New York, Mc-Graw Hill Book Company.

Novy, R. A. (1992, 4-7 October). *Pressure Drop in Horizontal Wells: When Can They Be Ignored?* Presented at the SPE 67^{th} Annual Technical Conference and Exhibition, Washington, D.C.

Oddie, G., Shi, H., Durlofsky, L.J., Aziz, K., Pfeffer, B., and Holmes, J.A. (2003). Experimental Study of Two and Three Phase Flows in Large Diameter Inclined Pipes. *International Journal of Multiphase Flow*, 29, 527-558.

Omega. (2002). *PX-603, Thin Film Transducer for Gage or Vacuum.* Retrieved August 25, 2004 from http://www.omega.ca/shop/pptsc.asp?ref=PX603

Omega. (2002). *TC-NPT, Rugged Pipe Plug Probe with 1/4 NPT Fitting.* Retrieved August 25, 2004 from http://www.omega.com/ppt/pptsc.asp?ref=TC-NPT

Omega. (2002). *FTB-730, Turbine Flow Meters.* Retrieved August 25, 2004 from http://www.omega.ca/shop/pptsc.asp?ref=FTB700

Omega. (2002). *FTB-930, Economical Ball Bearing Gas Turbine Flow Meters.* Retrieved August 25, 2004 from http://www.omega.ca/shop/pptsc.asp?ref=FTB930

Omega. (2002) *Pressure Transducers, Differential Pressure Transducers, DPT.* Retrieved July 26, 2005 from http://www.omega.ca/shop/subsectionSC.asp?subsection =B05&book=Pressure

Ouyang, L-B., Arbabi, S., and Aziz, K. (1997). *General Single Phase Wellbore Flow Model.* Unpublished Topical Report, Stanford University, California, USA.

Ouyang, L-B. and Aziz, K. (1996, October). *General Wellbore Flow Model for Horizontal, Vertical, and Slanted Well Completions.* Presented at the 71^{st} SPE Annual Technical Conference and Exhibition, Denver, Colorado.

Ouyang, L-B., and Aziz, K.: Steady State Gas Flow in Pipes, Journal of Petroleum Science and Engineering (1996).

Papadimitriou, D.A., and Shoham, O. (1991, 7-9 April) *A Mechanistic Model for Predicting Annulus Bottomhole Pressures in Pumping Wells.* Presented at the SPE Production Operation Symposium, Oklahoma City, Oklahoma. ***NOTE..done right***

Potter, M.C., and Wiggert, D.C. (1997). *Mechanics of Fluids* (2^{nd} Edition). New Jersey: Prentice-Hall Inc.

Sadatomi, M., Sato, Y., and Saruwatari, Y. (1982). Two-Phase Flow in Vertical Noncircular Channels. *International Journal of Multiphase Flow*, 8, 641-655.

Schulkes, R.M.S.M., Rinde, T, and Utvik, O.H. (1999). Pipe Flow With Radial Inflow: Experimental and Modeling Work. *Journal of Fluids Engineering*, 121, 106-111.

Schulkes, R.M.S.M., and Utvik, O.H. (1998). Pressure Drop in a Perforated Pipe With Radial Inflow: Single-Phase Flow. *Society of Petroleum Engineering Journal*, 3(1), 177-85.

Schulkes, R., Utvik, O. H., and Rinde, T., 1997. Pressure drop in horizontal wells: multiphase flow with radial inflow. Proceedings from 8th International Conference, Cannes, France: 18-20 June 1997: 45-55.

Shean, A.R. (1976). Pressure Drop and Phase Fraction in Oil-Water-Air Vertical

Pipe Flow. PhD Thesis (MIT)

Shi, H., Holmes, J. A., Diaz, L. R., and Aziz, K. (2004, 26-29 Septemeber) *Drift-Flux Parameters for Three-Phase Steady State Flow in Wellbores.* Presented at the SPE Annual Technical Conference and Exhibition, Houston, Texas.

Smith, S.P., Gregory, G.A., Murno, N., and Muqeem, M. (1998, 10-11 June). *Application of Multiphase Flow Methods to Horizontal Underbalanced Drilling.* Presented at the 1st North American Conference on Multiphase Technology: Technology from the Arctic to the Tropics, Banff, Canada.

Su, Z. and Gudmundsson, J. S. (1993, 3-6 October) *Friction Factor of Perforation Roughness in Pipes.* Presented at the SPE 68th Annual Technical Conference and Exhibition, Houston, Texas.

Su, Z., and Gudmundsson, J. S. (1995). Pressure Drop in Perforated Pipes. PROFIT Project Summary Reports, Norwegian Petroleum Directorate, Stavanger.

Su, Z., and Gudmundsson, J. S. (1995). Pressure Drop in Perforated Pipes. Report Department of Petroleum Engineering and Applied Geophysics, U. Trandheim, Norway.

Suiru, W. D. Jr., and Logan, E. Jr. (1977). Response of a Turbulent Pipe Flow to a Change in Roughness. *Journal of Fluids Engineering*, 99(3), 548-553.

Tshuva, M., Barnea, D., and Taitel, Y. (1999). Two-phase Flow in Inclined Parallel Pipes. *International Journal of Multiphase Flow*, 25, 1491-1503.

US Energy Information Administration. *EIA Supply.* Retrieved December 6, 2004 from web site: http://www.eia.doe.gov/pub/oil_gas/petroleum/analysis_publications /oil_market_basics/Supply_text.htm

Western Dynamics. (2004). *Friction Losses in Pipe Fittings Resistance Coefficient K.* Retrieved on September 17, 2005, from http://www.westerndynamics.com/Download /friclossfittings.pdf.

White, F. M. (1991). *Viscous Fluid Flow, second edition.* New York, Mc-Graw Hill Companies Inc.

Woods, G.S., Spedding, P.L., Watterson, J.K., and Raghunathan, R.S. (1998). Three Phase Oil/Water/Air Vertical Flow. *Institute for Chemical Engineers*, 76, 571-584.

Yuan, H., Sarica, C., and Brill, J.P. (1996, 18-20 November). *Effect of Perforation Density on a Single Phase Liquid Flow Behavior in Horizontal Wells.* Presented at the 2nd International Conference on Horizontal Well Technology, Calgary, Alberta.

Yuan, S.W. and Finkelstein, A.B.: Laminar Pipe Flow with Injection and Suction through a Porous Wall, Transactions of ASME, vol 78 (1956) 719-724.

Appendix A

Simulator Code for Pressure Gradient Comparison

```
import java.math.*;
import java.io.*;
import java.lang.*;

public class Simulator {

        //Constructor

        public Simulator() {

        }

        //OTHER

        public FileWriter fileWriter;
        public int flowRateStart;
        public int flowRateEnd;

        //COMPUTED VALUES

        public double flowArea;
        public double perimeter;
        public double hydrDiameter;
        public double fricLam;
        public double fricTurb;
        public double flowVel;
        public double volFlowRate;
        public double rEffektive;
        public double fluidVel2pow;
        public double[] dataM1;
        public double[] dataM2;
        public double[] dataM3;

        //INPUT VARIABLES

        public double outerRadius;
        public double innerRadius;
        public double density;
        public double length;
        public double wallRough;
        public double fluidVisc;
        public double volFlowRateTemp;
        public double flowType;
```

```
        //this variable states whether the taylorseries expansion or the logarithmic
expression should be used for computing fLaminar
        public double type;

        public void cFlowVel(double q) {

                flowVel = (q/flowArea);
        }

        public void cFlowArea() {

                flowArea = Math.PI*(Math.pow(outerRadius, 2) - Math.pow(innerRadius,
2));
        }

        public void cPerimeter() {

                perimeter = 2*Math.PI*(outerRadius + innerRadius);
        }

        public void cHydraulicDiameter() {

                hydrDiameter = 2*(outerRadius - innerRadius);
        }

        public double cReynold(double q) {

                double reynold =
(((density)*(q/flowArea)*(hydrDiameter))/fluidVisc);

                return reynold;
        }

        public double cReynoldEff(double q) {

                        double reynold =
(((density)*(q/flowArea)*(cDEffektive(q)))/fluidVisc);

                        return reynold;
        }

        public double cDEffektive(double q) {

                double dEffektive =
((64)*(hydrDiameter))/((this.cFlaminar(q))*(this.cReynold(q)));

                return dEffektive;

        }

//***************************************************************************************
*****

        //FRICTION FACTORS

        //METHOD 1 FINDING FRICTION FACTOR FOR TURBULENT FLOW ;
        //the Haaland friction factor must be implemented

        public double f1(double q) {

                double f1 = Math.pow(1.8*Math.log(6.9/cReynold(q) +
Math.pow(wallRough/3.7*hydrDiameter,10/9)),-2)*4;

                return f1;
        }
```

```
        public double f2(double q) {

                        double f2 = Math.pow(1.8*Math.log(6.9/cReynoldEff(q) +
Math.pow(wallRough/3.7*cDEffektive(q),10/9)),-2)*4;

                        return f2;
        }

        public double cFlaminar(double q) {

                double outer2pow = Math.pow(outerRadius,2);
                double inner2pow = Math.pow(innerRadius,2);
                double log = Math.pow(outerRadius,4) - Math.pow(innerRadius,4) -
(Math.pow(outer2pow - inner2pow,2)/Math.log(outerRadius/innerRadius));

                double fLam = (16*fluidVisc*hydrDiameter*(outer2pow -
inner2pow))/(density*(q/flowArea)*log);

                return fLam;
        }

        public double pressureDropM1T(double q) {

                double pressureDropM1T;

                pressureDropM1T =
(this.f1(q))*(density)*(Math.pow(q/flowArea,2))/((2)*(hydrDiameter));

                return pressureDropM1T;
        }

        //METHOD 2, Turbulent flow using the effective diameter

        public double pressureDropM2T(double q) {

                double pressureDropM2T;

                pressureDropM2T =
(this.f2(q))*(density)*(Math.pow(q/flowArea,2))/((2)*(cDEffektive(q)));

                return pressureDropM2T;
        }

        //COLLECTING DATA IN ARRAYS SO THAT TABELS AND GRAPHS MAY BE INITIATED
        //the integers a and b define the length of the interval

        public void dataM1() {

                dataM1 = new double[flowRateEnd-flowRateStart];
                int counter = 0;

                        for (int i=flowRateStart; i<flowRateEnd +40; i = i + 20) {

                                double number = (double) i;
                                double input = number/86400;

                                dataM1[counter] = pressureDropM1T(input);

                                //"Q = " + i + "                PressureDropGradient =
" +

                                System.out.println(dataM1[counter] + " Q :" +i);
                                counter++;
                        }
        }
```

```
	public void dataM2() {

		dataM2 = new double[flowRateEnd-flowRateStart];
		int counter = 0;

			for (int i=flowRateStart; i<flowRateEnd + 40; i = i + 20) {

				double number = (double) i;
				double input = number/86400;

				dataM2[counter] = pressureDropM2T(input);

				//"Q = " + i + "                PressureDropGradient =
" +

				System.out.println(dataM2[counter] + " Q :" +i);
				counter++;
			}
	}

	//KEYBOARD READER

	public String readString() {
		InputStreamReader read = new InputStreamReader(System.in);
		BufferedReader gattered = new BufferedReader(read);

			try {
				String readLine = gattered.readLine();
				return readLine;
				}
			catch (IOException i) {System.out.println("Error when
reading from keyboard!");
				return null;
				}
	}

	public double readDouble() {

		double number=0;

			try {
				number = Double.parseDouble(readString());
				}

			catch (NumberFormatException n) {System.out.println("This is
not a number, rerun program!");
				return 0;
				}
		return number;
	}

	public int readInt() {

		int number = 0;

		try {

			number = Integer.parseInt(readString());

		}

		catch (NumberFormatException n) {System.out.println("This is not a
number, rerun program!");

		return 0;

		}

	return number;

	}

	//THE PROGRAM
```

```
	public static void main(String[] args) {
		Simulator sim = new Simulator();

		System.out.println("Calculation of the pressuredrop gradient dp/dx
in a Concentric Annulus");

		System.out.println("Please set variables, SI units");
		System.out.println("");

		//System.out.println("Set Volume Flow rate (m^3/Dag)");

		//sim.volFlowRateTemp = sim.readDouble();

		System.out.println("Set the outher Radius (m)");

		sim.outerRadius = sim.readDouble();

		System.out.println("Set the inner Radius (m)");

		sim.innerRadius = sim.readDouble();

		System.out.println("Set fluid density (kg/m^3)");

		sim.density = sim.readDouble();

		//System.out.println("Set pipe length (m)");

		//sim.length = sim.readDouble();

		System.out.println("Set Wall Roughness (scalar)");

		sim.wallRough = sim.readDouble();

		System.out.println("Set fluid viscosity (Pa/s)");

		sim.fluidVisc = sim.readDouble();

		System.out.println("");

		System.out.println("Set flowRate interval");

		System.out.println("");

		System.out.println("Set starting value");

		sim.flowRateStart = sim.readInt();

		System.out.println("");

		System.out.println("Set end value");

		sim.flowRateEnd = sim.readInt();

		System.out.println("");

		//FIXED VARIABLES CALCULATED, NOW COMPARE THE DIFFERENT METHODS FOR
VARYING Q
		//= VOLUME FLOW RATE

		sim.cHydraulicDiameter();
		sim.cFlowArea();
		sim.cPerimeter();

		System.out.println("--------------Method 1 (LOG) using the hydraulic
diameter---------------");
		System.out.println("");
		sim.dataM1();
		System.out.println("---------------------Method 2 (LOG) using the
effective diameter-----------");
		System.out.println("");
		sim.dataM2();
		System.out.println("");
	}
}
```

Appendix B

Operating and Maintaining the Multiphase Flow Loop

B.1 Turning on the Flow Loop

To operate the multiphase flow loop, one must use the correct procedures. Without this, one poses the risk of damaging the equipment or even hurting themselves, therefore step by step instructions must be followed.

To begin operating the flow loop the first thing to be done is to turn on the breaker switch labeled FLOW LOOP. If it is not on, power will not be supplied to the system. This breaker switch is located on a side wall near the mixing tank.

Next, open the air valve that supplies the actuators located near the pressure regulator in the main line near the mixing and separating tanks.

The LabView program can now be opened on the flow loop's computer located on the second floor in the fluids lab behind the platform that supports the vertical test section. The program used to run the system is called *Kelly's Flow Loop DAQ Program.vi.* When the program opens, run it and fully open the FLUID OUT and FLUID RETURN actuators. This must be done before the pump can be turned on.

With the actuators open in the data acquisition system, the inverter on the wall can now be turned on, done by pressing the FWD button. The frequency should be set above 40 Hz to begin to ensure there is enough power to propel the fluid up the vertical portion of the flow loop and over the top. The default frequency for the inverter is set at 60 Hz and is adequate for most situations.

Data measurements can now be taken.

B.2 Shutting Down the Flow Loop

To shut down the multiphase flow loop, a similar procedure is always used to ensure it is shut down correctly. If air has been used as a working fluid, the slider which controls the air flow rate on the LabView screen must be slid all the way down. This is necessary to prevent any damage to the pump. Next, press STOP on the inverter to stop pumping fluid through the system.

The next step is to move the FLUID OUT and FLUID RETURN sliders to zero. With this done, the LabView program can now be stopped by pressing both STOP buttons in the bottom right hand corner of the screen. The entire program can now be closed down and the computer can be shut off.

The valve supplying air to the actuators is closed next. To bleed off excess pressure in the actuators, the air valve is opened to 45 degrees.

The final thing step in shutting down the multiphase flow loop is to turn off the breaker switches labeled FLOW LOOP located on the side wall near the mixing tank. The flow loop is now completely shut down and the user can leave the laboratory.

Appendix C

Benchmarking Calculations

Table A.1 Benchmark Data Analysis: Trial 1

KNOWNS:

$d=$	0.08255	m	$L_{p1\text{-}p6}=$	18.72	m	$\mu_w=$	0.00113	Pa.s
$A=$	0.00535	m^2	$z_6=$	1.07	m	$\rho_w=$	1000	kg/m^3
						$k_E=$	0.25	

TRIAL 1

For 130 LPM, 60 hz					
$Q_{130}=$	132.99	L/min	$V_{130}=$	0.414	m/s
$Q_{130}=$	0.0022	m^3/s	$Re_{D130}=$	30,254.22	
$P_1=$	12.245	kPa	$f_{exp}=$	**0.0041**	
$P_6=$	1.369	kPa	$f_{theory}=$	**0.0060**	
$\Delta P=$	10.876	kPa			

For 240 LPM, 45 hz					
$Q_{240}=$	241.79	L/min	$V_{240}=$	0.753	m/s
$Q_{240}=$	0.0040	m^3/s	$Re_{D240}=$	55,005.25	
$P_1=$	15.214	kPa	$f_{exp}=$	**0.0072**	
$P_6=$	2.648	kPa	$f_{theory}=$	**0.0052**	
$\Delta P=$	12.566	kPa			

For 350 LPM, 60 hz					
$Q_{350}=$	358.88	L/min	$V_{350}=$	1.118	m/s
$Q_{350}=$	0.0060	m^3/s	$Re_{D350}=$	81,642.05	
$P_1=$	20.237	kPa	$f_{exp}=$	**0.0043**	
$P_6=$	6.820	kPa	$f_{theory}=$	**0.0047**	
$\Delta P=$	13.417	kPa			

For 500 LPM, 45 hz					
$Q_{500}=$	503.54	L/min	$V_{500}=$	1.568	m/s
$Q_{500}=$	0.0084	m^3/s	$Re_{D500}=$	114,550.56	
$P_1=$	29.840	kPa	$f_{exp}=$	**0.0042**	
$P_6=$	13.697	kPa	$f_{theory}=$	**0.0043**	
$\Delta P=$	16.143	kPa			

For 550 LPM, 60 hz					
$Q_{550}=$	559.38	L/min	$V_{550}=$	1.742	m/s
$Q_{550}=$	0.0093	m^3/s	$Re_{D550}=$	127,253.49	
$P_1=$	34.258	kPa	$f_{exp}=$	**0.0042**	
$P_6=$	16.833	kPa	$f_{theory}=$	**0.0042**	
$\Delta P=$	17.424	kPa			

For 690 LPM, 45 hz					
$Q_{690}=$	690.33	L/min	$V_{690}=$	2.150	m/s
$Q_{690}=$	0.0115	m^3/s	$Re_{D690}=$	157,044.36	
$P_1=$	41.262	kPa	$f_{exp}=$	**0.0018**	
$P_6=$	25.224	kPa	$f_{theory}=$	**0.0040**	
$\Delta P=$	16.038	kPa			

For 770 LPM, 60 hz					
$Q_{770}=$	772.08	L/min	$V_{770}=$	2.404	m/s
$Q_{770}=$	0.0129	m^3/s	$Re_{D770}=$	175,641.06	
$P_1=$	35.825	kPa	$f_{exp}=$	**-0.0031**	
$P_6=$	31.353	kPa	$f_{theory}=$	**0.0039**	
$\Delta P=$	4.472	kPa			

For 850 LPM, 45 hz					
$Q_{850}=$	840.19	L/min	$V_{850}=$	2.616	m/s
$Q_{850}=$	0.0140	m^3/s	$Re_{D850}=$	191,134.62	
$P_1=$	60.494	kPa	$f_{exp}=$	**0.0034**	
$P_6=$	36.892	kPa	$f_{theory}=$	**0.0038**	
$\Delta P=$	23.602	kPa			

For 1020 LPM, 60 hz					
$Q_{1020}=$	1018.82	L/min	$V_{1020}=$	3.173	m/s
$Q_{1020}=$	0.0170	m^3/s	$Re_{D1020}=$	231,772.23	
$P_1=$	79.111	kPa	$f_{exp}=$	**0.0023**	
$P_6=$	54.308	kPa	$f_{theory}=$	**0.0592**	
$\Delta P=$	24.803	kPa			

Table A.2 Benchmark Data Analysis: Trial 2

TRIAL 2

For 125 LPM, 45 hz					
Q_{125}=	125.59	L/min	V_{125}=	0.391	m/s
Q_{125}=	0.0021	m^3/s	Re_{D125}=	28,569.62	
P_1=	12.111	kPa	f_{exp}=	**0.0047**	
P_6=	1.229	kPa	f_{theory}=	**0.0061**	
ΔP=	10.882	kPa			

For 230 LPM, 60 hz					
Q_{230}=	226.64	L/min	V_{230}=	0.706	m/s
Q_{230}=	0.0038	m^3/s	Re_{D230}=	51,558.06	
P_1=	13.6305	kPa	f_{exp}=	**0.0029**	
P_6=	2.2938	kPa	f_{theory}=	**0.0052**	
ΔP=	11.3367	kPa			

For 250 LPM, 45 hz					
Q_{250}=	249.59	L/min	V_{250}=	0.777	m/s
Q_{250}=	0.0042	m^3/s	Re_{D250}=	56,778.58	
P_1=	15.2083	kPa	f_{exp}=	**0.0053**	
P_6=	3.0219	kPa	f_{theory}=	**0.0051**	
ΔP=	12.1864	kPa			

For 300 LPM, 60 hz					
Q_{300}=	300.00	L/min	V_{300}=	0.934	m/s
Q_{300}=	0.0050	m^3/s	Re_{D300}=	68,248.10	
P_1=	17.052	kPa	f_{exp}=	**0.0032**	
P_6=	4.977	kPa	f_{theory}=	**0.0049**	
ΔP=	12.076	kPa			

For 530 LPM, 45 hz					
Q_{530}=	529.80	L/min	V_{530}=	1.650	m/s
Q_{530}=	0.0088	m^3/s	Re_{D530}=	120,524.32	
P_1=	31.296	kPa	f_{exp}=	**0.0038**	
P_6=	15.109	kPa	f_{theory}=	**0.0042**	
ΔP=	16.187	kPa			

For 550 LPM, 60 hz					
Q_{550}=	524.87	L/min	V_{550}=	1.634	m/s
Q_{550}=	0.0087	m^3/s	Re_{D550}=	119,402.81	
P_1=	34.561	kPa	f_{exp}=	**0.0046**	
P_6=	17.485	kPa	f_{theory}=	**0.0042**	
ΔP=	17.076	kPa			

For 690 LPM, 45 hz					
Q_{690}=	693.92	L/min	V_{690}=	2.161	m/s
Q_{690}=	0.0116	m^3/s	Re_{D690}=	157,859.33	
P_1=	45.150	kPa	f_{exp}=	**0.0035**	
P_6=	25.500	kPa	f_{theory}=	**0.0040**	
ΔP=	19.650	kPa			

For 750 LPM, 60 hz					
Q_{750}=	754.97	L/min	V_{750}=	2.351	m/s
Q_{750}=	0.0126	m^3/s	Re_{D750}=	171,749.49	
P_1=	45.510	kPa	f_{exp}=	**0.0012**	
P_6=	29.891	kPa	f_{theory}=	**0.0039**	
ΔP=	15.619	kPa			

For 850 LPM, 45 hz					
Q_{850}=	849.30	L/min	V_{850}=	2.645	m/s
Q_{850}=	0.0142	m^3/s	Re_{D850}=	193,208.40	
P_1=	61.013	kPa	f_{exp}=	**0.0032**	
P_6=	37.858	kPa	f_{theory}=	**0.0038**	
ΔP=	23.155	kPa			

For 950 LPM, 60 hz					
Q_{950}=	125.59	L/min	V_{950}=	0.391	m/s
Q_{950}=	0.0021	m^3/s	Re_{D950}=	28,569.62	
P_1=	12.111	kPa	f_{exp}=	**0.0047**	
P_6=	1.229	kPa	f_{theory}=	**0.0061**	
ΔP=	10.882	kPa			

For 1020 LPM, 60 hz					
Q_{1020}=	1022.98	L/min	V_{1020}=	3.186	m/s
Q_{1020}=	0.0170	m^3/s	Re_{D1020}=	232,718.21	
P_2=	77.671	kPa	f_{exp}=	**0.0020**	
P_6=	54.274	kPa	f_{theory}=	**0.0036**	
ΔP=	23.397	kPa			

Table A.3 Benchmark Data Analysis: Trial 3

TRIAL 3

For 290 LPM, 60 hz					
Q_{290}=	291.93	L/min	V_{10}=	0.909	m/s
Q_{290}=	0.0049	m^3/s	Re_{D10}=	66,412.28	
P_1=	16.866	kPa	f_{exp}=	**0.0041**	
P_6=	4.511	kPa	f_{theory}=	**0.0049**	
ΔP=	12.355	kPa			
For 410 LPM, 60 hz					
Q_{410}=	412.8691	L/min	V_{43}=	1.286	m/s
Q_{410}=	0.0069	m^3/s	Re_{D43}=	93,923.81	
P_1=	23.0921	kPa	f_{exp}=	**0.0034**	
P_6=	9.3894	kPa	f_{theory}=	**0.0045**	
ΔP=	13.7027	kPa			
For 630 LPM, 60 hz					
Q_{630}=	630.98	L/min	V_{45}=	1.965	m/s
Q_{630}=	0.0105	m^3/s	Re_{D45}=	143,542.60	
P_1=	39.140	kPa	f_{exp}=	**0.0033**	
P_6=	21.359	kPa	f_{theory}=	**0.0041**	
ΔP=	17.781	kPa			
For 780 LPM, 60 hz					
Q_{780}=	783.33	L/min	V_{115}=	2.439	m/s
Q_{780}=	0.0131	m^3/s	Re_{D115}=	178,200.69	
P_1=	53.614	kPa	f_{exp}=	**0.0032**	
P_6=	32.379	kPa	f_{theory}=	**0.0038**	
ΔP=	21.236	kPa			
For 870 LPM, 60 hz					
Q_{870}=	873.73	L/min	V_{125}=	2.721	m/s
Q_{870}=	0.0146	m^3/s	Re_{D125}=	198,765.53	
P_1=	63.620	kPa	f_{exp}=	**0.0032**	
P_6=	39.693	kPa	f_{theory}=	**0.0037**	
ΔP=	23.927	kPa			

For 875 LPM, 75 hz					
Q_{875}=	877.22	L/min	V_{230}=	2.732	m/s
Q_{875}=	0.0146	m^3/s	Re_{D230}=	199,559.59	
P_1=	63.927	kPa	f_{exp}=	**0.0030**	
P_6=	40.530	kPa	f_{theory}=	**0.0037**	
ΔP=	23.396	kPa			
For 950 LPM, 75 hz					
Q_{950}=	952.32	L/min	V_{250}=	2.966	m/s
Q_{950}=	0.0159	m^3/s	Re_{D250}=	216,642.66	
P_1=	71.942	kPa	f_{exp}=	**0.0027**	
P_6=	47.183	kPa	f_{theory}=	**0.0037**	
ΔP=	24.759	kPa			
For 1030 LPM, 75 hz					
Q_{1030}=	1022.91	L/min	V_{300}=	3.185	m/s
Q_{1030}=	0.0170	m^3/s	Re_{D300}=	232,702.41	
P_1=	82.077	kPa	f_{exp}=	**0.0029**	
P_6=	54.212	kPa	f_{theory}=	**0.0036**	
ΔP=	27.865	kPa			
For 1125 LPM, 75 hz					
Q_{1125}=	1122.57	L/min	V_{530}=	3.496	m/s
Q_{1125}=	0.0187	m^3/s	Re_{D530}=	255,373.90	
P_1=	95.796	kPa	f_{exp}=	**0.0029**	
P_6=	64.913	kPa	f_{theory}=	**0.0035**	
ΔP=	30.883	kPa			
For 1200 LPM, 75 hz					
Q_{1200}=	1183.11	L/min	V_{550}=	3.684	m/s
Q_{1200}=	0.0197	m^3/s	Re_{D550}=	269,146.39	
P_1=	104.804	kPa	f_{exp}=	**0.0028**	
P_6=	72.007	kPa	f_{theory}=	**0.0035**	
ΔP=	32.797	kPa			

Appendix D

Radial Inflow Experimental Results

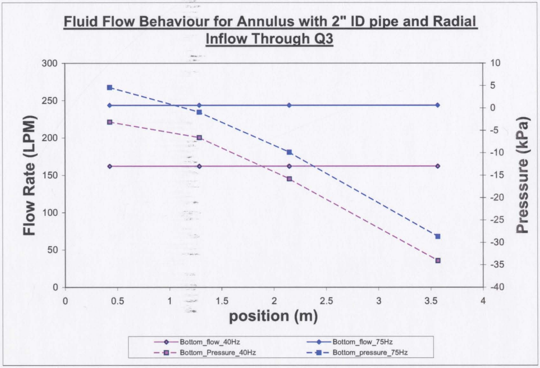

Figure B.1 Fluid Flow Behaviour with a 2" ID Annular Channel with Radial Inflow Through Q_3

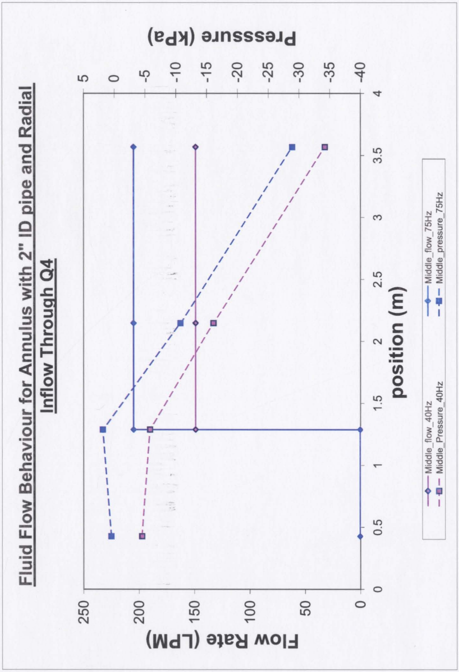

Figure B.2 Fluid Flow Behaviour with a 2" ID Annular Channel with Radial Inflow Through Q_4

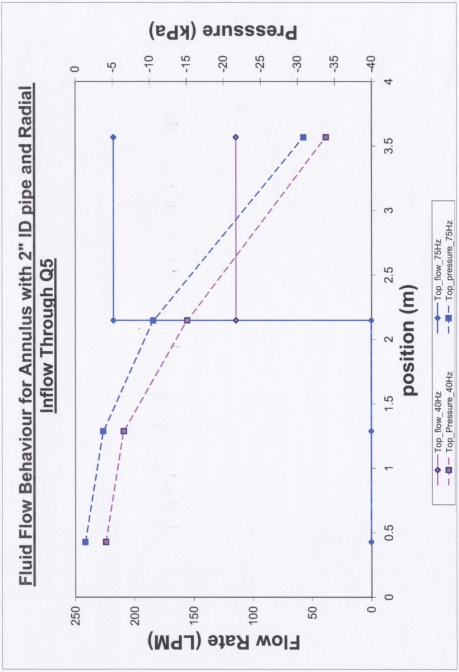

Figure B.3 Fluid Flow Behaviour with a 2" ID Annular Channel with Radial Inflow Through Q_5

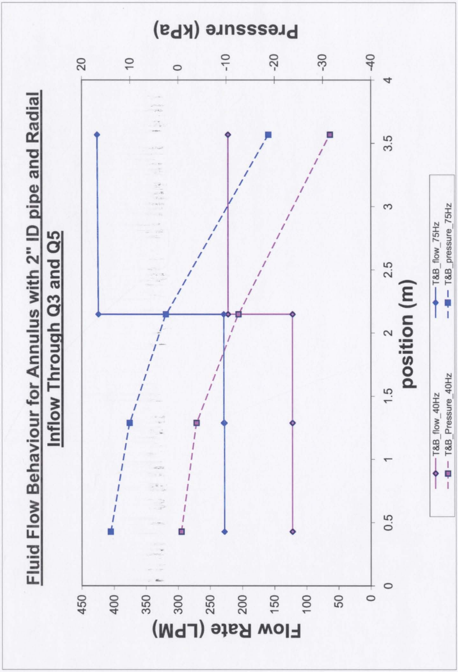

Figure B.4 Fluid Flow Behaviour with a 2" ID Annular Channel with Radial Inflow Through Q_3 and Q_5

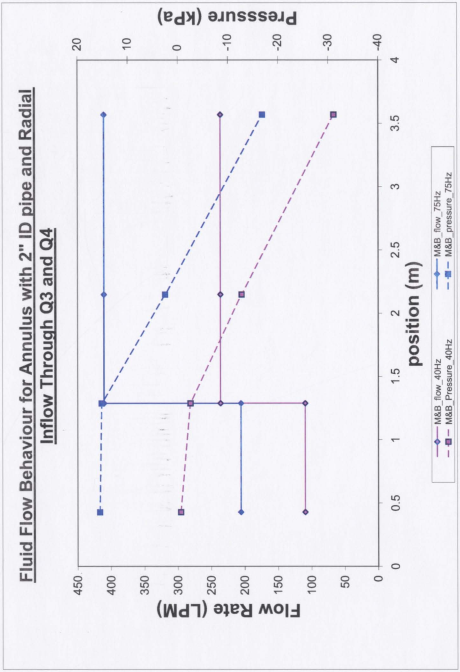

Figure B.5 Fluid Flow Behaviour with a 2" ID Annular Channel with Radial Inflow Through Q_3 and Q_4

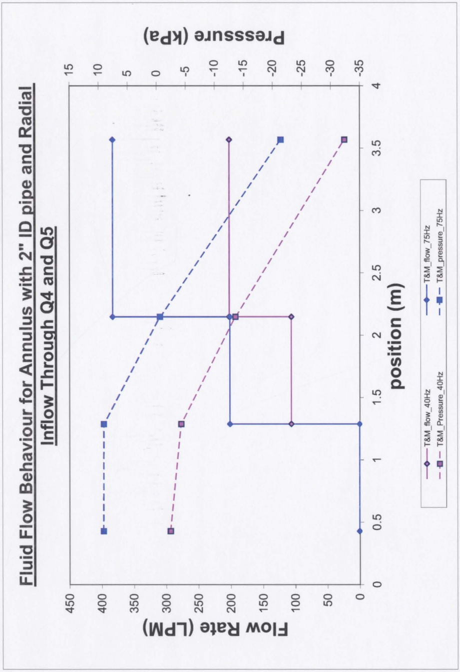

Figure B.6 Fluid Flow Behaviour with a 2" ID Annular Channel with Radial Inflow Through Q_4 and Q_5

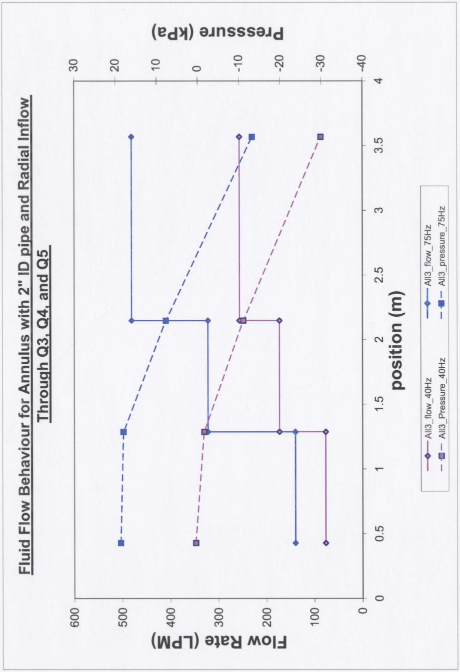

Figure B.7 Fluid Flow Behaviour with a 2" ID Annular Channel with Radial Inflow Through Q_3, Q_4 and Q_5

Table B.1 Data Summary for Radial Inflow with a 2" ID Annular Channel

File Name		Position (m)	Pressure (kPa)	Flow Rates (LPM)
6to2in_40hz_all3_002	*Bottom (P3)*	0.43	0.441	76.07
	Middle (P4)	1.29	-1.605	172.43
	Top (P5)	2.15	-11.146	255.31
	P6	3.57	-29.980	255.31
6to2in_40hz_Bot_002	*Bottom (P3)*	0.43	-3.080	162.33
	Middle (P4)	1.29	-6.555	162.33
	Top (P5)	2.15	-15.765	162.33
	P6	3.57	-34.023	162.33
6to2in_40hz_Mid_002	*Bottom (P3)*	0.43	-4.522	0
	Middle (P4)	1.29	-5.826	148.64
	Top (P5)	2.15	-16.149	148.636
	P6	3.57	-34.248	148.636
6to2in_40hz_Top_002	*Bottom (P3)*	0.43	-4.144	0
	Middle (P4)	1.29	-6.552	0
	Top (P5)	2.15	-15.136	114.31
	P6	3.57	-33.852	114.311
6to2in_40hz_Top&Mid_002	*Bottom (P3)*	0.43	-2.441	0
	Middle (P4)	1.29	-4.289	105.76
	Top (P5)	2.15	-13.632	201.81
	P6	3.57	-32.405	201.81
6to2in_40hz_Top&Bot_002	*Bottom (P3)*	0.43	-0.747	121.51
	Middle (P4)	1.29	-3.896	121.51
	Top (P5)	2.15	-12.589	221.69
	P6	3.57	-31.573	221.69
6to2in_40hz_Mid&Bot_002	*Bottom (P3)*	0.43	-0.646	109.06
	Middle (P4)	1.29	-2.558	235.85
	Top (P5)	2.15	-12.797	235.85
	P6	3.57	-31.164	235.85
6to2in_75hz_all3_002	*Bottom (P3)*	0.43	18.693	139.20
	Middle (P4)	1.29	18.013	321.12
	Top (P5)	2.15	7.693	480.12
	P6	3.57	-13.305	480.12
6to2in_75hz_Bot_002	*Bottom (P3)*	0.43	4.669	244.01
	Middle (P4)	1.29	-0.866	244.010
	Top (P5)	2.15	-9.811	244.010
	P6	3.57	-28.636	244.010
6to2in_75hz_Mid_002	*Bottom (P3)*	0.43	0.460	0
	Middle (P4)	1.29	1.859	204.81
	Top (P5)	2.15	-10.792	204.813
	P6	3.57	-28.940	204.813
6to2in_75hz_Top_002	*Bottom (P3)*	0.43	-1.370	0
	Middle (P4)	1.29	-3.797	0
	Top (P5)	2.15	-10.544	217.69
	P6	3.57	-30.828	217.688
6to2in_75hz_Top&Mid_002	*Bottom (P3)*	0.43	9.102	0.00
	Middle (P4)	1.29	9.041	200.90
	Top (P5)	2.15	-0.650	382.62
	P6	3.57	-21.449	382.62
6to2in_75hz_Top&Bot_002	*Bottom (P3)*	0.43	13.941	227.32
	Middle (P4)	1.29	10.033	228.32
	Top (P5)	2.15	2.465	423.71
	P6	3.57	-18.817	425.71
6to2in_75hz_Mid&Bot_002	*Bottom (P3)*	0.43	15.522	205.42
	Middle (P4)	1.29	15.178	410.23
	Top (P5)	2.15	2.468	410.23
	P6	3.57	-16.930	410.23

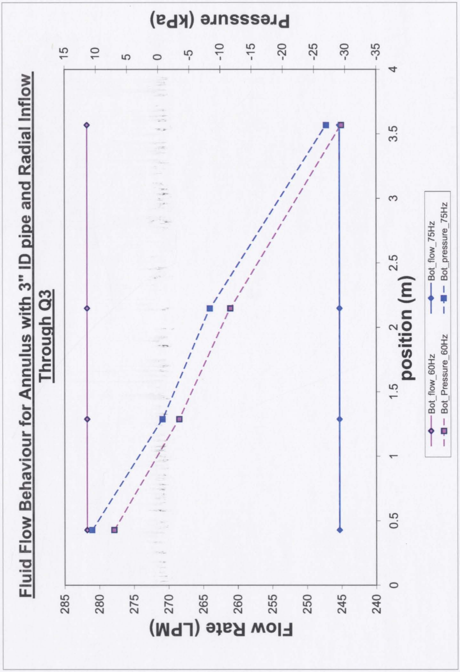

Figure B.8 Fluid Flow Behaviour with a 3" ID Annular Channel with Radial Inflow Through Q_3

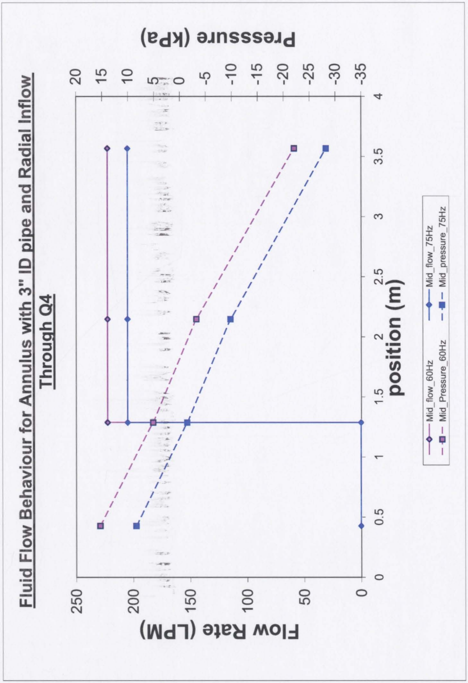

Figure B.9 Fluid Flow Behaviour with a 3" ID Annular Channel with Radial Inflow Through Q_4

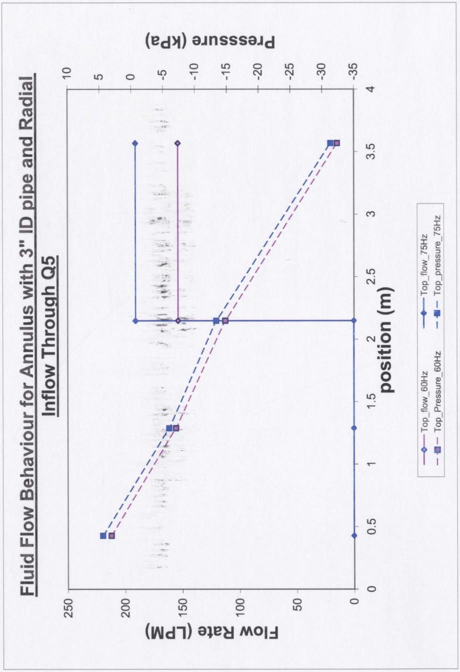

Figure B.10 Fluid Flow Behaviour with a 3" ID Annular Channel with Radial Inflow Through Q_5

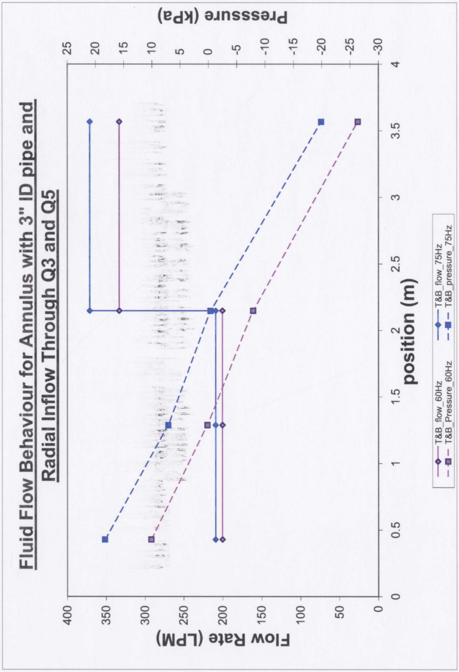

Figure B.11 Fluid Flow Behaviour with a 3" ID Annular Channel with Radial Inflow Through Q_3 and Q_5

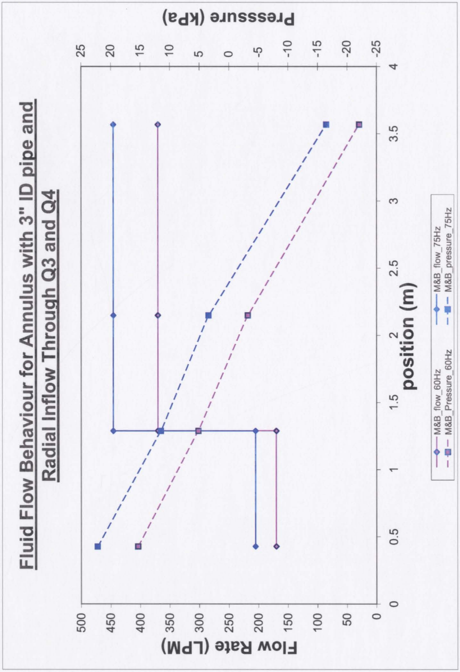

Figure B.12 Fluid Flow Behaviour with a 3" ID Annular Channel with Radial Inflow Through Q_3 and Q_4

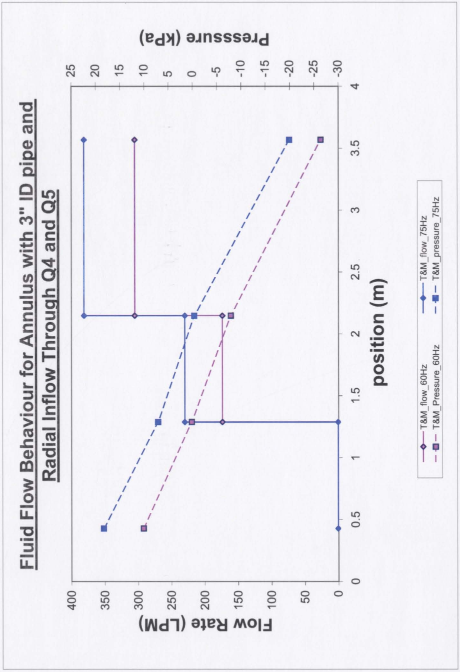

Figure B.13 Fluid Flow Behaviour with a 3" ID Annular Channel with Radial Inflow Through Q_4 and Q_5

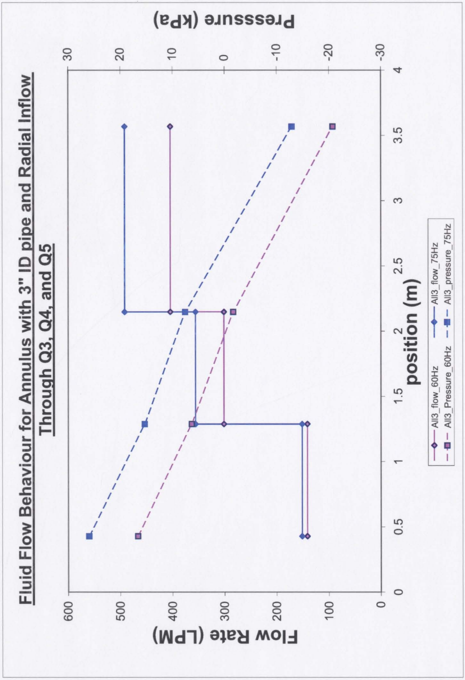

Figure B.14 Fluid Flow Behaviour with a 3" ID Annular Channel with Radial Inflow Through Q_3, Q_4 and Q_5

Table B.2 Data Summary for Radial Inflow with a 3" ID Annular Channel

File Name		Position (m)	Pressure (kPa)	Flow Rates (LPM)
6to3in_60hz_all3_001	***Bottom (P3)***	0.43	16.617	140.86
	Middle (P4)	1.29	6.275	300.81
	Top (P5)	2.15	-1.692	403.66
	P6	3.57	-20.795	403.66
6to3in_60hz_Bot_001	***Bottom (P3)***	0.43	7.036	281.72
	Middle (P4)	1.29	-3.427	281.72
	Top (P5)	2.15	-11.648	281.72
	P6	3.57	-29.434	281.72
6to3in_60hz_Mid_001	***Bottom (P3)***	0.43	15.358	0
	Middle (P4)	1.29	5.135	222.25
	Top (P5)	2.15	-3.232	222.25
	P6	3.57	-22.103	222.25
6to3in_60hz_Top_001	***Bottom (P3)***	0.43	3.153	0
	Middle (P4)	1.29	-7.018	0
	Top (P5)	2.15	-14.787	153.37
	P6	3.57	-32.388	153.37
6to3in_60hz_Top&Mid_001	***Bottom (P3)***	0.43	10.119	0
	Middle (P4)	1.29	0.150	173.40
	Top (P5)	2.15	-7.903	304.74
	P6	3.57	-26.419	304.74
6to3in_60hz_Top&Bot_001	***Bottom (P3)***	0.43	13.016	199.97
	Middle (P4)	1.29	2.197	199.97
	Top (P5)	2.15	-5.466	332.92
	P6	3.57	-24.286	332.92
6to3in_60hz_Mid&Bot_001	***Bottom (P3)***	0.43	15.358	169.37
	Middle (P4)	1.29	5.135	369.86
	Top (P5)	2.15	-3.232	369.86
	P6	3.57	-22.103	369.86
6to3in_75hz_all3_001	***Bottom (P3)***	0.43	25.968	150.98
	Middle (P4)	1.29	15.304	355.25
	Top (P5)	2.15	7.525	491.48
	P6	3.57	-12.936	491.48
6to3in_75hz_Bot_001-MAXED	***Bottom (P3)***	0.43	10.589	245.27
	Middle (P4)	1.29	-0.753	245.270
	Top (P5)	2.15	-8.364	245.270
	P6	3.57	-27.021	245.270
6to3in_75hz_Mid_001	***Bottom (P3)***	0.43	8.392	0
	Middle (P4)	1.29	-1.461	204.79
	Top (P5)	2.15	-9.822	204.794
	P6	3.57	-28.273	204.794
6to2in_75hz_Top_002	***Bottom (P3)***	0.43	4.468	0
	Middle (P4)	1.29	-5.963	0
	Top (P5)	2.15	-13.373	190.54
	P6	3.57	-31.363	190.54
6to3in_75hz_Top&Mid_001	***Bottom (P3)***	0.43	15.655	0.00
	Middle (P4)	1.29	5.596	229.62
	Top (P5)	2.15	-2.522	380.71
	P6	3.57	-21.863	380.71
6to3in_75hz_Top&Bot_001	***Bottom (P3)***	0.43	18.302	208.74
	Middle (P4)	1.29	7.101	208.74
	Top (P5)	2.15	-0.391	370.85
	P6	3.57	-19.948	370.85
6to2in_75hz_Mid&Bot_002	***Bottom (P3)***	0.43	22.203	204.79
	Middle (P4)	1.29	11.480	445.30
	Top (P5)	2.15	3.409	445.30
	P6	3.57	-16.501	445.30

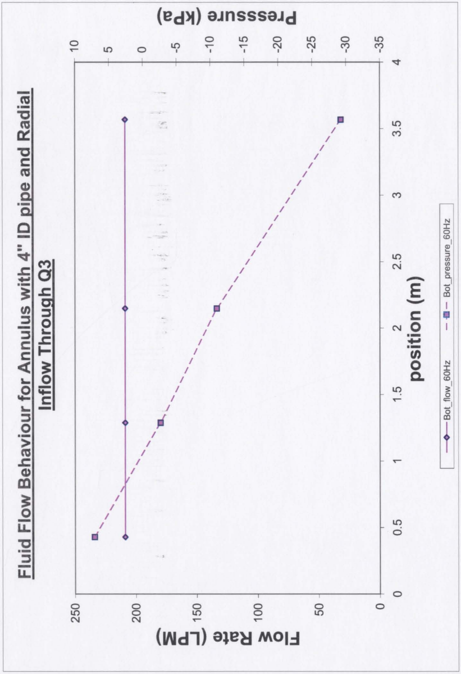

Figure B.15 Fluid Flow Behaviour with a 4" ID Annular Channel with Radial Inflow Through Q_3

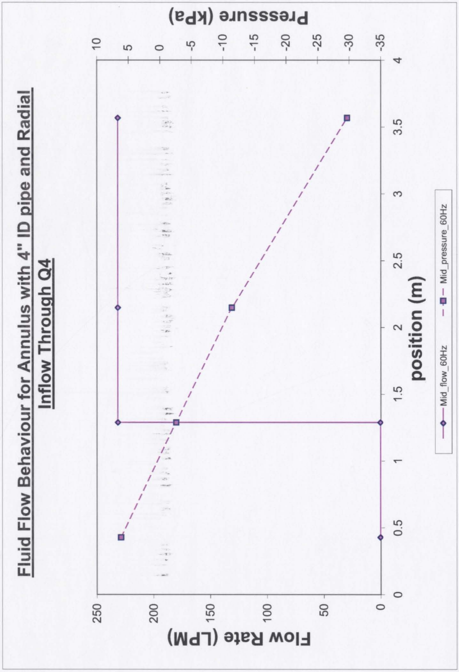

Figure B.16 Fluid Flow Behaviour with a 4" ID Annular Channel with Radial Inflow Through Q_4

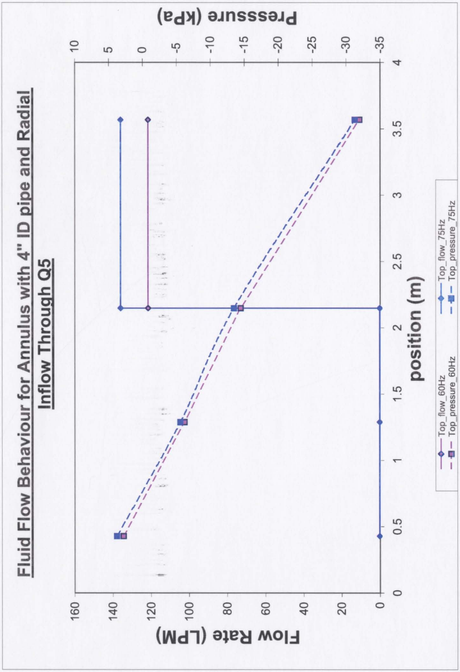

Figure B.17 Fluid Flow Behaviour with a 4" ID Annular Channel with Radial Inflow Through Q_5

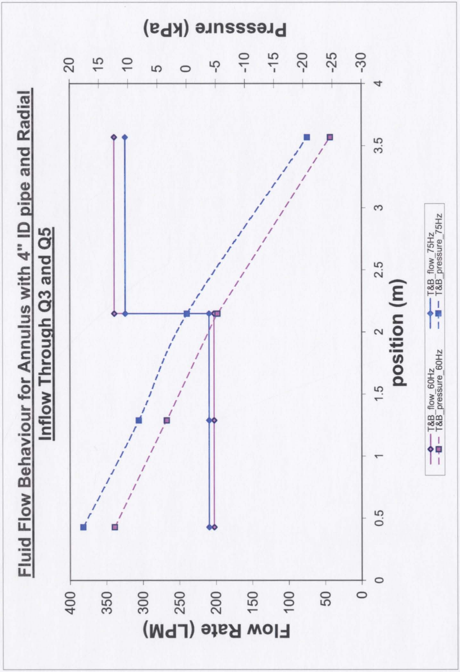

Figure B.18 Fluid Flow Behaviour with a 4" ID Annular Channel with Radial Inflow Through Q_3 and Q_5

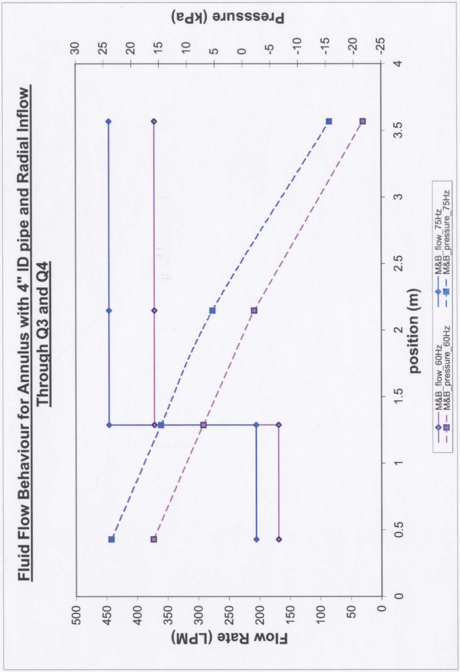

Figure B.19 Fluid Flow Behaviour with a 4" ID Annular Channel with Radial Inflow Through Q_3 and Q_4

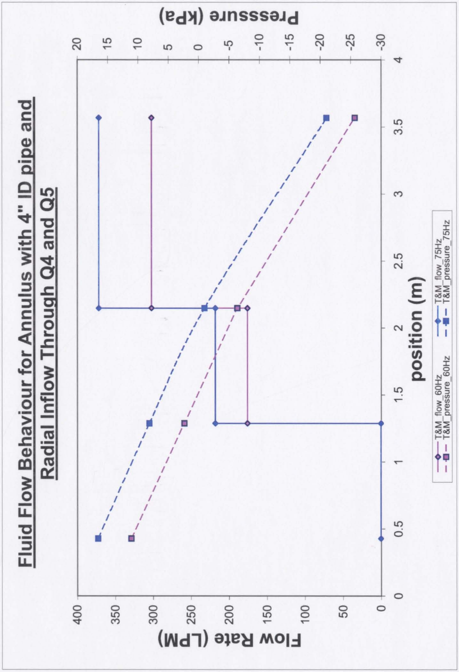

Figure B.20 Fluid Flow Behaviour with a 4" ID Annular Channel with Radial Inflow Through Q_4 and Q_5

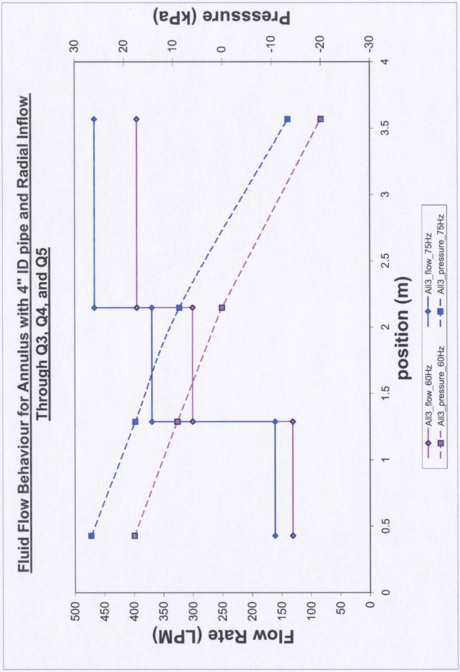

Figure B.21 Fluid Flow Behaviour with a 4" ID Annular Channel with Radial Inflow Through Q_3, Q_4 and Q_5

Table B.3 Data Summary for Radial Inflow with a 4" ID Annular Channel

File Name		Position (m)	Pressure (kPa)	Flow Rates (LPM)
6to4in_60hz_all3_001	***Bottom (P3)***	0.43	17.872	130.62
	Middle (P4)	1.29	9.109	299.91
	Top (P5)	2.15	0.045	394.36
	P6	3.57	-20.100	394.36
6to4in_60hz_Bot_001-MAXED	***Bottom (P3)***	0.43	7.094	208.74
	Middle (P4)	1.29	-2.660	208.74
	Top (P5)	2.15	-10.977	208.74
	P6	3.57	-29.291	208.74
6to4in_60hz_Mid_001	***Bottom (P3)***	0.43	6.138	0
	Middle (P4)	1.29	-2.607	231.23
	Top (P5)	2.15	-11.434	231.23
	P6	3.57	-29.735	231.23
6to4in_60hz_Top_001	***Bottom (P3)***	0.43	2.802	0
	Middle (P4)	1.29	-6.209	0
	Top (P5)	2.15	-14.484	121.48
	P6	3.57	-32.008	121.48
6to4in_60hz_Top&Mid_001	***Bottom (P3)***	0.43	11.098	0
	Middle (P4)	1.29	2.322	175.64
	Top (P5)	2.15	-6.377	302.00
	P6	3.57	-25.691	302.00
6to4in_60hz_Top&Bot_001	***Bottom (P3)***	0.43	12.330	201.88
	Middle (P4)	1.29	3.366	201.88
	Top (P5)	2.15	-5.334	338.72
	P6	3.57	-24.680	338.72
6to4in_60hz_Mid&Bot_001	***Bottom (P3)***	0.43	16.005	168.08
	Middle (P4)	1.29	7.021	370.97
	Top (P5)	2.15	-2.133	370.97
	P6	3.57	-21.771	370.97
6to4in_75hz_all3_001	***Bottom (P3)***	0.43	26.659	160.70
	Middle (P4)	1.29	17.693	369.18
	Top (P5)	2.15	8.689	466.33
	P6	3.57	-13.344	466.33
6to4in_75hz_Bot_001	***Bottom (P3)***			0
	Middle (P4)			0
	Top (P5)			0
	P6			0
6to4in_75hz_Mid_001 - MAXED	***Bottom (P3)***	0.43	9.290	0
	Middle (P4)	1.29	0.778	235.65
	Top (P5)	2.15	-9.115	235.651
	P6	3.57	-27.755	235.651
6to4in_75hz_Top_001	***Bottom (P3)***	0.43	3.770	0
	Middle (P4)	1.29	-5.598	0
	Top (P5)	2.15	-13.488	135.94
	P6	3.57	-31.322	135.94
6to3in_75hz_Top&Mid_001	***Bottom (P3)***	0.43	16.548	0.00
	Middle (P4)	1.29	8.107	217.91
	Top (P5)	2.15	-0.987	371.41
	P6	3.57	-21.051	371.41
6to3in_75hz_Top&Bot_001	***Bottom (P3)***	0.43	17.697	208.74
	Middle (P4)	1.29	8.168	208.74
	Top (P5)	2.15	-0.120	323.75
	P6	3.57	-20.733	323.75
6to2in_75hz_Mid&Bot_002	***Bottom (P3)***	0.43	23.600	204.76
	Middle (P4)	1.29	14.638	445.35
	Top (P5)	2.15	5.352	445.35
	P6	3.57	-15.687	445.35

Table B.4 Friction Factors Evaluated at P_3 to P_4 for Varying Annular Channels

KNOWNS

μ_w=	0.00113	Pa.s	Z_3=	0.43	m	D_2=	0.05715	m	D_4=	0.10795	m
ρ_w=	1000	kg/m^3	Z_4=	1.29	m	D_3=	0.08255	m	D_6=	0.1524	m
D_{tube}=	0.03175	m	Z_5=	2.15	m						

Between P3 and P4 - 6-2 inch Annulus

Case 1) Q3 is the only flow (i.e. bottom valve open)

Dh=	0.09525	m	Q3=	272.43	LPM
			Q=	0.004540	m^3/s
P3=	-1238.51	Pa	V_{tube}=	5.735	m/s
P4=	-3144.46	Pa	m dot=	4.540	L/s = kg/s
			V_3=	3.041	m/s
P_{34} term =	1905.95		Re=	256316.39	
height term =	8436.6		Cd=	0.61	
Pstag =	10030.90	Pa	f_{EXP}=	-0.09449	
Pacc =	9246.55	Pa	f_{THEORY}=	0.00351	

Case 1) Q3 is the only flow (i.e. bottom valve open)

Dh=	0.09525	m	Q3=	327.64	LPM
			Q=	0.005461	m^3/s
P3=	-2570.702	Pa	V_{tube}=	6.897	m/s
P4=	-960.238	Pa	m dot=	5.461	L/s = kg/s
			V_3=	3.657	m/s
P_{34} term =	-1610.46		Re=	308263.15	
height term =	8436.6		Cd=	0.61	
Pstag =	14508.76	Pa	f_{EXP}=	-0.09698	
Pacc =	13374.27	Pa	f_{THEORY}=	0.00335	

Between P3 and P4 - 6-3 inch Annulus

Case 1) Q3 is the only flow (i.e. bottom valve open)

Dh=	0.06985	m	Q3=	219.48	LPM
P3=	525.253	Pa	V_{tube}=	4.620	m/s
P4=	-3427.077	Pa	m dot=	3.658	L/s = kg/s
			V_3=	4.063	m/s
P_{34} term =	3952.33		Re=	251148.87	
height term =	8436.6		Cd=	0.61	
Pstag =	6510.70		f_{EXP}=	-0.05164	
Pacc =	16507.70		f_{THEORY}=	0.00353	

Case 1) Q3 is the only flow (i.e. bottom valve open)

Dh=	0.06985	m	Q3=	289.74	LPM
P3=	-757.750	Pa	V_{tube}=	6.099	m/s
P4=	-752.925	Pa	m dot=	4.829	L/s = kg/s
			V_3=	5.364	m/s
P_{34} term =	-4.82		Re=	331552.07	
height term =	8436.6		Cd=	0.61	
Pstag =	11346.69	Pa	f_{EXP}=	-0.05253	
Pacc =	28769.18544		f_{THEORY}=	0.00329	

Case 1) Q3 is the only flow (i.e. bottom valve open)

Dh=	0.06985	m	Q3=	277.47	LPM
P3=	-3787.543	Pa	V_{tube}=	5.841	m/s
P4=	-2792.408	Pa	m dot=	4.624	L/s = kg/s
			V_3=	5.136	m/s
P_{34} term =	-995.14		Re=	317505.55	
height term =	8436.6		Cd=	0.61	
Pstag =	10405.63	Pa	f_{EXP}=	-0.05513	
Pacc =	26383.15		f_{THEORY}=	0.00333	

Case 1) Q3 is the only flow (i.e. bottom valve open)

Dh=	0.06985	m	Q3=	327.03	LPM
P3=	-4766.623	Pa	V_{tube}=	6.884	m/s
P4=	-517.429	Pa	m dot=	5.451	L/s = kg/s
			V_3=	6.054	m/s
P_{34} term =	-4249.19		Re=	374221.05	
height term =	8436.6		Cd=	0.61	
Pstag =	14455.13	Pa	f_{EXP}=	-0.05467	
Pacc =	36650.55		f_{THEORY}=	0.00319	

Case 1) Q3 is the only flow (i.e. bottom valve open)

Dh=	0.06985	m	Q3=	239.49	LPM
P3=	-2701.024	Pa	V_{tube}=	5.042	m/s
P4=	-4427.368	Pa	m dot=	3.992	L/s = kg/s
			V_3=	4.433	m/s
P_{34} term =	1726.34		Re=	274050.60	
height term =	8436.6		Cd=	0.61	
Pstag =	7752.24	Pa	f_{EXP}=	-0.05447	
Pacc =	19655.57		f_{THEORY}=	0.00345	

Case 1) Q3 is the only flow (i.e. bottom valve open)

Dh=	0.06985	m	Q3=	329.14	LPM
P3=	-4381.666	Pa	V_{tube}=	6.929	m/s
P4=	-361.804	Pa	m dot=	5.486	L/s = kg/s
			V_3=	6.093	m/s
P_{34} term =	-4019.86		Re=	376632.74	
height term =	8436.6		Cd=	0.61	
Pstag =	14642.04	Pa	f_{EXP}=	-0.05424	
Pacc =	37124.47		f_{THEORY}=	0.00319	

Between P3 and P4 - 6-4 inch Annulus

Case 1) Q3 is the only flow (i.e. bottom valve open)

Dh=	0.04445	m	Q3=	278.98	LPM
P3=	-4632.34	Pa	V_{tube}=	5.873	m/s
P4=	-2659.86	Pa	m dot=	4.650	L/s = kg/s
			V_3=	11.509	m/s
P_{34} term =	-1972.48		Re=	452713.08	
height term =	8436.6		Cd=	0.68	
Pstag =	11726.43	Pa	f_{EXP}=	-0.02787	
Pacc =	132452.28		f_{THEORY}=	0.00305	

Case 1) Q3 is the only flow (i.e. bottom valve open)

Dh=	0.04445	m	Q3=	327.47	LPM
P3=	-6243.84	Pa	V_{tube}=	6.894	m/s
P4=	-159.30	Pa	m dot=	5.458	L/s = kg/s
			V_3=	13.509	m/s
P_{34} term =	-6084.54		Re=	531399.09	
height term =	8436.6		Cd=	0.68	
Pstag =	16157.02	Pa	f_{EXP}=	-0.02790	
Pacc =	182496.68		f_{THEORY}=	0.00293	

Case 1) Q3 is the only flow (i.e. bottom valve open)

Dh=	0.04445	m	Q3=	278.69	LPM
P3=	-4695.30	Pa	V_{tube}=	5.867	m/s
P4=	-2188.85	Pa	m dot=	4.645	L/s = kg/s
			V_3=	11.497	m/s
P_{34} term =	-2506.45		Re=	452240.52	
height term =	8436.6		Cd=	0.68	
Pstag =	11701.96	Pa	f_{EXP}=	-0.02798	
Pacc =	132175.90		f_{THEORY}=	0.00305	

Case 1) Q3 is the only flow (i.e. bottom valve open)

Dh=	0.04445	m	Q3=	326.52	LPM
P3=	-6325.45	Pa	V_{tube}=	6.874	m/s
P4=	234.15	Pa	m dot=	5.442	L/s = kg/s
			V_3=	13.470	m/s
P_{34} term =	-6559.60		Re=	529864.67	
height term =	8436.6		Cd=	0.68	
Pstag =	16063.84	Pa	f_{EXP}=	-0.02798	
Pacc =	181444.28		f_{THEORY}=	0.00293	

Appendix E

Smooth Axial Flow Calculations

Table C.1 Part 1: Smooth Axial Flow Through a 3" ID Annular Channel - Horizontal Analysis

KNOWNS:

$d_{3"}$=	0.08255	m	L_{P1-P2}=	4.68	m	ρ_w=	1000	kg/m^3
$A_{3"}$=	0.00535	m^2	μ_w=	0.00113	Pa.s			

TRIAL 1- HORIZONTAL TEST SECTION

For 73 hz					
Q=	1000.22	L/min	$V_{3"}$=	3.11	m/s
Q=	0.0167	m^3/s	$Re_{D\,3"}$=	227,541.35	
P_1=	115.664	kPa	f_{exp}=	**0.00369**	
P_2=	111.610	kPa	f_{theory}=	**0.00362**	
ΔP=	4.054	kPa			
For 67 hz					
Q=	944.34	L/min	$V_{3"}$=	2.94	m/s
Q=	0.0157	m^3/s	$Re_{D\,3"}$=	214,828.69	
P_1=	104.955	kPa	f_{exp}=	**0.00388**	
P_2=	101.155	kPa	f_{theory}=	**0.00367**	
ΔP=	3.800	kPa			
For 60 hz					
Q=	852.11	L/min	$V_{3"}$=	2.65	m/s
Q=	0.0142	m^3/s	$Re_{D\,3"}$=	193,847.04	
P_1=	89.869	kPa	f_{exp}=	**0.00393**	
P_2=	86.733	kPa	f_{theory}=	**0.00376**	
ΔP=	3.135	kPa			
For 52 hz					
Q=	756.38	L/min	$V_{3"}$=	2.36	m/s
Q=	0.0126	m^3/s	$Re_{D\,3"}$=	172,069.13	
P_1=	71.868	kPa	f_{exp}=	**0.00433**	
P_2=	69.145	kPa	f_{theory}=	**0.00388**	
ΔP=	2.723	kPa			

For 45 hz					
Q=	652.54	L/min	$V_{3"}$=	2.03	m/s
Q=	0.0109	m^3/s	$Re_{D\,3"}$=	148,447.39	
P_1=	57.030	kPa	f_{exp}=	**0.00469**	
P_2=	54.832	kPa	f_{theory}=	**0.00402**	
ΔP=	2.198	kPa			
For 37 hz					
Q=	534.38	L/min	$V_{3"}$=	1.66	m/s
Q=	0.0089	m^3/s	$Re_{D\,3"}$=	121,567.41	
P_1=	41.944	kPa	f_{exp}=	**0.00423**	
P_2=	40.617	kPa	f_{theory}=	**0.00423**	
ΔP=	1.327	kPa			
For 30 hz					
Q=	431.84	L/min	$V_{3"}$=	1.34	m/s
Q=	0.0072	m^3/s	$Re_{D\,3"}$=	98,240.38	
P_1=	30.823	kPa	f_{exp}=	**0.00175**	
P_2=	30.463	kPa	f_{theory}=	**0.00446**	
ΔP=	0.359	kPa			
For 22 hz					
Q=	313.86	L/min	$V_{3"}$=	0.98	m/s
Q=	0.0052	m^3/s	$Re_{D\,3"}$=	71,400.21	
P_1=	20.981	kPa	f_{exp}=	**-0.00069**	
P_2=	21.056	kPa	f_{theory}=	**0.00483**	
ΔP=	-0.075	kPa			

Table C.2 Part 2: Smooth Axial Flow Through a 3" ID Annular Channel - Horizontal Analysis

TRIAL 2- HORIZONTAL TEST SECTION

For 73 hz

Q=	966.67	L/min	$V_{3"}$=	3.01	m/s
Q=	0.0161	m^3/s	$Re_{D\,3"}$=	219,909.21	
P_1=	107.130	kPa	f_{exp}=	0.00457	
P_2=	102.436	kPa	f_{theory}=	0.00365	
ΔP=	4.694	kPa			

For 67 hz

Q=	912.90	L/min	$V_{3"}$=	2.84	m/s
Q=	0.0152	m^3/s	$Re_{D\,3"}$=	207,675.67	
P_1=	98.301	kPa	f_{exp}=	0.00517	
P_2=	93.567	kPa	f_{theory}=	0.00370	
ΔP=	4.734	kPa			

For 60 hz

Q=	823.60	L/min	$V_{3"}$=	2.56	m/s
Q=	0.0137	m^3/s	$Re_{D\,3"}$=	187,361.01	
P_1=	85.860	kPa	f_{exp}=	0.00609	
P_2=	81.318	kPa	f_{theory}=	0.00380	
ΔP=	4.542	kPa			

For 56 hz

Q=	773.94	L/min	$V_{3"}$=	2.41	m/s
Q=	0.0129	m^3/s	$Re_{D\,3"}$=	176,062.91	
P_1=	77.569	kPa	f_{exp}=	0.00492	
P_2=	74.327	kPa	f_{theory}=	0.00386	
ΔP=	3.242	kPa			

For 52 hz

Q=	719.04	L/min	$V_{3"}$=	2.24	m/s
Q=	0.0120	m^3/s	$Re_{D\,3"}$=	163,575.43	
P_1=	69.609	kPa	f_{exp}=	0.00558	
P_2=	66.440	kPa	f_{theory}=	0.00393	
ΔP=	3.169	kPa			

For 45 hz

Q=	633.73	L/min	$V_{3"}$=	1.97	m/s
Q=	0.0106	m^3/s	$Re_{D\,3"}$=	144,168.16	
P_1=	56.469	kPa	f_{exp}=	0.00614	
P_2=	53.758	kPa	f_{theory}=	0.00405	
ΔP=	2.712	kPa			

For 40 hz

Q=	561.31	L/min	$V_{3"}$=	1.75	m/s
Q=	0.0094	m^3/s	$Re_{D\,3"}$=	127,692.68	
P_1=	47.759	kPa	f_{exp}=	0.00576	
P_2=	45.763	kPa	f_{theory}=	0.00418	
ΔP=	1.995	kPa			

For 36 hz

Q=	505.08	L/min	$V_{3"}$=	1.57	m/s
Q=	0.0084	m^3/s	$Re_{D\,3"}$=	114,901.79	
P_1=	41.729	kPa	f_{exp}=	0.00671	
P_2=	39.848	kPa	f_{theory}=	0.00429	
ΔP=	1.881	kPa			

For 30 hz

Q=	419.99	L/min	$V_{3"}$=	1.31	m/s
Q=	0.0070	m^3/s	$Re_{D\,3"}$=	95,543.97	
P_1=	33.516	kPa	f_{exp}=	0.00747	
P_2=	32.066	kPa	f_{theory}=	0.00449	
ΔP=	1.450	kPa			

For 26 hz

Q=	362.99	L/min	$V_{3"}$=	1.13	m/s
Q=	0.0060	m^3/s	$Re_{D\,3"}$=	82,577.38	
P_1=	28.735	kPa	f_{exp}=	0.00792	
P_2=	27.588	kPa	f_{theory}=	0.00466	
ΔP=	1.147	kPa			

For 20 hz

Q=	277.29	L/min	$V_{3"}$=	0.86	m/s
Q=	0.0046	m^3/s	$Re_{D\,3"}$=	63,080.55	
P_1=	22.490	kPa	f_{exp}=	0.00618	
P_2=	21.967	kPa	f_{theory}=	0.00498	
ΔP=	0.523	kPa			

TRIAL 3- HORIZONTAL TEST SECTION

For 73 hz

Q=	997.51	L/min	$V_{3"}$=	3.11	m/s
Q=	0.0166	m^3/s	$Re_{D\,3"}$=	226,924.79	
P_1=	113.288	kPa	f_{exp}=	0.00399	
P_2=	108.926	kPa	f_{theory}=	0.00362	
ΔP=	4.362	kPa			

For 67 hz

Q=	933.65	L/min	$V_{3"}$=	2.91	m/s
Q=	0.0156	m^3/s	$Re_{D\,3"}$=	212,395.88	
P_1=	101.340	kPa	f_{exp}=	0.00397	
P_2=	97.540	kPa	f_{theory}=	0.00368	
ΔP=	3.801	kPa			

For 60 hz

Q=	849.48	L/min	$V_{3"}$=	2.65	m/s
Q=	0.0142	m^3/s	$Re_{D\,3"}$=	193,248.40	
P_1=	86.679	kPa	f_{exp}=	0.00421	
P_2=	83.340	kPa	f_{theory}=	0.00377	
ΔP=	3.339	kPa			

For 56 hz

Q=	796.08	L/min	$V_{3"}$=	2.48	m/s
Q=	0.0133	m^3/s	$Re_{D\,3"}$=	181,101.22	
P_1=	78.922	kPa	f_{exp}=	0.00420	
P_2=	75.997	kPa	f_{theory}=	0.00383	
ΔP=	2.925	kPa			

For 40 hz

Q=	565.99	L/min	$V_{3"}$=	1.76	m/s
Q=	0.0094	m^3/s	$Re_{D\,3"}$=	128,757.41	
P_1=	47.821	kPa	f_{exp}=	0.00477	
P_2=	46.142	kPa	f_{theory}=	0.00417	
ΔP=	1.679	kPa			

For 36 hz

Q=	507.70	L/min	$V_{3"}$=	1.58	m/s
Q=	0.0085	m^3/s	$Re_{D\,3"}$=	115,497.54	
P_1=	41.692	kPa	f_{exp}=	0.00509	
P_2=	40.249	kPa	f_{theory}=	0.00429	
ΔP=	1.443	kPa			

For 30 hz

Q=	421.65	L/min	$V_{3"}$=	1.31	m/s
Q=	0.0070	m^3/s	$Re_{D\,3"}$=	95,921.12	
P_1=	32.877	kPa	f_{exp}=	0.00782	
P_2=	31.348	kPa	f_{theory}=	0.00449	
ΔP=	1.529	kPa			

For 26 hz

Q=	364.24	L/min	$V_{3"}$=	1.13	m/s
Q=	0.0061	m^3/s	$Re_{D\,3"}$=	82,862.25	
P_1=	27.391	kPa	f_{exp}=	0.00918	
P_2=	26.051	kPa	f_{theory}=	0.00466	
ΔP=	1.340	kPa			

Table C.3 Part 3: Smooth Axial Flow Through a 3" ID Annular Channel - Horizontal Analysis

For 52 hz					
Q=	738.53	L/min	$V_{3''}$=	2.30	m/s
Q=	0.0123	m^3/s	$Re_{D\,3''}$=	168,009.38	
P_1=	70.910	kPa	f_{exp}=	**0.00437**	
P_2=	68.287	kPa	f_{theory}=	**0.00390**	
ΔP=	2.622	kPa			

For 45 hz					
Q=	637.36	L/min	$V_{3''}$=	1.98	m/s
Q=	0.0106	m^3/s	$Re_{D\,3''}$=	144,994.50	
P_1=	56.569	kPa	f_{exp}=	**0.00458**	
P_2=	54.523	kPa	f_{theory}=	**0.00405**	
ΔP=	2.046	kPa			

For 20 hz					
Q=	278.08	L/min	$V_{3''}$=	0.87	m/s
Q=	0.0046	m^3/s	$Re_{D\,3''}$=	63,261.23	
P_1=	20.564	kPa	f_{exp}=	**0.00919**	
P_2=	19.783	kPa	f_{theory}=	**0.00498**	
ΔP=	0.782	kPa			

Table C.4 Part 1: Smooth Axial Flow Through a 3" ID Annular Channel - Annular Flow Analysis

KNOWNS

Do=	0.1524	m	A_{ann}=	0.01289	m^2	μ_w=	0.00113	Pa.m
Di=	0.08255	m	$L_{P3\text{-}P5}$=	1.727	m	ρ_w=	1000	kg/m^3
Dh=	0.06985	m				z_5=	1.727	m (z_3=0)

TRIAL 2- ANNULAR TEST SECTION

For 73 hz					
Q=	966.67	L/min	V_{ann}=	1.250	m/s
Q=	0.0161	m^3/s	Re_D=	77,265.40	
P_3=	87.462	kPa	f_{exp}=	**0.01734**	
P_5=	69.180	kPa	f_{theory}=	**0.00474**	
ΔP=	18.281	kPa			

For 67 hz					
Q=	912.90	L/min	V_{ann}=	1.180	m/s
Q=	0.0152	m^3/s	Re_D=	72,967.13	
P_3=	78.859	kPa	f_{exp}=	**0.02017**	
P_5=	60.528	kPa	f_{theory}=	**0.00481**	
ΔP=	18.332	kPa			

For 60 hz					
Q=	823.60	L/min	V_{ann}=	1.065	m/s
Q=	0.0137	m^3/s	Re_D=	65,829.54	
P_3=	67.190	kPa	f_{exp}=	**0.01637**	
P_5=	49.330	kPa	f_{theory}=	**0.00493**	
ΔP=	17.860	kPa			

For 56 hz					
Q=	773.94	L/min	V_{ann}=	1.001	m/s
Q=	0.0129	m^3/s	Re_D=	61,859.94	
P_3=	59.738	kPa	f_{exp}=	**0.01427**	
P_5=	42.089	kPa	f_{theory}=	**0.00501**	
ΔP=	17.648	kPa			

For 40 hz					
Q=	561.31	L/min	V_{ann}=	0.726	m/s
Q=	0.0094	m^3/s	Re_D=	44,865.00	
P_3=	31.822	kPa	f_{exp}=	**-0.00653**	
P_5=	15.051	kPa	f_{theory}=	**0.00543**	
ΔP=	16.772	kPa			

For 36 hz					
Q=	505.08	L/min	V_{ann}=	0.653	m/s
Q=	0.0084	m^3/s	Re_D=	40,370.90	
P_3=	26.324	kPa	f_{exp}=	**-0.00842**	
P_5=	9.560	kPa	f_{theory}=	**0.00557**	
ΔP=	16.764	kPa			

For 30 hz					
Q=	419.99	L/min	V_{ann}=	0.543	m/s
Q=	0.0070	m^3/s	Re_D=	33,569.50	
P_3=	18.901	kPa	f_{exp}=	**-0.01177**	
P_5=	2.131	kPa	f_{theory}=	**0.00584**	
ΔP=	16.770	kPa			

For 26 hz					
Q=	362.99	L/min	V_{ann}=	0.469	m/s
Q=	0.0060	m^3/s	Re_D=	29,013.68	
P_3=	14.758	kPa	f_{exp}=	**-0.00424**	
P_5=	-2.138	kPa	f_{theory}=	**0.00605**	
ΔP=	16.896	kPa			

Table C.5 Part 2: Smooth Axial Flow Through a 3" ID Annular Channel - Annular Flow Analysis

For 52 hz					
Q=	719.04	L/min	V_{ann}=	0.930	m/s
Q=	0.0120	m^3/s	Re_D=	57,472.45	
P_3=	51.872	kPa	f_{exp}=	**0.00288**	
P_5=	34.807	kPa	f_{theory}=	**0.00510**	
ΔP=	17.065	kPa			

For 45 hz					
Q=	633.73	L/min	V_{ann}=	0.819	m/s
Q=	0.0106	m^3/s	Re_D=	50,653.68	
P_3=	39.559	kPa	f_{exp}=	**-0.00222**	
P_5=	22.691	kPa	f_{theory}=	**0.00527**	
ΔP=	16.868	kPa			

For 20 hz					
Q=	277.29	L/min	V_{ann}=	0.359	m/s
Q=	0.0046	m^3/s	Re_D=	22,163.44	
P_3=	9.590	kPa	f_{exp}=	**0.02291**	
P_5=	-7.498	kPa	f_{theory}=	**0.00647**	
ΔP=	17.088	kPa			

TRIAL 3- ANNULAR TEST SECTION

73 hz pump speed					
Q=	997.51	L/min	V_{ann}=	1.290	m/s
Q=	0.0166	m^3/s	Re_D=	79,730.33	
P_3=	93.450	kPa	f_{exp}=	**0.01861**	
P_5=	74.977	kPa	f_{theory}=	**0.00470**	
ΔP=	18.473	kPa			

67 hz pump speed					
Q=	933.65	L/min	V_{ann}=	1.207	m/s
Q=	0.0156	m^3/s	Re_D=	74,625.58	
P_3=	82.514	kPa	f_{exp}=	**0.01383**	
P_5=	64.576	kPa	f_{theory}=	**0.00478**	
ΔP=	17.938	kPa			

60 hz pump speed					
Q=	849.48	L/min	V_{ann}=	1.098	m/s
Q=	0.0142	m^3/s	Re_D=	67,898.09	
P_3=	69.165	kPa	f_{exp}=	**0.01579**	
P_5=	51.282	kPa	f_{theory}=	**0.00489**	
ΔP=	17.884	kPa			

56 hz pump speed					
Q=	796.08	L/min	V_{ann}=	1.029	m/s
Q=	0.0133	m^3/s	Re_D=	63,630.16	
P_3=	61.353	kPa	f_{exp}=	**0.01592**	
P_5=	43.577	kPa	f_{theory}=	**0.00497**	
ΔP=	17.776	kPa			

52 hz pump speed					
Q=	738.53	L/min	V_{ann}=	0.955	m/s
Q=	0.0123	m^3/s	Re_D=	59,030.32	
P_3=	53.275	kPa	f_{exp}=	**0.01047**	
P_5=	35.861	kPa	f_{theory}=	**0.00507**	
ΔP=	17.414	kPa			

45 hz pump speed					
Q=	637.36	L/min	V_{ann}=	0.824	m/s
Q=	0.0106	m^3/s	Re_D=	50,944.01	
P_3=	40.546	kPa	f_{exp}=	**0.00210**	
P_5=	23.533	kPa	f_{theory}=	**0.00526**	
ΔP=	17.012	kPa			

40 hz pump speed					
Q=	565.99	L/min	V_{ann}=	0.732	m/s
Q=	0.0094	m^3/s	Re_D=	45,239.09	
P_3=	33.137	kPa	f_{exp}=	**0.01415**	
P_5=	15.821	kPa	f_{theory}=	**0.00542**	
ΔP=	17.317	kPa			

36 hz pump speed					
Q=	507.70	L/min	V_{ann}=	0.656	m/s
Q=	0.0085	m^3/s	Re_D=	40,580.22	
P_3=	27.005	kPa	f_{exp}=	**0.00918**	
P_5=	9.867	kPa	f_{theory}=	**0.00557**	
ΔP=	17.137	kPa			

30 hz pump speed					
Q=	421.65	L/min	V_{ann}=	0.545	m/s
Q=	0.0070	m^3/s	Re_D=	33,702.02	
P_3=	18.668	kPa	f_{exp}=	**0.00388**	
P_5=	1.670	kPa	f_{theory}=	**0.00583**	
ΔP=	16.999	kPa			

26 hz pump speed					
Q=	364.24	L/min	V_{ann}=	0.471	m/s
Q=	0.0061	m^3/s	Re_D=	29,113.76	
P_3=	13.790	kPa	f_{exp}=	**0.01744**	
P_5=	-3.343	kPa	f_{theory}=	**0.00605**	
ΔP=	17.133	kPa			

20 hz pump speed					
Q=	278.08	L/min	V_{ann}=	0.360	m/s
Q=	0.0046	m^3/s	Re_D=	22,226.92	
P_3=	7.771	kPa	f_{exp}=	**0.01891**	
P_5=	-9.292	kPa	f_{theory}=	**0.00647**	
ΔP=	17.063	kPa			

Table C.6 Part 1: Smooth Axial Flow Through a 4" ID Annular Channel - Horizontal Analysis

KNOWNS

d_3=	0.08255	m	L_{P1-P2}=	4.68	m	ρ_w=	1000	kg/m^3
A_3=	0.00535	m^2	μ_w=	0.00113	Pa.s			

TRIAL 1- HORIZONTAL TEST SECTION

	Q= (L/min)	Q= (m^3/s)	P_1= (kPa)	P_2= (kPa)	ΔP= (kPa)	V_3= (m/s)	Re_{D3}=	f_{exp}=	f_{theory}=
For 73 hz	948.33	0.0158	116.049	111.795	4.254	2.953	215,736.36	0.00430	0.00367
For 67 hz	889.10	0.0148	103.965	100.222	3.743	2.769	202,262.51	0.00431	0.00373
For 60 hz	811.29	0.0135	88.776	85.731	3.045	2.526	184,560.50	0.00421	0.00381
For 56 hz	758.66	0.0126	79.363	76.531	2.832	2.363	172,588.87	0.00448	0.00388
For 52 hz	702.79	0.0117	70.520	68.064	2.456	2.189	159,877.54	0.00452	0.00395
45 hz pump speed	607.87	0.0101	55.558	53.687	1.871	1.893	138,284.74	0.00460	0.00410
For 40 hz	539.10	0.0090	46.381	44.885	1.496	1.679	122,641.01	0.00468	0.00422
For 36 hz	482.84	0.0080	39.485	38.373	1.112	1.504	109,841.02	0.00434	0.00434
For 30 hz	401.48	0.0067	30.321	29.742	0.579	1.250	91,333.07	0.00326	0.00454
For 26 hz	347.32	0.0058	25.152	24.833	0.319	1.082	79,012.92	0.00240	0.00471

TRIAL 2- HORIZONTAL TEST SECTION

	Q= (L/min)	Q= (m^3/s)	P_1= (kPa)	P_2= (kPa)	ΔP= (kPa)	V_3= (m/s)	Re_{D3}=	f_{exp}=	f_{theory}=
For 72 hz	946.88	0.0158	114.029	109.851	4.178	2.95	215,407.31	0.00424	0.00367
For 67 hz	891.31	0.0149	102.812	99.450	3.362	2.78	202,764.34	0.00385	0.00372
For 64 hz	858.86	0.0143	96.802	92.460	4.342	2.67	195,382.26	0.00535	0.00376
For 60 hz	807.33	0.0135	86.957	83.838	3.119	2.51	183,659.97	0.00435	0.00382
For 48 hz	647.09 (set)	0.0108	61.072 (meas.)	58.718 (meas.)	2.354	2.02	147,207.67	0.00511	0.00403
For 45 hz	603.11	0.0101	54.932	52.288	2.644	1.88	137,201.52	0.00661	0.00410
For 40 hz	538.15	0.0090	45.771	44.047	1.724	1.68	122,423.18	0.00541	0.00422
For 36 hz	479.31	0.0080	39.411	37.762	1.649	1.49	109,037.71	0.00653	0.00435

Table C.7 Part 2: Smooth Axial Flow Through a 4" ID Annular Channel - Horizontal Analysis

For 56 hz					
Q=	757.64	L/min	V_3=	2.36	m/s
Q=	0.0126	m^3/s	Re_{D3}=	172,356.05	
P_1=	78.837	kPa	f_{exp}=	**0.00547**	
P_2=	75.385	kPa	f_{theory}=	**0.00388**	
ΔP=	3.452	kPa			

For 52 hz					
Q=	703.80	L/min	V_3=	2.19	m/s
Q=	0.0117	m^3/s	Re_{D3}=	160,107.80	
P_1=	69.763	kPa	f_{exp}=	**0.00464**	
P_2=	67.236	kPa	f_{theory}=	**0.00395**	
ΔP=	2.527	kPa			

For 30 hz					
Q=	402.37	L/min	V_3=	1.25	m/s
Q=	0.0067	m^3/s	Re_{D3}=	91,536.17	
P_1=	30.059	kPa	f_{exp}=	**0.00282**	
P_2=	29.557	kPa	f_{theory}=	**0.00454**	
ΔP=	0.502	kPa			

For 26 hz					
Q=	346.82	L/min	V_3=	1.08	m/s
Q=	0.0058	m^3/s	Re_{D3}=	78,898.02	
P_1=	24.863	kPa	f_{exp}=	**0.00354**	
P_2=	24.395	kPa	f_{theory}=	**0.00471**	
ΔP=	0.468	kPa			

TRIAL 3- HORIZONTAL TEST SECTION

For 72 hz					
Q=	957.47	L/min	V_3=	2.98	m/s
Q=	0.0160	m^3/s	Re_{D3}=	217,816.15	
P_1=	116.067	kPa	f_{exp}=	**0.00394**	
P_2=	112.100	kPa	f_{theory}=	**0.00366**	
ΔP=	3.967	kPa			

For 67 hz					
Q=	902.37	L/min	V_3=	2.81	m/s
Q=	0.0150	m^3/s	Re_{D3}=	205,281.32	
P_1=	103.986	kPa	f_{exp}=	**0.00352**	
P_2=	100.832	kPa	f_{theory}=	**0.00371**	
ΔP=	3.154	kPa			

For 64 hz					
Q=	866.73	L/min	V_3=	2.70	m/s
Q=	0.0144	m^3/s	Re_{D3}=	197,173.16	
P_1=	97.462	kPa	f_{exp}=	**0.00401**	
P_2=	94.148	kPa	f_{theory}=	**0.00375**	
ΔP=	3.314	kPa			

For 60 hz					
Q=	814.29	L/min	V_3=	2.54	m/s
Q=	0.0136	m^3/s	Re_{D3}=	185,242.14	
P_1=	87.356	kPa	f_{exp}=	**0.00316**	
P_2=	85.049	kPa	f_{theory}=	**0.00381**	
ΔP=	2.307	kPa			

For 56 hz					
Q=	764.99	L/min	V_3=	2.38	m/s
Q=	0.0127	m^3/s	Re_{D3}=	174,027.27	
P_1=	78.855	kPa	f_{exp}=	**0.00377**	
P_2=	76.432	kPa	f_{theory}=	**0.00387**	
ΔP=	2.424	kPa			

For 52 hz					
Q=	706.63	L/min	V_3=	2.20	m/s
Q=	0.0118	m^3/s	Re_{D3}=	160,752.46	
P_1=	69.359	kPa	f_{exp}=	**0.00392**	
P_2=	67.205	kPa	f_{theory}=	**0.00395**	
ΔP=	2.154	kPa			

For 48 hz					
Q=	653.33	L/min	V_3=	2.03	m/s
Q=	0.0109	m^3/s	Re_{D3}=	148,626.98	
P_1=	60.793	kPa	f_{exp}=	**0.00380**	
P_2=	59.011	kPa	f_{theory}=	**0.00402**	
ΔP=	1.781	kPa			

For 45 hz					
Q=	608.96	L/min	V_3=	1.90	m/s
Q=	0.0101	m^3/s	Re_{D3}=	138,532.35	
P_1=	54.754	kPa	f_{exp}=	**0.00394**	
P_2=	53.147	kPa	f_{theory}=	**0.00409**	
ΔP=	1.606	kPa			

For 40 hz					
Q=	541.86	L/min	V_3=	1.69	m/s
Q=	0.0090	m^3/s	Re_{D3}=	123,267.51	
P_1=	45.501	kPa	f_{exp}=	**0.00298**	
P_2=	44.538	kPa	f_{theory}=	**0.00422**	
ΔP=	0.963	kPa			

For 36 hz					
Q=	489.27	L/min	V_3=	1.52	m/s
Q=	0.0082	m^3/s	Re_{D3}=	111,304.35	
P_1=	39.076	kPa	f_{exp}=	**0.00312**	
P_2=	38.255	kPa	f_{theory}=	**0.00433**	
ΔP=	0.822	kPa			

For 30 hz					
Q=	404.90	L/min	V_3=	1.26	m/s
Q=	0.0067	m^3/s	Re_{D3}=	92,111.12	
P_1=	29.989	kPa	f_{exp}=	**0.00126**	
P_2=	29.762	kPa	f_{theory}=	**0.00453**	
ΔP=	0.228	kPa			

Table C.8 Part 1: Smooth Axial Flow Through a 4" ID Annular Channel - Annular Flow Analysis

KNOWNS:

D_o=	0.1524	m	A_{ann}=	0.00909	m^2	μ_w=	0.00113	Pa.s
D_i=	0.10795	m	$L_{P3\text{-}P5}$=	1.727	m	ρ_w=	1000	kg/m^3
D_h=	0.04445	m				z_5=	1.727	m (z_3=0)

TRIAL 1- ANNULAR TEST SECTION

For 73 hz

Q=	948.33	L/min	V_{ann}=	1.739	m/s
Q=	0.0158	m^3/s	Re_D=	68,404.21	
P_3=	90.478	kPa	f_{exp}=	**0.00693**	
P_5=	71.907	kPa	f_{theory}=	**0.00488**	
ΔP=	18.571	kPa			

For 67 hz

Q=	889.10	L/min	V_{ann}=	1.630	m/s
Q=	0.0148	m^3/s	Re_D=	64,132.01	
P_3=	79.386	kPa	f_{exp}=	**0.00540**	
P_5=	61.329	kPa	f_{theory}=	**0.00496**	
ΔP=	18.057	kPa			

For 60 hz

Q=	811.29	L/min	V_{ann}=	1.488	m/s
Q=	0.0135	m^3/s	Re_D=	58,519.18	
P_3=	66.127	kPa	f_{exp}=	**0.00554**	
P_5=	48.233	kPa	f_{theory}=	**0.00508**	
ΔP=	17.894	kPa			

For 56 hz

Q=	758.66	L/min	V_{ann}=	1.391	m/s
Q=	0.0126	m^3/s	Re_D=	54,723.30	
P_3=	58.078	kPa	f_{exp}=	**0.00619**	
P_5=	40.206	kPa	f_{theory}=	**0.00517**	
ΔP=	17.872	kPa			

For 52 hz

Q=	702.79	L/min	V_{ann}=	1.289	m/s
Q=	0.0117	m^3/s	Re_D=	50,692.88	
P_3=	49.984	kPa	f_{exp}=	**0.00359**	
P_5=	32.579	kPa	f_{theory}=	**0.00526**	
ΔP=	17.405	kPa			

For 45 hz

Q=	607.87	L/min	V_{ann}=	1.115	m/s
Q=	0.0101	m^3/s	Re_D=	43,846.38	
P_3=	36.658	kPa	f_{exp}=	**0.00036**	
P_5=	19.682	kPa	f_{theory}=	**0.00546**	
ΔP=	16.977	kPa			

For 40 hz

Q=	539.10	L/min	V_{ann}=	0.989	m/s
Q=	0.0090	m^3/s	Re_D=	38,886.17	
P_3=	28.320	kPa	f_{exp}=	**-0.00334**	
P_5=	11.631	kPa	f_{theory}=	**0.00563**	
ΔP=	16.689	kPa			

For 36 hz

Q=	482.84	L/min	V_{ann}=	0.885	m/s
Q=	0.0080	m^3/s	Re_D=	34,827.64	
P_3=	22.337	kPa	f_{exp}=	**-0.00465**	
P_5=	5.678	kPa	f_{theory}=	**0.00578**	
ΔP=	16.659	kPa			

For 30 hz

Q=	401.48	L/min	V_{ann}=	0.736	m/s
Q=	0.0067	m^3/s	Re_D=	28,959.27	
P_3=	-24.808	kPa	f_{exp}=	**-0.94437**	
P_5=	-1.978	kPa	f_{theory}=	**0.00606**	
ΔP=	-22.830	kPa			

TRIAL 2- ANNULAR TEST SECTION

For 73 hz

Q=	946.88	L/min	V_{ann}=	1.736	m/s
Q=	0.0158	m^3/s	Re_D=	68,299.88	
P_3=	88.817	kPa	f_{exp}=	**0.00579**	
P_5=	70.519	kPa	f_{theory}=	**0.00489**	
ΔP=	18.297	kPa			

For 67 hz

Q=	891.31	L/min	V_{ann}=	1.634	m/s
Q=	0.0149	m^3/s	Re_D=	64,291.13	
P_3=	78.897	kPa	f_{exp}=	**0.00531**	
P_5=	60.853	kPa	f_{theory}=	**0.00496**	
ΔP=	18.044	kPa			

For 64 hz

Q=	858.86	L/min	V_{ann}=	1.575	m/s
Q=	0.0143	m^3/s	Re_D=	61,950.47	
P_3=	73.335	kPa	f_{exp}=	**0.00641**	
P_5=	55.158	kPa	f_{theory}=	**0.00501**	
ΔP=	18.177	kPa			

For 60 hz

Q=	807.33	L/min	V_{ann}=	1.480	m/s
Q=	0.0135	m^3/s	Re_D=	58,233.65	
P_3=	64.866	kPa	f_{exp}=	**0.00405**	
P_5=	47.235	kPa	f_{theory}=	**0.00509**	
ΔP=	17.631	kPa			

For 48 hz

Q=	647.09	L/min	V_{ann}=	1.187	m/s
Q=	0.0108	m^3/s	Re_D=	46,675.60	
P_3=	41.655	kPa	f_{exp}=	**-0.00117**	
P_5=	24.841	kPa	f_{theory}=	**0.00537**	
ΔP=	16.813	kPa			

For 45 hz

Q=	603.11	L/min	V_{ann}=	1.106	m/s
Q=	0.0101	m^3/s	Re_D=	43,502.92	
P_3=	36.095	kPa	f_{exp}=	**-0.00003**	
P_5=	19.156	kPa	f_{theory}=	**0.00547**	
ΔP=	16.939	kPa			

For 40 hz

Q=	538.15	L/min	V_{ann}=	0.987	m/s
Q=	0.0090	m^3/s	Re_D=	38,817.11	
P_3=	28.188	kPa	f_{exp}=	**-0.00534**	
P_5=	11.650	kPa	f_{theory}=	**0.00563**	
ΔP=	16.538	kPa			

For 36 hz

Q=	479.31	L/min	V_{ann}=	0.879	m/s
Q=	0.0080	m^3/s	Re_D=	34,572.93	
P_3=	22.476	kPa	f_{exp}=	**-0.01148**	
P_5=	6.223	kPa	f_{theory}=	**0.00579**	
ΔP=	16.253	kPa			

Table C.9 Part 2: Smooth Axial Flow Through a 4" ID Annular Channel - Annular Flow Analysis

For 56 hz

Q=	757.64	L/min	V_{ann}=	1.389	m/s
Q=	0.0126	m^3/s	Re_D=	54,649.48	
P_3=	56.946	kPa	f_{exp}=	0.00352	
P_5=	39.476	kPa	f_{theory}=	0.00517	
ΔP=	17.470	kPa			

For 52 hz

Q=	703.80	L/min	V_{ann}=	1.291	m/s
Q=	0.0117	m^3/s	Re_D=	50,765.89	
P_3=	49.229	kPa	f_{exp}=	0.00004	
P_5=	32.282	kPa	f_{theory}=	0.00526	
ΔP=	16.947	kPa			

For 30 hz

Q=	402.37	L/min	V_{ann}=	0.738	m/s
Q=	0.0067	m^3/s	Re_D=	29,023.66	
P_3=	14.618	kPa	f_{exp}=	-0.01767	
P_5=	-1.576	kPa	f_{theory}=	0.00605	
ΔP=	16.194	kPa			

TRIAL 3- ANNULAR TEST SECTION

For 72 hz

Q=	957.47	L/min	V_{ann}=	1.756	m/s
Q=	0.0160	m^3/s	Re_D=	69,063.66	
P_3=	90.051	kPa	f_{exp}=	0.00553	
P_5=	71.784	kPa	f_{theory}=	0.00487	
ΔP=	18.267	kPa			

For 67 hz

Q=	902.37	L/min	V_{ann}=	1.655	m/s
Q=	0.0150	m^3/s	Re_D=	65,089.20	
P_3=	79.605	kPa	f_{exp}=	0.00526	
P_5=	61.544	kPa	f_{theory}=	0.00495	
ΔP=	18.062	kPa			

For 64 hz

Q=	866.73	L/min	V_{ann}=	1.589	m/s
Q=	0.0144	m^3/s	Re_D=	62,518.32	
P_3=	73.893	kPa	f_{exp}=	0.00541	
P_5=	55.889	kPa	f_{theory}=	0.00500	
ΔP=	18.005	kPa			

For 60 hz

Q=	814.29	L/min	V_{ann}=	1.493	m/s
Q=	0.0136	m^3/s	Re_D=	58,735.31	
P_3=	65.663	kPa	f_{exp}=	0.00521	
P_5=	47.819	kPa	f_{theory}=	0.00507	
ΔP=	17.844	kPa			

For 56 hz

Q=	764.99	L/min	V_{ann}=	1.403	m/s
Q=	0.0127	m^3/s	Re_D=	55,179.38	
P_3=	57.832	kPa	f_{exp}=	0.00454	
P_5=	40.197	kPa	f_{theory}=	0.00515	
ΔP=	17.635	kPa			

For 52 hz

Q=	706.63	L/min	V_{ann}=	1.296	m/s
Q=	0.0118	m^3/s	Re_D=	50,970.29	
P_3=	49.194	kPa	f_{exp}=	0.00451	
P_5=	31.664	kPa	f_{theory}=	0.00526	
ΔP=	17.530	kPa			

For 48 hz

Q=	653.33	L/min	V_{ann}=	1.198	m/s
Q=	0.0109	m^3/s	Re_D=	47,125.63	
P_3=	41.621	kPa	f_{exp}=	0.00020	
P_5=	24.657	kPa	f_{theory}=	0.00536	
ΔP=	16.964	kPa			

For 45 hz

Q=	608.96	L/min	V_{ann}=	1.117	m/s
Q=	0.0101	m^3/s	Re_D=	43,924.89	
P_3=	36.091	kPa	f_{exp}=	0.00197	
P_5=	18.958	kPa	f_{theory}=	0.00546	
ΔP=	17.133	kPa			

For 40 hz

Q=	541.86	L/min	V_{ann}=	0.994	m/s
Q=	0.0090	m^3/s	Re_D=	39,084.82	
P_3=	28.238	kPa	f_{exp}=	-0.00161	
P_5=	11.420	kPa	f_{theory}=	0.00562	
ΔP=	16.818	kPa			

For 36 hz

Q=	489.27	L/min	V_{ann}=	0.897	m/s
Q=	0.0082	m^3/s	Re_D=	35,291.62	
P_3=	22.383	kPa	f_{exp}=	-0.00294	
P_5=	5.625	kPa	f_{theory}=	0.00576	
ΔP=	16.758	kPa			

For 30 hz

Q=	404.90	L/min	V_{ann}=	0.742	m/s
Q=	0.0067	m^3/s	Re_D=	29,205.96	
P_3=	14.581	kPa	f_{exp}=	-0.00606	
P_5=	-2.101	kPa	f_{theory}=	0.00604	
ΔP=	16.682	kPa			

Table C.10 Part 1: Smooth Axial Flow Through a 5" ID Annular Channel - Horizontal Analysis

KNOWNS

$d_{3"}$=	0.08255	m	L_{P1-P2}=	4.68	m	ρ_w=	1000	kg/m^3
$A_{3"}$=	0.00535	m^2	μ_w=	0.00113	Pa.s			

TRIAL 1- HORIZONTAL TEST SECTION

Frequency	Q (L/min)	Q (m^3/s)	P_1 (kPa)	P_2 (kPa)	ΔP (kPa)	$V_{3"}$ (m/s)	$Re_{D\,3"}$	f_{exp}	f_{theory}
For 73 hz	962.33	0.0160	126.377	120.754	5.623	2.997	218,920.17	**0.00552**	**0.00365**
For 67 hz	893.43	0.0149	112.387	107.588	4.799	2.782	203,245.84	**0.00547**	**0.00372**
For 60 hz	811.66	0.0135	95.997	91.903	4.094	2.528	184,644.02	**0.00565**	**0.00381**
For 56 hz	759.25	0.0127	86.999	82.713	4.286	2.364	172,722.66	**0.00676**	**0.00388**
For 52 hz	702.10	0.0117	77.433	73.624	3.809	2.186	159,720.69	**0.00703**	**0.00395**
For 45 hz	601.34	0.0100	62.045	59.104	2.941	1.873	136,798.97	**0.00740**	**0.00411**
For 40 hz	539.35	0.0090	52.731	49.983	2.749	1.680	122,697.93	**0.00859**	**0.00422**
For 36 hz	475.79	0.0079	45.545	43.401	2.144	1.482	108,238.74	**0.00861**	**0.00436**
For 30 hz	400.72	0.0067	36.319	34.593	1.726	1.248	91,160.23	**0.00977**	**0.00455**
For 26 hz	346.70	0.0058	30.955	29.628	1.327	1.080	78,870.29	**0.01004**	**0.00471**
For 20 hz	264.59	0.0044	24.184	23.414	0.770	0.824	60,191.83	**0.01000**	**0.00504**

Table C.11 Part 2: Smooth Axial Flow Through a 5" ID Annular Channel - Annular Flow Analysis

KNOWNS:

Do=	0.1524	m	A_{ann}=	0.00429	m^2	μ_w=	0.00113	Pa.m
Di=	0.1333	m	L_{P3-P5}=	1.727	m	ρ_w=	1000	kg/m^3
Dh=	0.0191	m				z_5=	1.727	m (z_3=0)

TRIAL 1- ANNULAR TEST SECTION

Pump speed	Q (L/min)	Q (m^3/s)	P_3 (kPa)	P_5 (kPa)	ΔP (kPa)	V_{ann} (m/s)	Re_D	f_{exp}	f_{theory}
73 hz pump speed	962.33	0.0160	97.069	72.046	25.024	3.742	63,254.67	**0.00319**	**0.00498**
67 hz pump speed	893.43	0.0149	85.544	60.723	24.821	3.474	58,725.74	**0.00361**	**0.00507**
60 hz pump speed	811.66	0.0135	72.032	47.936	24.096	3.156	53,350.94	**0.00397**	**0.00520**
56 hz pump speed	759.25	0.0127	64.159	40.655	23.504	2.953	49,906.39	**0.00416**	**0.00529**
52 hz pump speed	702.10	0.0117	56.327	33.592	22.735	2.730	46,149.61	**0.00430**	**0.00539**
45 hz pump speed	601.34	0.0100	43.577	21.912	21.666	2.338	39,526.62	**0.00478**	**0.00560**
40 hz pump speed	539.35	0.0090	35.638	14.720	20.917	2.097	35,452.27	**0.00500**	**0.00576**
36 hz pump speed	475.79	0.0079	30.013	9.567	20.446	1.850	31,274.44	**0.00566**	**0.00594**
30 hz pump speed	400.72	0.0067	22.573	2.469	20.103	1.558	26,339.79	**0.00720**	**0.00620**
26 hz pump speed	346.70	0.0058	18.502	-1.489	19.991	1.348	22,788.74	**0.00927**	**0.00643**
20 hz pump speed	264.59	0.0044	13.256	-6.421	19.677	1.029	17,391.79	**0.01429**	**0.00688**

Appendix F

Rough Axial Flow Calculations

Table D.1 Part 1: Horizontal Pipe Flow with 1 Roughened Surface in the Annular Channel

KNOWNS

d_{3*}=	0.08255	m	$L_{P1\text{-}P2}$=	4.68	m	ρ_w=	1000	kg/m^3
A_{3*}=	0.00535	m^2	μ_w=	0.00113	Pa.m			

TRIAL 1- HORIZONTAL TEST SECTION

For 73 hz

Q=	928.69	L/min	V_{3*}=	2.892	m/s
Q=	0.0155	m^3/s	$Re_{D\,3*}$=	211,267.47	
P_1=	110.761	kPa	f_{exp}=	**0.00420**	
P_2=	106.776	kPa	f_{theory}=	**0.00368**	
ΔP=	3.985	kPa			

For 67 hz

Q=	881.39	L/min	V_{3*}=	2.745	m/s
Q=	0.0147	m^3/s	$Re_{D\,3*}$=	200,507.39	
P_1=	102.103	kPa	f_{exp}=	**0.00357**	
P_2=	99.055	kPa	f_{theory}=	**0.00373**	
ΔP=	3.048	kPa			

For 64 hz

Q=	843.16	L/min	V_{3*}=	2.626	m/s
Q=	0.0141	m^3/s	$Re_{D\,3*}$=	191,809.81	
P_1=	93.447	kPa	f_{exp}=	**0.00392**	
P_2=	90.381	kPa	f_{theory}=	**0.00377**	
ΔP=	3.066	kPa			

For 60 hz

Q=	948.33	L/min	V_{3*}=	2.953	m/s
Q=	0.0158	m^3/s	$Re_{D\,3*}$=	215,736.36	
P_1=	116.049	kPa	f_{exp}=	**0.00430**	
P_2=	111.795	kPa	f_{theory}=	**0.00367**	
ΔP=	4.254	kPa			

For 56 hz

Q=	743.01	L/min	V_{3*}=	2.314	m/s
Q=	0.0124	m^3/s	$Re_{D\,3*}$=	169,027.87	
P_1=	75.553	kPa	f_{exp}=	**0.00387**	
P_2=	73.204	kPa	f_{theory}=	**0.00390**	
ΔP=	2.349	kPa			

For 52 hz

Q=	683.24	L/min	V_{3*}=	2.128	m/s
Q=	0.0114	m^3/s	$Re_{D\,3*}$=	155,431.26	
P_1=	66.221	kPa	f_{exp}=	**0.00473**	
P_2=	63.790	kPa	f_{theory}=	**0.00398**	
ΔP=	2.430	kPa			

For 48 hz

Q=	632.36	L/min	V_{3*}=	1.969	m/s
Q=	0.0105	m^3/s	$Re_{D\,3*}$=	143,856.89	
P_1=	58.389	kPa	f_{exp}=	**0.00434**	
P_2=	56.481	kPa	f_{theory}=	**0.00406**	
ΔP=	1.908	kPa			

For 45 hz

Q=	593.51	L/min	V_{3*}=	1.848	m/s
Q=	0.0099	m^3/s	$Re_{D\,3*}$=	135,017.28	
P_1=	53.032	kPa	f_{exp}=	**0.00363**	
P_2=	51.626	kPa	f_{theory}=	**0.00412**	
ΔP=	1.406	kPa			

For 40 hz

Q=	527.33	L/min	V_{3*}=	1.642	m/s
Q=	0.0088	m^3/s	$Re_{D\,3*}$=	119,963.65	
P_1=	44.500	kPa	f_{exp}=	**0.00424**	
P_2=	43.204	kPa	f_{theory}=	**0.00424**	
ΔP=	1.296	kPa			

For 36 hz

Q=	466.86	L/min	V_{3*}=	1.454	m/s
Q=	0.0078	m^3/s	$Re_{D\,3*}$=	106,205.48	
P_1=	37.086	kPa	f_{exp}=	**0.00435**	
P_2=	36.043	kPa	f_{theory}=	**0.00438**	
ΔP=	1.043	kPa			

For 30 hz

Q=	388.90	L/min	V_{3*}=	1.211	m/s
Q=	0.0065	m^3/s	$Re_{D\,3*}$=	88,471.87	
P_1=	28.527	kPa	f_{exp}=	**-0.00015**	
P_2=	28.552	kPa	f_{theory}=	**0.00458**	
ΔP=	-0.024	kPa			

For 26 hz

Q=	334.28	L/min	V_{3*}=	1.041	m/s
Q=	0.0056	m^3/s	$Re_{D\,3*}$=	76,046.64	
P_1=	23.552	kPa	f_{exp}=	**-0.00350**	
P_2=	23.983	kPa	f_{theory}=	**0.00476**	
ΔP=	-0.430	kPa			

Table D.2 Part 2: Horizontal Pipe Flow with 1 Roughened Surface in the Annular Channel

TRIAL 2- HORIZONTAL TEST SECTION

For	Q= (L/min)	Q= (m^3/s)	V_{3^*}= (m/s)	$Re_{D\,3^*}$=	P_1= (kPa)	P_2= (kPa)	ΔP= (kPa)	f_{exp}=	f_{theory}=
73 hz	925.79	0.0154	2.883	210,609.29	110.321	106.268	4.053	0.00430	0.00369
67 hz	873.55	0.0146	2.720	198,725.12	99.248	95.752	3.495	0.00417	0.00374
64 hz	840.30	0.0140	2.617	191,159.50	92.468	89.178	3.290	0.00424	0.00378
60 hz	788.42	0.0131	2.455	179,358.79	84.825	81.918	2.907	0.00425	0.00384
56 hz	739.33	0.0123	2.302	168,190.51	75.330	72.516	2.813	0.00468	0.00390
52 hz	675.56	0.0113	2.104	153,682.40	66.685	64.248	2.436	0.00486	0.00399
48 hz	634.94	0.0106	1.977	144,443.41	58.948	56.944	2.004	0.00452	0.00405
45 hz	588.48	0.0098	1.833	133,872.72	52.473	50.511	1.962	0.00515	0.00413
40 hz	525.86	0.0088	1.638	119,628.49	44.146	42.700	1.446	0.00476	0.00425
36 hz	469.73	0.0078	1.463	106,860.19	37.509	36.306	1.203	0.00496	0.00437
30 hz	390.47	0.0065	1.216	88,827.53	29.010	28.668	0.342	0.00204	0.00458
26 hz	333.77	0.0056	1.039	75,930.63	23.751	23.886	-0.135	-0.00110	0.00476

TRIAL 3- HORIZONTAL TEST SECTION

For	Q= (L/min)	Q= (m^3/s)	V_{3^*}= (m/s)	$Re_{D\,3^*}$=	P_1= (kPa)	P_2= (kPa)	ΔP= (kPa)	f_{exp}=	f_{theory}=
72 hz	928.13	0.0155	2.890	211,140.30	109.780	105.922	3.858	0.00407	0.00369
67 hz	874.45	0.0146	2.723	198,929.81	99.188	95.625	3.564	0.00424	0.00374
64 hz	844.41	0.0141	2.630	192,096.27	93.568	90.475	3.093	0.00395	0.00377
60 hz	787.94	0.0131	2.454	179,247.98	82.887	80.444	2.443	0.00358	0.00384
48 hz	632.99	0.0105	1.971	143,999.43	58.400	56.349	2.051	0.00465	0.00406
45 hz	587.41	0.0098	1.829	133,629.14	52.280	50.421	1.859	0.00490	0.00413
40 hz	527.30	0.0088	1.642	119,955.18	44.111	42.881	1.230	0.00402	0.00424
36 hz	468.78	0.0078	1.460	106,643.54	37.249	36.406	0.842	0.00349	0.00437

Table D.3 Part 2: Horizontal Pipe Flow with 1 Roughened Surface in the Annular Channel

For 56 hz

Q=	742.05	L/min	$V_{3'}$=	2.311	m/s
Q=	0.0124	m^3/s	$Re_{D\,3'}$=	168,809.19	
P_1=	75.399	kPa	f_{exp}=	0.00408	
P_2=	72.931	kPa	f_{theory}=	0.00390	
ΔP=	2.468	kPa			

For 52 hz

Q=	682.74	L/min	$V_{3'}$=	2.126	m/s
Q=	0.0114	m^3/s	$Re_{D\,3'}$=	155,316.97	
P_1=	66.047	kPa	f_{exp}=	0.00444	
P_2=	63.773	kPa	f_{theory}=	0.00398	
ΔP=	2.274	kPa			

For 30 hz

Q=	390.56	L/min	$V_{3'}$=	1.216	m/s
Q=	0.0065	m^3/s	$Re_{D\,3'}$=	88,849.46	
P_1=	29.064	kPa	f_{exp}=	0.00301	
P_2=	28.559	kPa	f_{theory}=	0.00458	
ΔP=	0.505	kPa			

For 26 hz

Q=	335.25	L/min	$V_{3'}$=	1.044	m/s
Q=	0.0056	m^3/s	$Re_{D\,3'}$=	76,265.20	
P_1=	23.972	kPa	f_{exp}=	0.00079	
P_2=	23.874	kPa	f_{theory}=	0.00475	
ΔP=	0.098	kPa			

Table D.4 Part 1: Annular Flow with 1 Roughened Surface in the Annular Channel

KNOWNS

D_o=	0.1504	m	A_{ann}=	0.00861	m^2	μ_w=	0.00113	Pa.s	A_{holes}=	0.004516
D_i=	0.10795	m	$L_{P3\text{-}P5}$=	1.727	m	ρ_w=	1000	kg/m^3	σ=	0.5243
D_h=	0.04245	m	ε=	1.60E-03		z_5=	1.727	m (z_3=0)	k_{red}=	0.3045
			ε/D=	0.0377					k_{exp}=	0.2263

TRIAL 1- ANNULAR TEST SECTION

For 72 hz

Q=	928.69	L/min	V_{ann}=	1.80	m/s
Q=	0.0155	m^3/s	Re_D=	67,505.82	
P_3=	86.369	kPa	K_{losses}=	857.07	
P_5=	60.148	kPa			
ΔP=	26.221	kPa	f_{exp}=	0.03205	
			f_{theory}=	0.01592495	

For 67 hz

Q=	881.39	L/min	V_{ann}=	1.71	m/s
Q=	0.0147	m^3/s	Re_D=	64,067.68	
P_3=	78.608	kPa	K_{losses}=	771.99	
P_5=	52.175	kPa			
ΔP=	26.433	kPa	f_{exp}=	0.03684	
			f_{theory}=	0.01593327	

For 64 hz

Q=	843.16	L/min	V_{ann}=	1.63	m/s
Q=	0.0141	m^3/s	Re_D=	61,288.56	
P_3=	71.508	kPa	K_{losses}=	706.47	
P_5=	47.443	kPa			
ΔP=	24.065	kPa	f_{exp}=	0.02963	
			f_{theory}=	0.01594064	

For 60 hz

Q=	786.61	L/min	V_{ann}=	1.52	m/s
Q=	0.0131	m^3/s	Re_D=	57,177.98	
P_3=	65.814	kPa	K_{losses}=	614.88	
P_5=	40.205	kPa			
ΔP=	25.609	kPa	f_{exp}=	0.04272	
			f_{theory}=	0.01595278	

For 56 hz

Q=	743.01	L/min	V_{ann}=	1.44	m/s
Q=	0.0124	m^3/s	Re_D=	54,009.10	
P_3=	56.280	kPa	K_{losses}=	548.62	
P_5=	33.775	kPa			
ΔP=	22.505	kPa	f_{exp}=	0.02982	
			f_{theory}=	0.01596333	

For 52 hz

Q=	683.24	L/min	V_{ann}=	1.32	m/s
Q=	0.0114	m^3/s	Re_D=	49,664.60	
P_3=	48.003	kPa	K_{losses}=	463.90	
P_5=	26.096	kPa			
ΔP=	21.907	kPa	f_{exp}=	0.03165	
			f_{theory}=	0.01597986	

For 48 hz

Q=	632.36	L/min	V_{ann}=	1.22	m/s
Q=	0.0105	m^3/s	Re_D=	45,966.27	
P_3=	41.295	kPa	K_{losses}=	397.39	
P_5=	20.193	kPa			
ΔP=	21.102	kPa	f_{exp}=	0.03089	
			f_{theory}=	0.015996235	

For 45 hz

Q=	593.51	L/min	V_{ann}=	1.15	m/s
Q=	0.0099	m^3/s	Re_D=	43,141.77	
P_3=	37.016	kPa	K_{losses}=	350.05	
P_5=	15.686	kPa			
ΔP=	21.330	kPa	f_{exp}=	0.03763	
			f_{theory}=	0.016010525	

For 40 hz

Q=	527.33	L/min	V_{ann}=	1.02	m/s
Q=	0.0088	m^3/s	Re_D=	38,331.72	
P_3=	29.480	kPa	K_{losses}=	276.34	
P_5=	9.359	kPa			
ΔP=	20.121	kPa	f_{exp}=	0.03427	
			f_{theory}=	0.01603941	

For 36 hz

Q=	466.86	L/min	V_{ann}=	0.90	m/s
Q=	0.0078	m^3/s	Re_D=	33,935.60	
P_3=	23.285	kPa	K_{losses}=	216.59	
P_5=	3.957	kPa			
ΔP=	19.328	kPa	f_{exp}=	0.03268	
			f_{theory}=	0.016072521	

For 30 hz

Q=	388.90	L/min	V_{ann}=	0.75	m/s
Q=	0.0065	m^3/s	Re_D=	28,269.22	
P_3=	16.540	kPa	K_{losses}=	150.30	
P_5=	-2.211	kPa			
ΔP=	18.751	kPa	f_{exp}=	0.03601	
			f_{theory}=	0.016129386	

For 26 hz

Q=	334.28	L/min	V_{ann}=	0.65	m/s
Q=	0.0056	m^3/s	Re_D=	24,299.01	
P_3=	12.332	kPa	K_{losses}=	111.05	
P_5=	-5.870	kPa			
ΔP=	18.202	kPa	f_{exp}=	0.03376	
			f_{theory}=	0.016183968	

Table D.5 Part 2: Annular Flow with 1 Roughened Surface in the Annular Channel

TRIAL 2- ANNULAR TEST SECTION

For 72 hz

Q=	925.79	L/min	V_{ann}=	1.79	m/s
Q=	0.0154	m^3/s	Re_D=	67,295.52	
P_3=	84.475	kPa	K_{losses}=	851.74	
P_5=	60.823	kPa			
ΔP=	23.652	kPa	f_{exp}=	**0.02244**	
			f_{theory}=	**0.01592544**	

For 67 hz

Q=	873.55	L/min	V_{ann}=	1.69	m/s
Q=	0.0146	m^3/s	Re_D=	63,498.19	
P_3=	76.871	kPa	K_{losses}=	758.33	
P_5=	52.581	kPa			
ΔP=	24.290	kPa	f_{exp}=	**0.02835**	
			f_{theory}=	**0.01593473**	

For 64 hz

Q=	840.30	L/min	V_{ann}=	1.63	m/s
Q=	0.0140	m^3/s	Re_D=	61,080.77	
P_3=	71.251	kPa	K_{losses}=	701.69	
P_5=	47.616	kPa			
ΔP=	23.635	kPa	f_{exp}=	**0.02785**	
			f_{theory}=	**0.01594122**	

For 60 hz

Q=	788.42	L/min	V_{ann}=	1.53	m/s
Q=	0.0131	m^3/s	Re_D=	57,310.11	
P_3=	63.244	kPa	K_{losses}=	617.73	
P_5=	40.630	kPa			
ΔP=	22.614	kPa	f_{exp}=	**0.02669**	
			f_{theory}=	**0.01595237**	

For 56 hz

Q=	739.33	L/min	V_{ann}=	1.43	m/s
Q=	0.0123	m^3/s	Re_D=	53,741.54	
P_3=	56.076	kPa	K_{losses}=	543.19	
P_5=	33.872	kPa			
ΔP=	22.204	kPa	f_{exp}=	**0.02834**	
			f_{theory}=	**0.01596428**	

For 52 hz

Q=	675.56	L/min	V_{ann}=	1.31	m/s
Q=	0.0113	m^3/s	Re_D=	49,105.80	
P_3=	48.675	kPa	K_{losses}=	453.52	
P_5=	26.948	kPa			
ΔP=	21.727	kPa	f_{exp}=	**0.03116**	
			f_{theory}=	**0.01598218**	

For 48 hz

Q=	634.94	L/min	V_{ann}=	1.23	m/s
Q=	0.0106	m^3/s	Re_D=	46,153.68	
P_3=	42.130	kPa	K_{losses}=	400.63	
P_5=	21.150	kPa			
ΔP=	20.980	kPa	f_{exp}=	**0.02962**	
			f_{theory}=	**0.015995346**	

For 45 hz

Q=	588.48	L/min	V_{ann}=	1.14	m/s
Q=	0.0098	m^3/s	Re_D=	42,776.05	
P_3=	36.490	kPa	K_{losses}=	344.14	
P_5=	15.942	kPa			
ΔP=	20.548	kPa	f_{exp}=	**0.03092**	
			f_{theory}=	**0.016012505**	

For 40 hz

Q=	525.86	L/min	V_{ann}=	1.02	m/s
Q=	0.0088	m^3/s	Re_D=	38,224.63	
P_3=	29.493	kPa	K_{losses}=	274.80	
P_5=	9.752	kPa			
ΔP=	19.740	kPa	f_{exp}=	**0.02996**	
			f_{theory}=	**0.016040131**	

For 36 hz

Q=	469.73	L/min	V_{ann}=	0.91	m/s
Q=	0.0078	m^3/s	Re_D=	34,144.80	
P_3=	23.736	kPa	K_{losses}=	219.27	
P_5=	4.677	kPa			
ΔP=	19.059	kPa	f_{exp}=	**0.02823**	
			f_{theory}=	**0.016070764**	

For 30 hz

Q=	390.47	L/min	V_{ann}=	0.76	m/s
Q=	0.0065	m^3/s	Re_D=	28,382.86	
P_3=	16.901	kPa	K_{losses}=	151.51	
P_5=	-1.773	kPa			
ΔP=	18.673	kPa	f_{exp}=	**0.03402**	
			f_{theory}=	**0.016128036**	

For 26 hz

Q=	333.77	L/min	V_{ann}=	0.65	m/s
Q=	0.0056	m^3/s	Re_D=	24,261.94	
P_3=	12.796	kPa	K_{losses}=	110.71	
P_5=	-5.527	kPa			
ΔP=	18.322	kPa	f_{exp}=	**0.03742**	
			f_{theory}=	**0.016184557**	

Table D.6 Part 3: Annular Flow with 1 Roughened Surface in the Annular Channel

TRIAL 3- ANNULAR TEST SECTION

For 72 hz

Q=	928.13	L/min	V_{ann}=	1.80	m/s
Q=	0.0155	m^3/s	Re_D=	67,465.19	
P_3=	85.916	kPa	K_{losses}=	856.04	
P_5=	60.694	kPa			
ΔP=	25.223	kPa	f_{exp}=	**0.02829**	
			f_{theory}=	**0.01592504**	

For 67 hz

Q=	874.45	L/min	V_{ann}=	1.69	m/s
Q=	0.0146	m^3/s	Re_D=	63,563.60	
P_3=	76.914	kPa	K_{losses}=	759.89	
P_5=	52.501	kPa			
ΔP=	24.413	kPa	f_{exp}=	**0.02881**	
			f_{theory}=	**0.01593456**	

For 64 hz

Q=	844.41	L/min	V_{ann}=	1.63	m/s
Q=	0.0141	m^3/s	Re_D=	61,380.09	
P_3=	71.965	kPa	K_{losses}=	708.58	
P_5=	47.975	kPa			
ΔP=	23.990	kPa	f_{exp}=	**0.02919**	
			f_{theory}=	**0.01594039**	

For 60 hz

Q=	787.94	L/min	V_{ann}=	1.52	m/s
Q=	0.0131	m^3/s	Re_D=	57,274.71	
P_3=	63.404	kPa	K_{losses}=	616.97	
P_5=	40.460	kPa			
ΔP=	22.944	kPa	f_{exp}=	**0.02847**	
			f_{theory}=	**0.01595248**	

For 56 hz

Q=	742.05	L/min	V_{ann}=	1.44	m/s
Q=	0.0124	m^3/s	Re_D=	53,939.23	
P_3=	56.301	kPa	K_{losses}=	547.20	
P_5=	33.977	kPa			
ΔP=	22.324	kPa	f_{exp}=	**0.02882**	
			f_{theory}=	**0.01596358**	

For 52 hz

Q=	682.74	L/min	V_{ann}=	1.32	m/s
Q=	0.0114	m^3/s	Re_D=	49,628.09	
P_3=	48.122	kPa	K_{losses}=	463.22	
P_5=	26.898	kPa			
ΔP=	21.224	kPa	f_{exp}=	**0.02690**	
			f_{theory}=	**0.01598001**	

For 48 hz

Q=	632.99	L/min	V_{ann}=	1.22	m/s
Q=	0.0105	m^3/s	Re_D=	46,011.82	
P_3=	41.745	kPa	K_{losses}=	398.17	
P_5=	20.758	kPa			
ΔP=	20.988	kPa	f_{exp}=	**0.02988**	
			f_{theory}=	**0.015996018**	

For 45 hz

Q=	587.41	L/min	V_{ann}=	1.14	m/s
Q=	0.0098	m^3/s	Re_D=	42,698.22	
P_3=	36.392	kPa	K_{losses}=	342.89	
P_5=	16.072	kPa			
ΔP=	20.320	kPa	f_{exp}=	**0.02887**	
			f_{theory}=	**0.016012931**	

For 40 hz

Q=	527.30	L/min	V_{ann}=	1.02	m/s
Q=	0.0088	m^3/s	Re_D=	38,329.01	
P_3=	29.440	kPa	K_{losses}=	276.31	
P_5=	9.695	kPa			
ΔP=	19.744	kPa	f_{exp}=	**0.02982**	
			f_{theory}=	**0.016039428**	

For 36 hz

Q=	468.78	L/min	V_{ann}=	0.91	m/s
Q=	0.0078	m^3/s	Re_D=	34,075.57	
P_3=	23.820	kPa	K_{losses}=	218.38	
P_5=	4.380	kPa			
ΔP=	19.439	kPa	f_{exp}=	**0.03404**	
			f_{theory}=	**0.016071343**	

For 30 hz

Q=	390.56	L/min	V_{ann}=	0.76	m/s
Q=	0.0065	m^3/s	Re_D=	28,389.87	
P_3=	16.955	kPa	K_{losses}=	151.59	
P_5=	-1.778	kPa			
ΔP=	18.733	kPa	f_{exp}=	**0.03529**	
			f_{theory}=	**0.016127953**	

For 26 hz

Q=	335.25	L/min	V_{ann}=	0.65	m/s
Q=	0.0056	m^3/s	Re_D=	24,368.85	
P_3=	12.777	kPa	K_{losses}=	111.69	
P_5=	-5.528	kPa			
ΔP=	18.304	kPa	f_{exp}=	**0.03654**	
			f_{theory}=	**0.016182864**	

Table D.7 Part 1: Horizontal Pipe Flow with Two Roughened Surface in the Annular Channel

KNOWNS

d_3=	0.08255	m	$L_{P1\text{-}P2}$=	4.68	m	ρ_w=	1000	kg/m^3
A_3=	0.00535	m^2	μ_w=	0.00113	Pa.s			

TRIAL 1- HORIZONTAL TEST SECTION

For 73 hz					
Q=	835.94	L/min	V_3=	2.603	m/s
Q=	0.0139	m^3/s	$Re_{D\,3}$=	190,168.37	
P_1=	123.458	kPa	f_{exp}=	**0.00461**	
P_2=	119.916	kPa	f_{theory}=	**0.00378**	
ΔP=	3.542	kPa			

For 67 hz					
Q=	800.70	L/min	V_3=	2.493	m/s
Q=	0.0133	m^3/s	$Re_{D\,3}$=	182,152.57	
P_1=	110.587	kPa	f_{exp}=	**0.00447**	
P_2=	107.434	kPa	f_{theory}=	**0.00382**	
ΔP=	3.153	kPa			

For 64 hz					
Q=	774.68	L/min	V_3=	2.412	m/s
Q=	0.0129	m^3/s	$Re_{D\,3}$=	176,231.59	
P_1=	104.861	kPa	f_{exp}=	**0.00441**	
P_2=	101.955	kPa	f_{theory}=	**0.00386**	
ΔP=	2.907	kPa			

For 60 hz					
Q=	719.48	L/min	V_3=	2.240	m/s
Q=	0.0120	m^3/s	$Re_{D\,3}$=	163,674.24	
P_1=	93.134	kPa	f_{exp}=	**0.00520**	
P_2=	90.172	kPa	f_{theory}=	**0.00393**	
ΔP=	2.962	kPa			

For 56 hz					
Q=	669.07	L/min	V_3=	2.084	m/s
Q=	0.0112	m^3/s	$Re_{D\,3}$=	152,206.17	
P_1=	82.815	kPa	f_{exp}=	**0.00446**	
P_2=	80.620	kPa	f_{theory}=	**0.00400**	
ΔP=	2.196	kPa			

For 52 hz					
Q=	615.40	L/min	V_3=	1.916	m/s
Q=	0.0103	m^3/s	$Re_{D\,3}$=	139,998.26	
P_1=	72.591	kPa	f_{exp}=	**0.00543**	
P_2=	70.330	kPa	f_{theory}=	**0.00408**	
ΔP=	2.261	kPa			

For 48 hz					
Q=	564.99	L/min	V_3=	1.759	m/s
Q=	0.0094	m^3/s	$Re_{D\,3}$=	128,528.92	
P_1=	63.701	kPa	f_{exp}=	**0.00546**	
P_2=	61.784	kPa	f_{theory}=	**0.00417**	
ΔP=	1.917	kPa			

For 45 hz					
Q=	532.94	L/min	V_3=	1.660	m/s
Q=	0.0089	m^3/s	$Re_{D\,3}$=	121,238.35	
P_1=	57.427	kPa	f_{exp}=	**0.00540**	
P_2=	55.741	kPa	f_{theory}=	**0.00423**	
ΔP=	1.686	kPa			

For 40 hz					
Q=	465.09	L/min	V_3=	1.448	m/s
Q=	0.0078	m^3/s	$Re_{D\,3}$=	105,802.96	
P_1=	47.350	kPa	f_{exp}=	**0.00588**	
P_2=	45.951	kPa	f_{theory}=	**0.00438**	
ΔP=	1.399	kPa			

For 36 hz					
Q=	412.53	L/min	V_3=	1.285	m/s
Q=	0.0069	m^3/s	$Re_{D\,3}$=	93,847.51	
P_1=	40.232	kPa	f_{exp}=	**0.00555**	
P_2=	39.193	kPa	f_{theory}=	**0.00451**	
ΔP=	1.039	kPa			

For 30 hz					
Q=	342.12	L/min	V_3=	1.065	m/s
Q=	0.0057	m^3/s	$Re_{D\,3}$=	77,829.92	
P_1=	31.418	kPa	f_{exp}=	**0.00656**	
P_2=	30.573	kPa	f_{theory}=	**0.00473**	
ΔP=	0.845	kPa			

For 26 hz					
Q=	290.53	L/min	V_3=	0.905	m/s
Q=	0.0048	m^3/s	$Re_{D\,3}$=	66,093.13	
P_1=	26.198	kPa	f_{exp}=	**0.00956**	
P_2=	25.311	kPa	f_{theory}=	**0.00493**	
ΔP=	0.887	kPa			

TRIAL 2- HORIZONTAL TEST SECTION

For 73 hz					
Q=	871.57	L/min	V_3=	2.714	m/s
Q=	0.0145	m^3/s	$Re_{D\,3}$=	198,274.11	
P_1=	121.698	kPa	f_{exp}=	**0.00386**	
P_2=	118.471	kPa	f_{theory}=	**0.00374**	
ΔP=	3.227	kPa			

For 64 hz					
Q=	784.10	L/min	V_3=	2.442	m/s
Q=	0.0131	m^3/s	$Re_{D\,3}$=	178,375.57	
P_1=	101.338	kPa	f_{exp}=	**0.00368**	
P_2=	98.847	kPa	f_{theory}=	**0.00384**	
ΔP=	2.490	kPa			

For 52 hz					
Q=	638.94	L/min	V_3=	1.990	m/s
Q=	0.0106	m^3/s	$Re_{D\,3}$=	145,352.03	
P_1=	69.230	kPa	f_{exp}=	**0.00359**	
P_2=	67.618	kPa	f_{theory}=	**0.00405**	
ΔP=	1.612	kPa			

Table D.8 Part 2: Horizontal Pipe Flow with Two Roughened Surface in the Annular Channel

TRIAL 3- HORIZONTAL TEST SECTION

	Q= (L/min)	Q= (m^3/s)	$V_{3'}$= (m/s)	$Re_{D\,3'}$=	P_1= (kPa)	P_2= (kPa)	ΔP= (kPa)	f_{exp}=	f_{theory}=
For 73 hz	754.38	0.0126	2.349	171,614.46	104.614	102.046	2.568	0.00410	0.00388
For 67 hz	688.63	0.0115	2.144	156,657.85	86.958	84.764	2.194	0.00421	0.00397
For 64 hz	669.77	0.0112	2.086	152,367.15	84.149	82.118	2.031	0.00412	0.00400
For 60 hz	626.43	0.0104	1.951	142,507.75	75.503	73.715	1.788	0.00414	0.00407
For 56 hz	590.36	0.0098	1.838	134,301.93	68.067	66.209	1.858	0.00485	0.00413
For 52 hz	545.78	0.0091	1.700	124,159.71	60.125	58.881	1.244	0.00380	0.00421
For 48 hz	503.50	0.0084	1.568	114,541.41	54.094	52.867	1.226	0.00440	0.00429
For 36 hz	373.30	0.0062	1.162	84,921.12	34.736	33.787	0.949	0.00620	0.00463
For 30 hz	310.79	0.0052	0.968	70,701.19	27.746	26.928	0.818	0.00770	0.00484
For 26 hz	266.46	0.0044	0.830	60,617.26	23.266	22.692	0.573	0.00735	0.00503

TRIAL 4- HORIZONTAL TEST SECTION

	Q= (L/min)	Q= (m^3/s)	$V_{3'}$= (m/s)	$Re_{D\,3'}$=	P_1= (kPa)	P_2= (kPa)	ΔP= (kPa)	f_{exp}=	f_{theory}=
73 hz pump speed	762.30	0.0127	2.374	173,416.14	101.646	98.841	2.805	0.00439	0.00387
67 hz pump speed	697.22	0.0116	2.171	158,609.82	89.784	87.327	2.457	0.00460	0.00396
64 hz pump speed	678.16	0.0113	2.112	154,275.50	83.867	82.055	1.812	0.00358	0.00399
60 hz pump speed	641.29	0.0107	1.997	145,887.31	78.605	76.460	2.145	0.00474	0.00404
56 hz pump speed	602.22	0.0100	1.875	137,000.25	71.002	69.292	1.710	0.00429	0.00411
52 hz pump speed	543.18	0.0091	1.691	123,567.46	60.030	58.768	1.262	0.00389	0.00421
48 hz pump speed	503.67	0.0084	1.568	114,580.66	53.583	52.560	1.023	0.00367	0.00429
45 hz pump speed	466.71	0.0078	1.453	106,172.92	47.862	46.802	1.060	0.00442	0.00438
40 hz pump speed	418.17	0.0070	1.302	95,128.61	41.219	40.403	0.816	0.00424	0.00450
36 hz pump speed	378.44	0.0063	1.178	86,091.98	35.622	34.962	0.660	0.00419	0.00461
30 hz pump speed	314.69	0.0052	0.980	71,588.52	28.324	27.643	0.681	0.00626	0.00483
26 hz pump speed	269.08	0.0045	0.838	61,212.24	23.894	23.423	0.470	0.00591	0.00502

Table D.10 Part 1: Annular Flow with Two Roughened Surface in the Annular Channel

KNOWNS

Do=	0.1484	m (6")	A_{ann}=	0.00710	m^2	μ_w=	0.00113	Pa.m	A_{holes}=	0.004516
Di=	0.11395	m (4 1/4")	L_{P3-P5}=	1.727	m	ρ_w=	1000	kg/m^3	σ=	0.6362
Dh=	0.03445	m	ε=	2.01E-03		z_5=	1.727	m (z_3=0)	k_{red}=	0.2500
			ε/D=	0.0582					k_{exp}=	0.1324

TRIAL 1- ANNULAR TEST SECTION

For 72 hz					
Q=	835.94	L/min	V_{ann}=	1.96	m/s
Q=	0.0139	m^3/s	Re_D=	59,837.62	
P_3=	89.854	kPa	K_{losses}=	736.48	
P_5=	49.362	kPa			
ΔP=	40.492	kPa	f_{exp}=	**0.05907**	
			f_{theory}=	**0.019397**	

For 67 hz					
Q=	800.70	L/min	V_{ann}=	1.88	m/s
Q=	0.0133	m^3/s	Re_D=	57,315.40	
P_3=	81.237	kPa	K_{losses}=	675.71	
P_5=	44.202	kPa			
ΔP=	37.034	kPa	f_{exp}=	**0.05479**	
			f_{theory}=	**0.019403**	

For 64 hz					
Q=	774.68	L/min	V_{ann}=	1.82	m/s
Q=	0.0129	m^3/s	Re_D=	55,452.33	
P_3=	76.520	kPa	K_{losses}=	632.49	
P_5=	40.391	kPa			
ΔP=	36.128	kPa	f_{exp}=	**0.05594**	
			f_{theory}=	**0.019409**	

For 60 hz					
Q=	719.48	L/min	V_{ann}=	1.69	m/s
Q=	0.0120	m^3/s	Re_D=	51,501.08	
P_3=	66.168	kPa	K_{losses}=	545.57	
P_5=	33.041	kPa			
ΔP=	33.127	kPa	f_{exp}=	**0.05466**	
			f_{theory}=	**0.019421**	

For 56 hz					
Q=	669.07	L/min	V_{ann}=	1.57	m/s
Q=	0.0112	m^3/s	Re_D=	47,892.58	
P_3=	57.507	kPa	K_{losses}=	471.79	
P_5=	26.668	kPa			
ΔP=	30.839	kPa	f_{exp}=	**0.05426**	
			f_{theory}=	**0.019434**	

For 52 hz					
Q=	615.40	L/min	V_{ann}=	1.44	m/s
Q=	0.0103	m^3/s	Re_D=	44,051.29	
P_3=	48.284	kPa	K_{losses}=	399.15	
P_5=	20.190	kPa			
ΔP=	28.094	kPa	f_{exp}=	**0.05137**	
			f_{theory}=	**0.019450**	

For 48 hz					
Q=	564.99	L/min	V_{ann}=	1.33	m/s
Q=	0.0094	m^3/s	Re_D=	40,442.39	
P_3=	40.772	kPa	K_{losses}=	336.43	
P_5=	14.640	kPa			
ΔP=	26.132	kPa	f_{exp}=	**0.05018**	
			f_{theory}=	**0.019468**	

For 45 hz					
Q=	532.94	L/min	V_{ann}=	1.25	m/s
Q=	0.0089	m^3/s	Re_D=	38,148.37	
P_3=	31.211	kPa	K_{losses}=	299.34	
P_5=	10.452	kPa			
ΔP=	20.760	kPa	f_{exp}=	**0.02241**	
			f_{theory}=	**0.019481**	

For 40 hz					
Q=	465.09	L/min	V_{ann}=	1.09	m/s
Q=	0.0078	m^3/s	Re_D=	33,291.54	
P_3=	27.212	kPa	K_{losses}=	227.97	
P_5=	4.937	kPa			
ΔP=	22.275	kPa	f_{exp}=	**0.04270**	
			f_{theory}=	**0.019514**	

For 36 hz					
Q=	412.5337	L/min	V_{ann}=	0.97	m/s
Q=	0.0069	m^3/s	Re_D=	29,529.68	
P_3=	21.285	kPa	K_{losses}=	179.36	
P_5=	0.347	kPa			
ΔP=	20.94	kPa	f_{exp}=	**0.04058**	
			f_{theory}=	**0.019546**	

For 30 hz					
Q=	342.12	L/min	V_{ann}=	0.80	m/s
Q=	0.0057	m^3/s	Re_D=	24,489.65	
P_3=	13.930	kPa	K_{losses}=	123.36	
P_5=	-4.779	kPa			
ΔP=	18.709	kPa	f_{exp}=	**0.02541**	
			f_{theory}=	**0.019604**	

For 26 hz					
Q=	290.53	L/min	V_{ann}=	0.68	m/s
Q=	0.0048	m^3/s	Re_D=	20,796.60	
P_3=	9.446	kPa	K_{losses}=	88.96	
P_5=	-7.979	kPa			
ΔP=	17.425	kPa	f_{exp}=	**0.00846**	
			f_{theory}=	**0.019664**	

Table D.11 Part 2: Annular Flow with Two Roughened Surface in the Annular Channel

TRIAL 2 - ANNULAR TEST SECTION

For 72 hz

Q=	871.57	L/min	V_{ann}=	2.05	m/s
Q=	0.0145	m^3/s	Re_D=	62,388.14	
P_3=	95.366	kPa	K_{losses}=	800.61	
P_5=	52.246	kPa			
ΔP=	43.120	kPa	f_{exp}=	**0.06044**	
			f_{theory}=	**0.019390**	

For 64 hz

Q=	784.10	L/min	V_{ann}=	1.84	m/s
Q=	0.0131	m^3/s	Re_D=	56,126.94	
P_3=	77.343	kPa	K_{losses}=	647.97	
P_5=	39.736	kPa			
ΔP=	37.608	kPa	f_{exp}=	**0.05891**	
			f_{theory}=	**0.019407**	

For 52 hz

Q=	638.94	L/min	V_{ann}=	1.50	m/s
Q=	0.0106	m^3/s	Re_D=	45,735.89	
P_3=	48.153	kPa	K_{losses}=	430.26	
P_5=	20.778	kPa			
ΔP=	18.799	kPa	f_{exp}=	**0.04433**	
			f_{theory}=	**0.019443**	

TRIAL 3 - ANNULAR TEST SECTION

For 72 hz

Q=	754.38	L/min	V_{ann}=	1.77	m/s
Q=	0.0126	m^3/s	Re_D=	53,999.52	
P_3=	74.578	kPa	K_{losses}=	599.78	
P_5=	40.175	kPa			
ΔP=	34.403	kPa	f_{exp}=	**0.05360**	
			f_{theory}=	**0.019413**	

For 67 hz

Q=	688.63	L/min	V_{ann}=	1.62	m/s
Q=	0.0115	m^3/s	Re_D=	49,293.33	
P_3=	59.987	kPa	K_{losses}=	499.79	
P_5=	27.973	kPa			
ΔP=	32.014	kPa	f_{exp}=	**0.05560**	
			f_{theory}=	**0.019429**	

For 64 hz

Q=	669.77	L/min	V_{ann}=	1.57	m/s
Q=	0.0112	m^3/s	Re_D=	47,943.24	
P_3=	61.787	kPa	K_{losses}=	472.79	
P_5=	29.693	kPa			
ΔP=	32.095	kPa	f_{exp}=	**0.05921**	
			f_{theory}=	**0.019434**	

For 60 hz

Q=	626.43	L/min	V_{ann}=	1.47	m/s
Q=	0.0104	m^3/s	Re_D=	44,840.92	
P_3=	53.963	kPa	K_{losses}=	413.58	
P_5=	23.422	kPa			
ΔP=	30.541	kPa	f_{exp}=	**0.06079**	
			f_{theory}=	**0.019447**	

For 56 hz

Q=	590.36	L/min	V_{ann}=	1.39	m/s
Q=	0.0098	m^3/s	Re_D=	42,258.91	
P_3=	47.042	kPa	K_{losses}=	367.33	
P_5=	18.516	kPa			
ΔP=	28.526	kPa	f_{exp}=	**0.05823**	
			f_{theory}=	**0.019459**	

For 52 hz

Q=	545.78	L/min	V_{ann}=	1.28	m/s
Q=	0.0091	m^3/s	Re_D=	39,067.60	
P_3=	40.341	kPa	K_{losses}=	313.94	
P_5=	13.393	kPa			
ΔP=	26.948	kPa	f_{exp}=	**0.05887**	
			f_{theory}=	**0.019475**	

For 48 hz

Q=	503.50	L/min	V_{ann}=	1.18	m/s
Q=	0.0084	m^3/s	Re_D=	36,041.14	
P_3=	35.063	kPa	K_{losses}=	267.19	
P_5=	9.187	kPa			
ΔP=	25.876	kPa	f_{exp}=	**0.06185**	
			f_{theory}=	**0.019494**	

For 36 hz

Q=	373.30	L/min	V_{ann}=	0.88	m/s
Q=	0.0062	m^3/s	Re_D=	26,720.94	
P_3=	17.672	kPa	K_{losses}=	146.87	
P_5=	-2.329	kPa			
ΔP=	20.002	kPa	f_{exp}=	**0.03782**	
			f_{theory}=	**0.019576**	

For 30 hz

Q=	310.79	L/min	V_{ann}=	0.73	m/s
Q=	0.0052	m^3/s	Re_D=	22,246.55	
P_3=	11.487	kPa	K_{losses}=	101.80	
P_5=	-6.797	kPa			
ΔP=	18.284	kPa	f_{exp}=	**0.02324**	
			f_{theory}=	**0.019638**	

For 26 hz

Q=	266.46	L/min	V_{ann}=	0.63	m/s
Q=	0.0044	m^3/s	Re_D=	19,073.58	
P_3=	7.632	kPa	K_{losses}=	74.83	
P_5=	-9.489	kPa			
ΔP=	17.121	kPa	f_{exp}=	**0.00265**	
			f_{theory}=	**0.019699**	

Table D.12 Part 3: Annular Flow with Two Roughened Surface in the Annular Channel

TRIAL 4 - ANNULAR TEST SECTION

72 hz pump speed

Q=	762.30	L/min	(set)	V_{ann}=	1.79	m/s
Q=	0.0127	m^3/s		Re_D=	54,566.43	
P_3=	76.308	kPa		K_{losses}=	612.44	
P_5=	41.035	kPa				
ΔP=	35.273	kPa		f_{exp}=	**0.05516**	
				f_{theory}=	**0.019411**	

67 hz pump speed

Q=	697.22	L/min	(set)	V_{ann}=	1.64	m/s
Q=	0.0116	m^3/s		Re_D=	49,907.53	
P_3=	65.771	kPa		K_{losses}=	512.33	
P_5=	32.557	kPa				
ΔP=	33.214	kPa		f_{exp}=	**0.05866**	
				f_{theory}=	**0.019427**	

64 hz pump speed

Q=	678.16	L/min	(set)	V_{ann}=	1.59	m/s
Q=	0.0113	m^3/s		Re_D=	48,543.71	
P_3=	60.943	kPa		K_{losses}=	484.71	
P_5=	28.182	kPa				
ΔP=	32.761	kPa		f_{exp}=	**0.06033**	
				f_{theory}=	**0.019432**	

60 hz pump speed

Q=	641.29	L/min	(set)	V_{ann}=	1.51	m/s
Q=	0.0107	m^3/s		Re_D=	45,904.32	
P_3=	56.378	kPa		K_{losses}=	433.43	
P_5=	24.968	kPa				
ΔP=	31.410	kPa		f_{exp}=	**0.06174**	
				f_{theory}=	**0.019442**	

56 hz pump speed

Q=	602.22	L/min	(set)	V_{ann}=	1.41	m/s
Q=	0.0100	m^3/s		Re_D=	43,107.95	
P_3=	49.873	kPa		K_{losses}=	382.23	
P_5=	20.299	kPa				
ΔP=	29.574	kPa		f_{exp}=	**0.06111**	
				f_{theory}=	**0.019454**	

52 hz pump speed

Q=	543.18	L/min	(set)	V_{ann}=	1.28	m/s
Q=	0.0091	m^3/s		Re_D=	38,881.24	
P_3=	40.151	kPa		K_{losses}=	310.95	
P_5=	13.060	kPa				
ΔP=	27.091	kPa		f_{exp}=	**0.06033**	
				f_{theory}=	**0.019476**	

48 hz pump speed

Q=	503.67	L/min	(set)	V_{ann}=	1.18	m/s
Q=	0.0084	m^3/s		Re_D=	36,053.49	
P_3=	34.437	kPa		K_{losses}=	267.37	
P_5=	9.012	kPa				
ΔP=	25.425	kPa		f_{exp}=	**0.05859**	
				f_{theory}=	**0.019494**	

45 hz pump speed

Q=	466.71	L/min	(set)	V_{ann}=	1.10	m/s
Q=	0.0078	m^3/s		Re_D=	33,407.95	
P_3=	29.295	kPa		K_{losses}=	229.57	
P_5=	5.527	kPa				
ΔP=	23.769	kPa		f_{exp}=	**0.05480**	
				f_{theory}=	**0.019513**	

40 hz pump speed

Q=	418.17	L/min	(set)	V_{ann}=	0.98	m/s
Q=	0.0070	m^3/s		Re_D=	29,932.79	
P_3=	23.322	kPa		K_{losses}=	184.29	
P_5=	1.332	kPa				
ΔP=	21.990	kPa		f_{exp}=	**0.05033**	
				f_{theory}=	**0.019542**	

36 hz pump speed

Q=	378.44	L/min	(set)	V_{ann}=	0.89	m/s
Q=	0.0063	m^3/s		Re_D=	27,089.36	
P_3=	18.748	kPa		K_{losses}=	150.94	
P_5=	-1.616	kPa				
ΔP=	20.364	kPa		f_{exp}=	**0.04132**	
				f_{theory}=	**0.019572**	

30 hz pump speed

Q=	314.69	L/min	(set)	V_{ann}=	0.74	m/s
Q=	0.0052	m^3/s		Re_D=	22,525.76	
P_3=	12.254	kPa		K_{losses}=	104.37	
P_5=	-6.205	kPa				
ΔP=	18.459	kPa		f_{exp}=	**0.02581**	
				f_{theory}=	**0.019634**	

26 hz pump speed

Q=	269.08	L/min	(set)	V_{ann}=	0.63	m/s
Q=	0.0045	m^3/s		Re_D=	19,260.80	
P_3=	8.169	kPa		K_{losses}=	76.31	
P_5=	-9.242	kPa				
ΔP=	17.411	kPa		f_{exp}=	**0.00982**	
				f_{theory}=	**0.019695**	